NITRIC OXIDE PRODUCTION OF MENICAL EXPLANTS FOLLOWING DYNAMIC COMPRESSION

BY

JEFFREY A. MCHENRY

B.S.M.E., Michigan Technological University, 2005

A THESIS

Submitted in partial fulfillment of the

requirements for the degree of

MASTER OF SCIENCE IN MECHANICAL ENGINEERING

MICHIGAN TECHNOLOGICAL UNIVERSITY

2005

NITRIC OXIDE PRODUCTION BY MENISCAL EXPLANTS FOLLOWING DYNAMIC COMPRESSION

Jeffrey A. McHenry

Department of Mechanical Engineering and Engineering Mechanics

Michigan Technological University, 2005

ABSTRACT

Meniscal fibrochondrocytes have been suspected of producing nitric oxide in response to dynamic compression. The relationship of compressive strain and compressive stress to nitric oxide production in meniscal explants has not yet been characterized. It may be true that physiological strain and pressure conditions may decrease nitric oxide production compared to the unloaded state, thus reducing the harmful affects that nitric oxide has on matrix metabolism in the meniscus. It may also be true that overloading as well as unloading may produce an up-regulation of nitric oxide when compared to physiological conditions. The identity of nitric oxide producing cells in the meniscus is also still unclear. The chondrocytic cells found in the deep zones of the meniscus have been shown to produce nitric oxide in articular cartilage, while the fibroblastic cells in the superficial zone have recently been investigated. To further understand these relationships, the goals of the current project were to 1) validate a specially designed tissue compression bioreactor capable of a wide range of accurate displacement and load control; 2) determine the relationship of strain/pressure to nitric oxide production in both superficial and deep zones of meniscal explants.

ACKNOWLEDGEMENTS

First, I would like to thank my advisor Dr. Tammy Haut Donahue for her support, direction, and patience through this project. Her help and encouragement have been very important to me and to the success and completion of this work. I would also like to thank the Whitaker foundation that has provided funding for this research, allowing the use of proper equipment and supplies needed for these experiments. My committee members Dr. Seth Donahue, Dr. Jeff Burl, and Dr. Eric Blough have provided critique of my work and have directed me in my writing and experimentation, which is much appreciated. I want to thank them for this advice and also for their patience.

I am also grateful for the assistance of my lab group members Tumul, Basia, and Jason. They have provided much needed assistance while I was off campus and have provided a great working environment in the lab. I would also like to thank Jesse Nordeng for dedication to providing professional quality machining work that was necessary for the accurate function of the bioreactor used in these experiments.

I want to thank my family for their encouragement of me taking on and completing this project. Their support had helped push me to finish work that I can be proud of, and I greatly appreciate it.

TABLE OF CONTENTS

LIST OF TABLES

LIST OF FIGURES

CHAPTER ONE

INTRODUCTION

1.1 Functions of the Meniscus

The menisci are specialized fibrocartilaginous structures that play a crucial role in the maintenance of knee stability, load distribution, joint lubrication, and shock absorption [1-8]. They have a semicircular shape with a wedge-shaped cross-section that adapts the curvature of the femoral condyles to the flatter tibial plateau. The tibial surface of the meniscus is flat while the femoral surface is convex. Their shape increases the tibial plateau contact area, thereby decreasing the contact stresses significantly in the knee. It has been shown that between 30% and 65% of the total knee joint load is transmitted through the meniscus, reducing the compressive stress on the articular cartilage and subchondral bone[3, 9]. During compressive loading of the knee, pressure is added to the superior surfaces of the menisci that has both a horizontal and vertical component. The vertical component is balanced by the reaction force of the tibial plateau [4]. The horizontal force is opposed by the hoop stress that forms in the circumferential direction of the meniscus [3, 9].

Following partial and full meniscectomy, changes occur in the knee due to a loss in the weight bearing capacity of the menisci. Narrowing of the joint space, formation of an osteophytic ridge between the femoral condyles, flattening of the femoral articular

surface, and osteoarthritis are symptoms seen in meniscectomized knees [1, 3, 4, 10]. Osteoarthritis (OA), characterized as the loss of articular cartilage, has been investigated and is thought to be triggered by meniscectomy [1, 11]. OA following meniscectomy is hypothesized to be a result of the increased contact pressure between the femoral condyles and the tibial plateau, resulting in overstraining and degeneration of the articular cartilage. Thus, this demostrates the vital role the meniscus plays in the weight bearing function of the knee joint.

The meniscus also provides stability between the femur and tibial plateau. The semicircular shape and the meniscal attachments help keep the femoral chondyles in the correct location by providing resistance. This aids the other ligaments in the stability of the joint by reducing motion. The movement of each meniscus is restricted by the ligamentous anterior and posterior horns connecting the meniscus substance to the tibial plateau. The circumferential matrix fibers of the meniscus extend to the intercondylar area to secure the meniscus. The lateral meniscus is radially smaller than the medial and attaches centrally along the intercondylar eminence [1, 12]. The larger medial meniscus connects more on the anterior and posterior portion of the intercondylar area. The deep medial ligament and posterior portion of the superficial medial ligament also fix the medial meniscus to the femur. The lateral meniscus attachments are less firm allowing greater posterior displacement of the meniscus as the tibia rotates during flexion [1, 13]. The medial meniscus has been found to move a few millimeters while the lateral meniscus can move at least a centimeter [4, 12]. These attachments allow the meniscus to move slightly along the tibial plateau as the knee flexes.

The meniscus also serves as a limited shock absorbing medium [1, 8, 14] and aids in lubrication of the joint [4, 15]. These functions come from the composition of the meniscus and the ability of the tissue to allow fluid flow through the extra-cellular matrix. The smooth surface of the meniscus in the presence of the synovial fluid is nearly frictionless, allowing unrestricted motion in the knee. Permeability of the tissue allows fluid to leave during compression, reducing the hydrostatic pressure within the matrix. This mechanism allows the meniscus to be a natural shock absorber. The study performed by Voloshin, et al. (1980) concluded that removal of the meniscus reduces the knees shock absorbing capacity by 20%.

1.2 *In Vivo* Loading Environment

The meniscus experiences a complex loading due to its form and function as a weight bearing structure and joint stabilizer. Their location between round femoral condyles and the tibial plateau creates compressive and tensile forces in the tissue matrix. The loading is further complicated during joint flexion and extension as the tibia rotates and the knee locks during the "screwed home" process. This occurs when the knee reaches full extension and is actually in a few degrees of hyperextension, increasing the load on the anterior portion of the meniscus. However the menisci experience the highest level of loading during 0˚ flexion [1, 11, 16]. Overall, the meniscus experiences up to four times body weight (a range of 0-3000 N) of compressive loading during walking [17].

The applied forces generate both a horizontal and vertical component on the superior surface as previously described. The vertical components of force on the

superior surface are balanced by the vertical components on the inferior surface generated by the tibial plateau. This balance of vertical forces causes compressive stress in the meniscus and holds it tightly between the femur and tibia during high levels of joint load. The horizontal force component is created by the rounded femoral condyle and matching concave superior surface of the meniscus. This force component acts to displace the meniscus radially outward. Opposing this force is the circumferential Type I collagen bundles that continue into the menical attachments and connect to the tibia. These fiber bundles provide tension that resist stretching and displacement of the tissue. The tibia provides the anchor point for resisting radial displacement. During joint flexion, the central portion of the meniscus does displace slightly outward [9]. However, the anterior and posterior regions move inward to produce a more compressed C-shape meniscus than during the unloaded state.

The loading conditions on the meniscus also change as the knee moves from full flexion to full extension [1, 9, 13, 18]. This range of motion is approximately 140° [4, 16]. As the knee moves from 30° of flexion to full extension, 18° of internal rotation of the femur occurs with respect to the femur [4, 11]. During flexion, the distance between the femoral condyle increases and the radius of curvature increases. This keeps the contact area high and pushes the menisci away from the center [9]. As the knee moves to extension, the radii of the femoral condyles increase and the distance between them decreases. When load is applied during extension, the menisci deform anteroposteriorly [9]. During full extension the femoral condyles slide posteriorly as they contact the anterior horns of the menisci [4, 18, 19]. This motion tightens the anterior cruciate ligament and stops the extension of the lateral femoral condyle. The medial condyle

rotates further forward until the popliteal tendon, tibial and fibular collateral ligaments are tight [4, 20]. At this point in extension, the meniscal horns add further restriction since the anterior portions of the menisci are tightly wedged between the femur and tibia. This is when the knee has "screwed home." To unlock the knee, the popliteus muscle contracts and rotates the lateral femoral condyle posteriorly [20]. This is approximately 18° of rotation, which occurs in the first 30° of flexion [4]. As the knee unlocks and moves in flexion, the menisci move with the femoral condyles keeping a large contact area [9]. This happens when the meniscofemoral ligaments pull the posterior section of the lateral meniscus in the medial direction. The popliteus muscle also pulls the posterior section back over the tibial plateau. The medial meniscus is pulled forward during flexion by the deep and superficial medial ligaments.

The motion of the meniscus, as the knee flexes, shifts load constantly through the knee. The menisci shift constantly with the femur to keep contact area high and maintain their weight bearing function. Constant compressive and tensile forces are present on the structure making the material properties particularly important for the menisci to function properly.

1.3 Material Properties of the Meniscus

The complex loading environment shows that the meniscus requires different compressive and tensile strengths. The circumferential direction must have high tensile strength to resist the hoop stress generated by the radial force component during joint load. The meniscus must be strong enough in tension in the radial direction to keep the

tissue from tearing under normal loading condition. There also has to be a high compressive strength to distribute load from the femoral condyles.

The circumferential direction has shown to have the highest tensile strength [2, 21-23]. Tests performed on the meniscus have characterized the elastic modulus of the anterior, central, and posterior regions for both the lateral and medial meniscus. The results from Fithian (1989) show the anterior region to have an average elastic modulus in the circumferential of approximately 160 MPa for both menisci (Lateral: 159.07 ± 47.4; Medial: 159.58 ± 26.2). The central region showed 228.79 ± 51.4 MPa for the lateral and 93.18 ± 52.14 MPa for the medial. The posterior region showed 294.14 ± 90.4 MPa for the lateral and 110.23 ± 40.7 MPa for the medial. Tissakht (1994) documented changes through the depth of the tissue; proximal, middle, and distal circumferential tensile elastic modulus. On average, the middle portion had the lowest elastic modulus with proximal and distal being close to one another. Their results also showed the lateral meniscus had a higher elastic modulus than the medial meniscus for all regions.

The tensile modulus of the meniscus in the radial direction is much smaller than circumferential. The elastic modulus ranges from 2 MPa to 23 MPa depending on the region, layer, and location of the tissue [21]. On average the middle layer has the lowest elastic modulus with the proximal and distal layer being the highest. The posterior region has the highest modulus at the proximal and distal layers while the anterior seems to have the lowest at those layers.

The compressive strength of the meniscus depends largely on the strain rate at which the tissue is tested [3]. Krause (1976) et. al. tested percent energy reduction in

compressed canine menisci at 3 different deformation rates, $2.12x10^{-5}$, $4.23x10^{-5}$, and $21.16x10^{-5}$ (m/sec). The resulting percent reduction in energy was 46.8 ± 18.6, 42.3 ± 20.3, and 32.2 ± 1.6 (%), respectively. This data shows that a greater amount of energy is required to compress the meniscus at higher strain rates. The high water content of the tissue creates a hydrostatic pressure that provides the compressive strength. As load is added to the tissue, hydrostatic pressure increases and then decreases as fluid flows out of the tissue. The compressive strength has also been shown to increase exponentially with level of strain [14]. At 0.2 strain, the compressive elastic modulus for the circumferential, radial, and axial direction is 10 MPa, 13 MPa, and 19 MPa, respectively. At 0.8 strain, the compressive elastic modulus for the same three directions are 288 MPa, 287 MPa, and 299 MPa, respectively. This shows that the meniscus has the greatest compressive strength in the axial direction, which is expected.

1.4 Composition and Structure

The meniscus is a biphasic material that includes an extra-cellular matrix filled with interstitial fluid. It is composed of approximately 75% water, 20% collagen, and 5% non-collagenous substances such and proteoglycans, lipids, and cells [1, 7, 14, 23]. These components contribute to the specialized structure and function of the meniscus. The fluid within the matrix experiences limited flow through the boundaries [24]. As load is added to the meniscus, the hydrostatic pressure increases within the meniscus making it strong in compression [14]. This pressure decreases with time as fluid flows out of the meniscus, compressing the matrix. When load is removed, the matrix returns

and fluid flows back into the meniscus, returning it to equilibrium. This behavior makes the meniscus a natural load bearing and shock absorbing structure.

The extra-cellular matrix is dominated by collagen, specifically Type I with small amounts of Type II, III, and IV [1, 6, 23, 25]. Numerous bundles of circumferentially oriented Type I collagen fibers are dispersed throughout the meniscus giving its highest tensile strength in that direction (Figure 1) [1, 3, 12, 14, 21, 23, 26, 27]. Some of these layers extend past the meniscus and form the horn attachments. Other collagen fibers are oriented radially and woven into the circumferential bundles (Figure 1). There are also some superficial fibers with random orientation creating a mesh-like matrix on the femoral articular surface. Type I collagen is a fibrous component that is strong in tension. This collagen arrangement is ideal when resisting the hoop stress created during normal loading conditions.

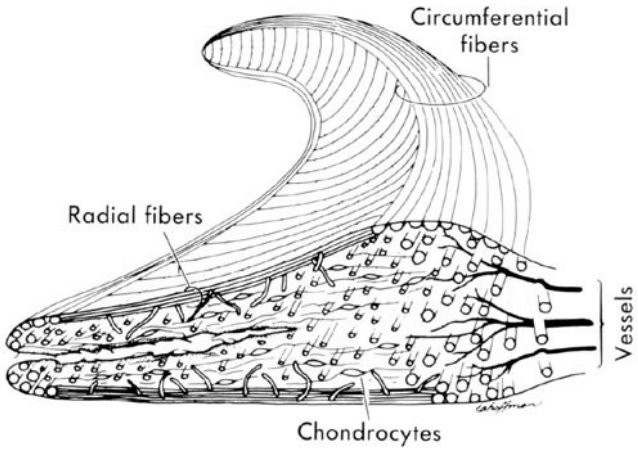

{www.orthoteers.co.uk/Nrujp~ij331m/orthkneemenisc.htm}

Figure 1.1: A cross-section of the meniscus showing the radial and circumferential collagen fiber orientation. Also shown are blood vessels penetrating the peripheral one-third of the tissue and location of chondrocytes.

Proteoglycans are another important component within the meniscus that add resilience and strength to the structure during compressive loading [1, 27]. Much of the noncollagenous portion of the extracellular matix is proteoglycans termed aggrecan, decorin, and biglycan, with aggrecan being the major type. These are large molecules with a core protein and a repeating sugar chain that is electronegative. These hydrophilic molecules can entrain 50 times their weight in free solution. The charge-charge repulsion force stiffly extends the proteoglycans in the matrix, making them naturally resistant to compression. Aggrecan is a type of proteoglycan that aggregates to hyaluronic acid to form a large molecule like those found in articular hyaline cartilage. These "cartilage-like" proteoglycans are the most abundant form in the adult human meniscus [5, 27, 28]. Proteoglycans that do not aggregate to hyaluronic acid are smaller, contain dermatan sulfate, and are either decorin or biglycan. Decorin has one dermatan sulfate chain and biglycan has two. Approxmimately 75% of the dermatan sulfate proteoglycans in the meniscus are decorin [28]. Proteoglycans are woven into the collagen matrix and distributed in an inhomogeneous manner allowing fluid flow in the meniscus. Therefore these molecules contribute in numerous ways to the compressive strength of the meniscus.

Some other elements present in small amounts in the meniscus are elastin, uronic acids, hexosamine, and ash [29]. These elements form very small amounts of the extra-cellular matrix. The cells in the meniscus, which are responsible for proper maintenance of the matrix, are called fibrochondrocytes.

1.5 Cellularity and Nutrition

The meniscus is composed of two distinct species of fibrochondrocytes that are generally distributed through the extra-cellular matrix in a homogenous manner [30]. The first species resembles fibroblasts and is found toward the superior surface. The second type resembles chondrocytes and is found closer to the inferior surface of the meniscus. Each type has a different phenotype, function, and distribution throughout the extra-cellular matrix. These fibrochondrocytes produce the components needed to maintain the fibrous tissue structure.

Fibroblasts are a type of connective-tissue cell that secretes extra-cellular matrix that is rich in Type I collagen. These cells are capable of differentiating into several different types of more specialized cells [31]. Fibroblasts can convert into chondrocytes, osteocytes, fat cells, and smooth muscle cells [31]. It appears that the conversion from fibroblast to chondrocyte is reversible. The differentiation of these cells seems to be influenced by the extra-cellular matrix through physical and chemical effects. An example is chondrocytes that are cultured in low density as a monolayer. Under these conditions, the chondrocytes lose their rounded shape, flatten, and stop producing collagen matrix [31]. Instead, the cells stop producing Type II collagen, and start producing Type I collagen, taking on the appearance of fibroblasts [31]. This helps explain why the cells within the meniscus appear as fibroblasts in some regions and chondrocytes in others. Since, the superficial region of meniscus has such a large amount of Type I collagen, the cells take on the fibroblast form and produce Type I collagen. The cells in the deep regions of the meniscus are surrounded by more proteoglycans and

small amounts of Type II collagen. These cells are chondrocytic and function to maintain the pericellular matrix.

The cells of the meniscus are set in well-defined lacunae and can be individual or paired [26]. The lacunae in the superficial layer are more compressed and fusiform than those in the interior layers. These superficial layers have a more homogenous extra-cellular matrix and appear to be more hyaline-like. This zone is a high-density, multilayer of fibroblastic cells that is surrounded by a large amount of Type I collagen. Cells in lower density surrounded by less Type I collagen will appear and behave like chondrocytes. In the deeper zones and closer to the inferior surface, there is a lower cell density of round or polygonal shaped chondrocytic cells. This subtype of cells synthesizes a large amount of sulfated proteoglycans and does not produce Type I collagen. This is a major component of articular cartilage that provides compressive strength, which is also found in the meniscus.

The lowest cell density is located in the central region of the meniscus [24, 30]. It is believed that cell density may be correlated to the supply of nutrition in the meniscus. The nutrient supply to the meniscal cells depends on two main sources, blood supply and synovial fluid. Only the peripheral 10 to 30% of the adult meniscus is vascularized, making the meniscus a relatively avascular structure (Figure 1). Blood is the main source of nutrients necessary to keep the fibrochondrocytes alive and the tissue healthy. This blood supply comes from the inferior, superior, and middle genicular arteries that run together in a capillary plexus on the periphery of the meniscus [1]. Radial branches penetrate and spread into the peripheral one-third of the structure. The components necessary for synthesis of the extracellular matrix are provided by the blood and by

synovial fluid. There is a larger population of cells near the surface of the meniscus with a decreasing population of cells towards the interior. The interior region is only nourished by diffusion of the blood from the periphery and diffusion of synovial fluid from the exterior. Cells that do not receive blood supply directly depend on fluid flow within the tissue. The nutrients are believed to diffuse through the tissue if the molecules are small enough [24]. Fluid is able to move through the articulating surface through canals 10-200 μm in diameter [1, 32]. These canals may play a role in nourishing the tissue even though they are not filled by the blood supply. Fluid motion associated with mechanical loading aids in nutrition by creating a greater flow of nutrition to cells.

The limited nutrient supply to the meniscus is believed to be the reason for its poor healing characteristics [24]. The inner two thirds of the meniscus heals poorly and is therefore frequently removed when torn. The vascularized portion is usually repaired because the vascularization increases the chances of healing. Sutures are often used to close tears, which occur in the outer one-third of the structure. This region is capable of cell proliferation and remodeling. The ability of a tissue to remodel depends on the chemical signaling between cells. These chemical signals require a pathway such as blood, synovial fluid, and gap junctions to create a healing response from distant cells. Without this pathway, the tissue is not capable of regeneration.

1.6 Mechanotransduction

Mechanotransduction is the mechanism that presumably leads to remodeling in several types of tissue. In this process, a mechanical signal creates a change in the environment of a cell, which produces a biochemical response. These chemical

responses are carried throughout the tissue serving as paracrine and autocrine signals to produce changes in cellular behavior throughout the tissue. This mechanism is responsible for the maintenance of matrix metabolism and the remodeling of many types of tissue. The process requires sensor cells, a pathway for signal transduction, and effector cells to respond to the signaling.

Mechanocoupling is the transduction of mechanical forces to a form that can be detected by cells [33]. Physical stimuli include factors such as tension, shear, hydrostatic pressure, fluid flow, and the frequently studied physical condition in the meniscus, compression. As these physical stimuli are imposed on tissue, the extracellular matrix deforms, transmitting the mechanical energy to the cells. Sensor cells respond to stimuli with various chemical signals with mechanisms that are not completely understood. Theory suggests there are multiple ways a cell can sense physical change. One way the cell may detect changes is through the activation of mechanosensitive (MS) ion channels [34]. These are gated channels that are found in the membrane of all types of living cells. The two basic types are stretch-activated and stretch-inactivated ion channels [34], both are used for electrical and/or chemical intracellular signaling. Stretch-activated MS channels are controlled by gates that respond to mechanical forces. The bilayer model and the tethered model are two theories used to describe gating of these channels [34]. In the bilayer model, mechanical forces produce tension in the lipid bilayer of the cell membrane, which directly gates the MS channels [34]. In the tethered model, there are direct connections between the cytoskeleton and MS channels [34]. Gating occurs when mechanical forces deform the cell and displace the channel gate relative to the cytoskeleton.

The cytoskeleton potentially plays a larger role in mechanotransduction than gating. It forms a network connecting the extracellular matrix to the nucleus and other organelles found within the cytoplasm. Glycoproteins called integrins extend from the actin of the cytoskeleton through the membrane to the extacellular matrix [33]. This allows for mechanical signals to be rapidly transmitted from the extracellular matrix to the nucleus, possibly altering gene expression. Recent studies have shown that deformation of tissue by compression brings distinct changes in cell and nucleus shape [35]. Static compression can alter the morphology of other organelles found in the cell, thereby altering the location and activity of intacellular enzymes. Compression is frequently studied in both articular cartilage and meniscus and is believed to play a major role in tissue homeostasis. In articular cartilage, compression alters the morphology and structure of the gogli apparatus and rough endoplasmic reticulum [35], which is believed to produce new matrix molecules with altered form and function.

Biochemical coupling is the mechanism of converting the physical stimuli sensed through mechanoncoupling into a biochemical signal [33]. Though not fully understood, the theory is that mechanical energy is transmitted to sensor cell through one of the mechanisms described above. This produces a change in the normal behavior of the cell leading to altered gene expression, enzyme production, and signaling. These factors produce autocrine and paracrine signaling that changes the function of the sensor cells and the effector cells. An effector cell receives the biochemical signal produced by the sensor cell, which alters the effector cells behavior. This type of signaling, paracrine, require a pathway such as gap junctions or interstitial fluid. Blood is a major pathway for biochemical signaling in many tissues. Fluid, either blood or interstitial fluid, carry

cytokines to and from cells creating a reaction. The result of such signaling is a response by cells that acts to regulate matrix metabolism. In the case of the meniscus, that response may be to increase or decrease the production of collagen, proteoglycans, or other matrix molecules [22, 32,33,34,39].

The biochemical factors produced by the mechanical stimulation of the meniscus are not fully understood, nor are the interactions of signaling molecules. Some of the biochemical factors that have been studied in the meniscus and articular cartilage are interleukin-1 (IL-1), tumor necrosis factor α (TNFα), Prostaglandin E_2 (PGE_2), and nitric oxide (NO)[7, 36-40]. These factors play a role in matrix metabolism and have been implicated in the onset of osteoarthritis [36, 41]. IL-1 and TNFα are proinflammatory cytokines that may induce production of the mediators NO and PGE_2. These cytokine have also been associated with up-regulation of genes responsible for possible matrix degradation and inflammation of cartilage such as inducible nitric oxide synthase (NOS2) and cyclooxygenase 2 (COX-2). Genes such as NOS2 and COX-2 are most likely responsible for production of NO and PGE_2, respectively. In the meniscus, IL-1β significantly increases production of NO [36, 41] and PGE_2 [36]. IL-17 and TNFα also increases NO production in the meniscus, although to a lesser extent. These cytokines also produce increased levels of COX-2 and NOS2 with IL-1 and IL-17 producing the greatest amount of NOS2 [36]. The highest levels of COX-2 are produced when meniscal tissue is incubated with IL-1 and the NOS2 inhibitor 1400W [36]. Taken together, these studies show the effect cytokines and gene expression have on production of matrix metabolism regulating factors such as PGE_2 and NO.

Although the signaling pathways in the meniscus are not fully understood, compression is believe to play a role in maintaining tissue metabolism through mechanontransduction. Unloading has been shown to decrease aggrecan [27] and collagen [42] in the meniscus. While conversely, dynamic compression has been shown to increase proteoglycan release rates from meniscal explants as well as increased NO and PGE_2 production[40]. The amount of proteoglycan release seems to be dependent on NO production. Also, the amount of NO produced seems to be dependent on the presence of IL-1 as well as compression. Although complex, understanding these mechanotransduction pathways is important because signaling molecules such as NO may play an important role in meniscal health and the onset of osteoarthritis [22, 32-34, 39, 46].

1.7 Nitric Oxide

Nitric Oxide (NO) is a gaseous free radical that acts as an intercellular and intracellular messenger in several different tissues [39]. It is a free radical that is synthesized from the conversion of L-arginine to L-citrulline and NO by a family of enzymes called nitric oxide sythases (NOS). There are three isoforms in this family of enzymes, NOS1, NOS2, and NOS3. NOS1 and NOS3 are calcium dependent while NOS2 is expressed after exposure to diverse stimuli such as inflammatory cytokines. NOS2, or iNOS, is the inducible form of nitric oxide synthase that is responsible for producing NO in tissues such as the meniscus and articular cartilage [36, 37, 39, 43, 44] . Nitric oxide is an important molecular messenger in mechanical signal transduction and has a very short half-life of less than 10 seconds, at which point it breaks down into stable

nitrite and nitrate [7, 45]. As a short acting signaling molecule, NO requires a fast acting signaling pathway in order to produce cellular response. Furthermore, NO should only act on nearby cells and proteins. How this molecule is produced, and its interaction with cytokines, cells, and tissue are important in determining the affect it has on articular cartilage and the meniscus.

NO has been found in high levels in the synovial fluid of patients with osteoarthritis and rheumatoid arthritis [39, 46]. Osteoarthritic cartilage has been shown to produce NO spontaneously. Healthy articular cartilage and meniscus have been studied to determine what loading and biochemical conditions produce an up-regulation in nitric oxide production by cells [7, 37, 38, 40, 43, 45, 47-49]. These studies in general have shown that both chondrocytes and fibrochondrocytes spontaneously produce NO. Also, dynamic compressive strain appears to increase NO production in both articular cartilage and meniscal explants. It is still unknown what levels of physiological load and strain produce harmful amounts. Stimulation with IL-1β and lipopolysaccarides (LPS), an endotoxin that activates iNOS, also increases NO in the meniscus suggesting high levels in osteoarthritic knees may be due to other factors in addition to mechanical stimulation.

In the meniscus, cytokines appear to play a major role in the up-regulation of nitric oxide. Inflammatory mediators IL-1β, IL-17, and TNFα have all shown to increase NO production in meniscal explants [36, 37, 40, 41]. On the other hand, hyaluronan (HA) has been shown to suppress NO production in the meniscus [45]. HA is glycosaminoglycan, which is often injected into the knee to slow osteoarthritic progression. HA is known to inhibit the release of glycosaminoglycans in articular

cartilage, delay degradation, and reduce inflammation. N^G-monomethyl-L-arginine (L-NMA), a commonly used inhibitor of nitric oxide sythase, was also found to strongly inhibit NO production in meniscal cell cultures [37]. Studies by Cao et. al. (1998) showed that meniscal explants did not produce nitric oxide in response to cytokine stimulation if only fibroblastic cells were present. However, enzymatic digestion of fresh meniscal fragments containing both fibroblastic and chondrocytic cells produced large quantities of NO in response to cytokine stimulation. This suggests that perhaps chondrocytes are a large source of nitric oxide in the meniscus. Since both articular caritlage and meniscus contain chondrocytic cells, NO studies performed on articular cartilage can be useful in understanding NO production in the meniscus.

Nitric oxide may decrease the synthesis of extracellular matrix, increase degradation of the matrix, and lead to cell apoptosis. Cao et. al. (1998) found that in the meniscus, NO inhibits collagen and proteoglycan [48] synthesis, yet protects proteoglycans from the catabolic effects of IL-1 [40]. Nitric oxide is also believed to cause extracellular matrix degradation due to its high concentrations in osteoarthritic joints. NO acts to break down collagen and proteoglycans through metalloproteases [39]. Matrix degradation may also be a result of fibrochondrocyte apoptosis. Hashimoto et. al. (1999) reported a high occurrence of apoptotic cell death associated with high levels of NO in the osteoarthritic knee. This suggest that NO may play a part in apoptosis which would result in the calcification and loss of the cells pericellular matrix [41].

Nitric oxide is suspected in playing a major role in the matrix metabolism of both the menisci and articular cartilage. The high concentration of NO in the osteoarthritic knee implys that it plays a role in tissue inflammation and matrix degradation. Whether

this cellular messenger is up-regulated primarily by other cytokines or mechanical stress is yet to be determined. The amount of NO present in the meniscus during healthy loading is also unknown. In order to better understand how nitric oxide mediates matrix metabolism in the meniscus, NO production should be measured during normal physiological loading and strain conditions, as well as pathophysiological conditions.

1.8 Hypotheses and Specific Aims

Osteoarthritis is a condition characterized by the degradation of articular cartilage and is positively associated with the presence of knee meniscectomy. The pathogenesis of osteoarthritis is not well understood, however it is well accepted that the removal of meniscal tissue associated with the mensicetomy procedure serves to increases the forces experienced by the remaining meniscal tissue. This increase in meniscal loading produced by the menisectomy has been postulated to underlie the etiology of this disorder. Elevations in nitric oxide production have been positively correlated to joint inflammation, matrix degradation and osteoarthritis progression [37, 39-41, 44, 46, 48, 50]. Evidence exists suggesting that mechanical compression up-regulates NO production in meniscal explants [7, 40], however neither the relationship between physiological loading conditions and meniscal nitric oxide production nor the identity of nitric oxide producing cells, if present, has been established. The objective therefore, of this study is to determine how loading influences meniscal nitric oxide production. The working hypothesis for this study is that increased mensical loading will be associated with an augmented nitric oxide production. To test this hypothesis and accomplish the objective of this study we will pursue the following two specific aims:

I. To establish the relationship between meniscal strain and meniscal nitric oxide production. Explants (n=6) will undergo unconfined compression to 0%, 5%, 10%, 15%, and 20% strain at a frequency of 1 Hz. for 2 hrs. Meniscal load will be calculated and correlated to meniscal nitric oxide production.

Hypothesis 1:

The meniscus produces low levels of nitric oxide without additional stimulation from cytokines or compression. This suggests that low levels of nitric oxide are present in the meniscus without unhealthy effects. We hypothesize that both overloading and underloading the meniscus results in increased NO production compared to the physiological levels of loading.

II. To determine the identity of nitric oxide producing cells. Following mechanical compression, explants will be cut into superficial and deep zones with each zone representing a different cell phenotype. Nitric oxide production from each zone quantified to establish the relationship between cell phenotype and NO production.

Hypothesis 2:

The meniscus contains fibroblastic cells that are prominent in the superior zone and chondrocytic cells that reside in the deep zone. Since chondrocytes have been shown to produce high levels of NO in articular cartilage following compression, we hypothesize that cells from the deep zones will produce more NO in response to mechanical stimulation compared to superficial zones.

REFERENCES

1. Aagaard, H. and R. Verdonk, *Function of the normal meniscus and consequences of meniscal resection.* Scand J Med Sci Sports, 1999. **9**(3): p. 134-40.
2. Fithian, D.C., et al., *Human meniscus tensile properties:Regional variation and biochemical correlation.* Trans. ORS, 1989. **35**: p. 205.
3. Krause, W.R., et al., *Mechanical changes in the knee after meniscectomy.* J Bone Joint Surg [Am], 1976. **58**(5): p. 599-604.
4. McBride, I.D. and J.G. Reid, *Biomechanical considerations of the menisci of the knee.* Can J Sport Sci, 1988. **13**(4): p. 175-87.
5. Roughley, P.J., et al., *The presence of a cartilage-like proteoglycan in the adult human meniscus.* Biochem J, 1981. **197**(1): p. 77-83.
6. Tanaka, T., K. Fujii, and Y. Kumagae, *Comparison of biochemical characteristics of cultured fibrochondrocytes isolated from the inner and outer regions of human meniscus.* Knee Surg Sports Traumatol Arthrosc, 1999. **7**(2): p. 75-80.
7. Fink, C., et al., *The effect of dynamic mechanical compression on nitric oxide production in the meniscus.* Osteoarthritis and Cartilage, 2001: p. 1-8.
8. Voloshin, A.S. and J. Wosk, *Shock absorption of meniscectomized and painful knees: a comparative in vivo study.* J Biomed Eng, 1983. **5**(2): p. 157-61.
9. Shrive, N.G., O.C. JJ, and J.W. Goodfellow, *Load-bearing in the knee joint.* Clinical Orthopedics, 1978. **131**: p. 279-87.
10. Kenny, C., *Radial displacement of the medial meniscus and Fairbank's signs.* Clin Orthop, 1997(339): p. 163-73.
11. Ahmed, A.M. and D.L. Burke, *In-vitro measurement of static pressure distribution in synovial joints--Part I: Tibial surface of the knee.* Journal of Biomechanical Engineering, 1983. **105**(3): p. 216-225.
12. Collier, S. and P. Ghosh, *Effects of transforming growth factor beta on proteoglycan synthesis by cell and explant cultures derived from the knee joint meniscus.* Osteoarthritis Cartilage, 1995. **3**(2): p. 127-38.
13. Bylski-Austrow, D.I., et al., *Displacements of the menisci under joint load: An in vitro study in human knees.* Journal of Biomechanics, 1994. **27**(4): p. 421-431.
14. Leslie, B.W., et al., *Anisotropic response of the human knee joint meniscus to unconfined compression.* Proc Inst Mech Eng [H], 2000. **214**(6): p. 631-5.
15. Grana, W.A., S. Connor, and S. Hollingsworth, *Partial arthroscopic meniscectomy: a preliminary report.* Clin Orthop Relat Res, 1982(164): p. 78-83.
16. Maquet, P.G., A.J. Van de Berg, and J.C. Simonet, *Femorotibial weight-bearing areas. Experimental determination.* J Bone Joint Surg Am, 1975. **57**(6): p. 766-71.
17. Kurosawa, H., T. Fukubayashi, and H. Nakajima, *Load-bearing mode of the knee joint; physical behavior of the knee with or without menisci.* Clinical Orthopaedics and Related Research, 1980. **149**: p. 283-290.
18. Walker, P.S. and M.J. Erkman, *The role of the menisci in force transmission across the knee.* Clinical Orthopedics, 1975. **109**: p. 184-92.
19. Seedhom, B.B. and D.J. Hargreaves, *Transmission of the load in the knee joint with special reference to the role of the menisci.* Engineering in Medicine, 1979. **8**: p. 220-228.

20. Welsh, R.P., *Knee joint structure and function.* Clin Orthop Relat Res, 1980(147): p. 7-14.
21. Tissakht, M. and A.M. Ahmed, *Tensile stress-strain characteristics of the human meniscal material.* Journal of Biomechanics, 1995. **28**(4): p. 411-422.
22. Fithian, D.C., et al., *Exponential law representation of tensile properties of human menisci.* IMechE, 1989: p. 85-90.
23. Proctor, C.S., Schmidt, M.B., Whipple, R.R., Kelly, M.A., Mow, V.C., *Material Properties of the normal medial bovine meniscus.* Journal of Orthopaedic Research, 1989. **7**(6): p. 771-782.
24. Gershuni, D.H., A.R. Hargens, and L.A. Danzig, *Regional nutrition and cellularity of the meniscus. Implications for tear and repair.* Sports Med, 1988. **5**(5): p. 322-7.
25. Upton, M.L., et al., *Differential effects of static and dynamic compression on meniscal cell gene expression.* J Orthop Res, 2003. **21**(6): p. 963-9.
26. Ahluwalia, S., et al., *Distribution of smooth muscle actin-containing cells in the human meniscus.* J Orthop Res, 2001. **19**(4): p. 659-64.
27. Djurasovic, M., et al., *Knee joint immobilization decreases aggrecan gene expression in the meniscus.* Am J Sports Med, 1998. **26**(3): p. 460-6.
28. Roughley, P.J. and R.J. White, *The dermatan sulfate proteoglycans of the adult human meniscus.* J Orthop Res, 1992. **10**(5): p. 631-7.
29. Peters, T.J. and I.S. Smillie, *Studies on the chemical composition of the menisci of the knee joint with special reference to the horizontal cleavage lesion.* Clin Orthop, 1972. **86**: p. 245-52.
30. Ghadially, F.N., J.M. Lalonde, and J.H. Wedge, *Ultrastructure of normal and torn menisci of the human knee joint.* J Anat, 1983. **136 (Pt 4)**: p. 773-91.
31. Alberts, B., et al., *Molecular Biology of the Cell*. Third ed, ed. M. Robertson. 1994: Garland Publishing, Inc. 1291.
32. Bird, M.D. and M.B. Sweet, *Canals in the semilunar meniscus: brief report.* J Bone Joint Surg Br, 1988. **70**(5): p. 839.
33. Duncan, R.L. and C.H. Turner, *Mechanotransduction and the functional response of bone to mechanical strain.* Calcif Tissue Int, 1995. **57**(5): p. 344-58.
34. Martinac, B., *Mechanosensitive ion channels: molecules of mechanotransduction.* J Cell Sci, 2004. **117**(Pt 12): p. 2449-60.
35. Grodzinsky, A.J., et al., *Cartilage tissue remodeling in response to mechanical forces.* Annu Rev Biomed Eng, 2000. **2**: p. 691-713.
36. LeGrand, A., et al., *Interleukin-1, tumor necrosis factor alpha, and interleukin-17 synergistically up-regulate nitric oxide and prostaglandin E2 production in explants of human osteoarthritic knee menisci.* Arthritis Rheum, 2001. **44**(9): p. 2078-83.
37. Cao, M., et al., *Generation of nitric oxide by lapine meniscal cells and its effect on matrix metabolism: stimulation of collagen production by arginine.* J Orthop Res, 1998. **16**(1): p. 104-11.
38. Maneiro, E., et al., *Aceclofenac increases the synthesis of interleukin 1 receptor antagonist and decreases the production of nitric oxide in human articular chondrocytes.* J Rheumatol, 2001. **28**(12): p. 2692-9.

39. Murrell, G.A., et al., *Nitric oxide: an important articular free radical.* J Bone Joint Surg Am, 1996. **78**(2): p. 265-74.
40. Shin, S.J., et al., *Regulation of matrix turnover in meniscal explants: role of mechanical stress, interleukin-1, and nitric oxide.* J Appl Physiol, 2003. **95**(1): p. 308-13.
41. Hashimoto, S., et al., *Nitric oxide production and apoptosis in cells of the meniscus during experimental osteoarthritis.* Arthritis Rheum, 1999. **42**(10): p. 2123-31.
42. Dowdy, P.A., et al., *The effect of cast immobilization on meniscal healing. An experimental study in the dog.* Am J Sports Med, 1995. **23**(6): p. 721-8.
43. Hayashi, T., et al., *Nitric oxide production by superficial and deep articular chondrocytes.* Arthritis Rheum, 1997. **40**(2): p. 261-9.
44. Kobayashi, K., et al., *Chondrocyte apoptosis and regional differential expression of nitric oxide in the medial meniscus following partial meniscectomy.* Journal of Orthopaedic Research, 2001. **19**: p. 802-808.
45. Takahashi, K., et al., *Hyaluronan suppressed nitric oxide production in the meniscus and synovium of rabbit osteoarthritis model.* J Orthop Res, 2001. **19**(3): p. 500-3.
46. Farrell, A.J., et al., *Increased concentrations of nitrite in synovial fluid and serum samples suggest increased nitric oxide synthesis in rheumatic diseases.* Ann Rheum Dis, 1992. **51**(11): p. 1219-22.
47. Sah, R.L., et al., *Biosynthetic response of cartilage explants to dynamic compression.* Journal of Orthopaedic Research, 1989. **7**: p. 619-636.
48. Taskiran, D., et al., *Nitric oxide mediates suppression of cartilage proteoglycan synthesis by interleukin-1.* Biochem Biophys Res Commun, 1994. **200**(1): p. 142-8.
49. Wiseman, M., et al., *Dynamic compressive strain inhibits nitric oxide synthesis by equine chondrocytes isolated from different areas of the cartilage surface.* Equine Vet J, 2003. **35**(5): p. 451-6.
50. Stefanovic-Racic, M., et al., *Nitric oxide and proteoglycan turnover in rabbit articular cartilage.* J Orthop Res, 1997. **15**(3): p. 442-9.

CHAPTER TWO

VALIDATION OF BIOREACTOR

A Tissue Engineering Bioreactor for Dynamically Compressing Meniscal Explants with Load or Displacement Control Capabilities

Jeffrey A. McHenry and Tammy L. Haut Donahue

2.1 Abstract

Motivated by our interest in examining meniscal mechanotransduction processes, we report on the validation of a new tissue engineering bioreactor. This paper describes the design and performance capabilities of a tissue engineering bioreactor for cyclic compression of meniscal explants. We showed that the system maintains a cell culture environment equivalent to that provided by conventional incubators and that its strain output was uniform and reproducible. The system incorporates a linear actuator and load cell aligned together in a frame that is contained within an incubator. The actuator has bi-directional repeatability of +/-.00762 mm and a uni-directional repeatability of +/-.00254 mm. The actuator can thrust to 2225 N with speed up to 50 cm/sec. The load cell has a 8895 N capacity with a sensitivity of 2.225 N. Explants (~5mm in height; 6 mm in diameter) are contained in a six well aluminum dish that is attached to the load cell. A plunger with six Teflon-filled Delrin compression rods is attached to the actuator, which is rigidly suspended above the load cell. System performance analysis showed that the

greatest difference in displacement between the wells was 0.0889 mm. Out of five tests, the maximum difference between each well ranged from 0.0813mm to 0.0889 mm with the same wells producing the greatest difference each time. Since this error is consistent, adjustments can be made to normalize meniscal explant test results. We conclude that this device will be useful in determining the biochemical response of tissue culture explants to dynamic compression.

2.2 Introduction

Mechanical loading of the meniscus plays a crucial role in the metabolic activity of fibrochondrocytes [1-5]. It is not fully understood how biomechanical and biochemical events interact to produce changes in the extracellular matrix. Recreating the physiological forces *in vitro* using tissue explants while measuring the biological response provides one method for observing the effect of mechanical stress on the meniscus [4, 6], however the majority of commercially available bioreactors may not be suitable for application to meniscal loading studies. Tissue explant culture studies allow control of loading and biochemical conditions. For these studies to be an accurate *in vivo* representation, the conditions within the body must be reproduced within the testing system.

A meniscal explant compression bioreactor must meet the following criteria to ensure successful experimentation. Explants must remain sterile throughout the entire procedure, thus all testing equipment and tools must be able to be sterilized by autoclave or alcohol before coming in contact with the tissue. Culture media and incubation (5% CO_2, 37°C) used with fresh tissue is necessary for the biological response to resemble the

in vivo response. To best create an *in vivo* response, mechanically loading explants requires the tissue to experience pressures that the meniscus would experience in the knee. Pressures up to 10 MPa and strains ranging from 2% to 20% are seen in the meniscus *in vivo* [7-9]. The anterior, central, and posterior regions experience different strain levels, making it necessary to test explants from all three regions. Testing 6 explants at once makes it possible to test how tissue from each region responds to the same level of loading or strain. If order to create repeatable results, and to show significance in data, all six explants must experience the same compression. Explants should receive the same strain within 5% error of each other throughout each test. For a 5mm explant, the displacement range has to be at least 0.1mm ± 2.5μm to 1.0 mm ± 2.5μm to achieve accurate displacement for strain levels ranging from 2% strain to 20%, respectively. Strains are relatively low in the normal healthy meniscus, but these strain levels increase with a partial menisectomy [9]. We hypothesized that higher strains would lead to degeneration of the meniscus by increased levels of nitric oxide.

Current systems for meniscal explant compression apply pressure near or below 1 MPa. The Biopress system (Flexcell International, Hillsborough, NC) uses air pressure applied to a flexible bottom under each well. It has been used to apply pressures of 0.1 MPa in previous studies done on meniscal explants [1, 3, 4], noting stain levels of approximately 10% due to the state of unconfined compression. Another biaxial tissue-loading device, previously used to compress articular cartilage explants, is able to create a maximum 400 N axial force on as many as 12 explants at once [10]. This device also has the ability to create rotational motion with a resolution of .0005°, and can only apply a sine wave with amplitudes as low as 10 μm and as large as 100 μm. Thus, this system

is not feasible for larger scale testing on 5mm meniscal explants which require displacements of 0.5mm for 10% strain.

The goal of this study was to design a tissue engineering bioreactor that cyclically compresses meniscal explants to physiological stresses and strains. The system had to meet the following criteria: 1) apply and measure compressive load up to 350 N per explants 2) create a cyclic compression test using load or displacement control accurate to within 1% and 3) maintain explants in a physiological environment. The subsequent sections describe the design of the system, accuracy evaluation, and application of the system to explant testing.

2.3 Materials and Methods

2.3.1 Design of Bioreactor

To create physiological loads, the system was based on a belt-driven linear actuator made by Ultramotion and Animatics. The Smartmotor 1720 (Ultramotion, Mattituck, NY) is an actuator that is part of the Bug series of actuators by Ultramotion, and utilizes a control package by Animatics. The actuator has a maximum stroke length of 5 cm and can thrust to 2225 N. It also has a maximum speed of 50 cm/sec with bi-directional repeatability of +/-.00762 mm and a unidirectional repeatability of +/-.00254 mm. Motor control was achieved by using the SmartMotor Interface (SMI), programs written with SMI programming language. This allows the motion of the actuator to be controlled by the signal generated by the load cell or by the displacement of the actuator. Displacement resolution for the actuator is .4 μm because a 2500 count on the encoder is equal to 1 mm.

Two dimensionally identical strain gage load cells (Interface, Scottsdale, AZ) with two different load capacities were used. This allows for a more flexible range of testing, combining higher accuracy at low range testing and greater capacity for high load applications. The first had a 1334 N capacity and the second has an 8896 N capacity. Tests that require loads near or above 1334 N will use the higher capacity load cell to reduce defection and therefore error. Tests run with the lower capacity load cell will have the advantage of a sensitivity of ~1.30 N and a more accurate signal. The sensitivity of the higher capacity load cell is ~2.17 N. A 2100 series signal conditioner (Vishay Intruments, Raleigh, NC) was used to amplify the load cell signal to produce a 5-volt signal (maximum allowable input voltage to the SmartMotor Interface) at the maximum load. The choice of load cell is critical because the movement of the actuator during testing needs to represent the displacement of the meniscal explant. Excess deflection of the load cell will lead to inaccurate displacement reading through the motor.

The load cell is centered on a 2.54 cm thick aluminum plate that is the base of the system frame (Fig. 2.1). A stud with a shoulder turned onto it is threaded into the load cell. This stud connects to the aluminum dish via a quick disconnect pin. The dish has six 10 mm deep wells equally spaced in a circular orientation. Teflon-filled Delrin compression rods (diameter= 8mm) for each well are press fit into a plunger which attaches to the actuator via a quick disconnect pin. The plunger also features two press-fit aluminum pins that slide into matching holes in the dish. This keeps the compression rods centered in each well and only allows for one plunger/dish orientation. To enclose the plunger and dish, an aluminum cap rests on the shoulder of the dish and houses a linear bearing that is press fit into the cap. Along the resting edge of the cap, four

shallow grooves were machined to allow carbon dioxide supply to the explants during testing. The linear bearing allows the plunger to move up and down within the cap and restricts the plunger to vertical motion.

The frame is the most critical component to maintaining equal well pressure in all 6 wells. An even well pressure will ensure all six explants experience the same mechanical stimulation. The frame is rigid to maintain alignment during handling or assembly. The frame is built out of two one-inch thick parallel aluminum plates separated by one-inch diameter aluminum support rods (Figure 2.2). Centered on the bottom plate is the load cell with the six well dish attached. The cylinder of the actuator is recessed into the top plate, and a collar holds the actuator tight and perpendicular to the plate.

2.3.2 Accuracy Evaluation of the System

Frame alignment and machining of the parts determined how accurately the system produced even pressure on all six wells. The length of each compression rod was measured using a micrometer with 2.54 μm resolution. Measurements of all of the wells were taken to ensure that they were all the same depth using a dial indicator with a resolution of 25.4 μm. The top surface of the dish was also measured using a dial indicator to prove that the top surface would be perpendicular to the axis of the load cell and actuator. Once these measurements were taken to prove the geometry was correct, ultra-low pressure film (Sensor Products Inc., East Hanover, NJ) was used to measure well pressure during compression.

Pressure film analysis was done using Scion Image (National Institute of Standards and Technology, Gaithersburg, MD) to measure the density of the pressure

film samples. When using the pressure film, repeatability tests were performed to determine the precision of the pressure film. The repeatability of the film was determined by loading the film in a materials testing machine (Instron Corp., Canton, MA) to 70 ± .2 N target load. This was repeated seven times. The film was placed on top of a 13.66 mm diameter by 3 mm thick piece of rubber, which was resting on the lower platen. The upper platen (2 cm square) was lowered to the surface of the film and compressed to the target load of 70 N corresponding to a pressure of 0.477 MPa. Once the target load was reached, the upper platen was immediately raised from the surface of the pressure film. Calibration of the pressure film was also done using the Instron and included loading pieces of pressure film ranging from 0.2 MPa to 1.64 MPa. All film samples were scanned and analyzed using Scion Image with the density scale for this program set at a range of 0-255 with 255 being completely saturated. Film was compressed between the platens and a piece of rubber similar to the rubber used for testing well pressure.

To determine well pressure in the bioreactor, a machined plate was set on top of the dish with a 3 mm thick piece of uniform rubber. Pressure film was placed on top of the rubber and the plunger was lowered near the surface of the film. Two different load settings of 24 N and 28 N on an area of 50.27 mm^2 corresponding to pressures of approximately 0.477 MPa and 0.564 MPa were tested with five tests per load. The 24 N and 28 N loads were the loads on each compression rod and each rod had a radius of 4 mm. These loads covered the upper end of the spectrum for the pressure film. The film from the bioreactor was analyzed and density measured to determine the difference

between each compression rod. The difference in film density and the maximum percentage error was determined to demonstrate the accuracy of the system.

2.3.3 Determination of Displacement Accuracy

A second technique for determining the accuracy of the system involved measuring the gap between the bottom of the compression rods and the bottom of the wells while the system was assembled into the bioreactor. This was done using auto body filler and a cream hardener that when mixed together, harden to form a rigid body. The actuator was used to compress the body filler until the gap between the bottom of the compression rod and well bottom was filled. The actuator remained at this position until the body filler hardened completely. The plunger was then removed along with the pieces of body filler. A micrometer (2.54 μm resolution) was then used to measure the thickness of the body filler. This process was repeated 5 times with the same plunger and dish orientation.

2.4 Results

2.4.1 Accuracy Evaluation of the System

The greatest difference in length between any of the compression rods was .0381 mm. All of the well depths were within 0.0254 mm of each other when measured with a dial indicator. The well depths were measured from the top surface of the aluminum dish, which was flat to within 0.0254 mm.

The densities produced for all the pressure film were compared to the calibration of the pressure film to determine the pressure. The results of the repeatability test showed there was an average of 0.4773 MPa with a standard deviation of 0.0003 MPa (Table 2.1). The pressure film from both the 0.477 MPa and 0.564 MPa tests appear to show equal pressure in each well for each load (Figures 2.3 and 2.4). There was 0.0912 to 0.1986 and 4.83 to 15.24 percent error for 0.477 MPa and 0.564 MPa respectively (Table 2.2). At higher loads there was an average difference in pressure of approximately 8.2% percent but at lower loads this error showed an average difference in pressure of approximately 0.18%. Due to the variability of the pressure film at higher pressures, these results alone were inconclusive in determining the accuracy of the system.

2.4.2 Determination of Displacement Accuracy

The micrometer measurements from the first samples of body filler showed that the greatest difference between any of the wells was .0813 mm with well 5 having the smallest gap. The second and fifth tests gave the same results as the first test. Test three showed .0864mm and test four showed .0889mm with both showing well 5 to have the smallest gap. All five tests were run with the same plunger/dish orientation and all tests showed compression rod 5 to produce a smaller gap. The percent error can be calculated from the amount of displacement that will be run during each test. If a test is run with a maximum displacement of 0.5 mm then there is approximately 16.76% difference in compression on average. For a 0.5 mm target compression, all the explants would be compressed between 0.4581 mm and 0.5419mm. A 1 mm displacement test would only see an 8.38% difference in compression on average. For a target of 1mm compression,

all explants would be compressed between 0.9581mm and 1.0419 mm. With this data, the results from testing of explants can be normalized for the difference in wells.

The results from the above gap testing can be seen in Table 2.3. For each test, the micrometer measurement is displayed for each well, along with the maximum difference, and average. Tests 3, 4, and 5 have higher values because the target displacement of the actuator was changed. This was done to show that the difference in the wells would stay the same regardless of the target displacement. The average maximum gap difference value is displayed below Table 2.3.

2.5 Discussion

The explant compression system meets the criteria necessary to obtain a realistic representation of physiological forces present in the knee joint. This system is able to apply known pressures to six explants at once, which is important when trying to gather data for hypothesis testing. It is capable of applying physiological levels of load and displacement, and has the ability to test in load or displacement control. SMI programming allows for flexibility in frequency, duration, amplitude, and waveform. The system is small enough to fit in a standard incubator and is made of materials that can endure autoclaving and alcohol. An important feature to this system is the ability to keep the explants and media sterile from the culture hood to the incubator. The plunger, dish, and cap form an enclosure that allow easy transport without allowing open air and bacteria to infect the sample. Since the cap incorporates a linear bearing it does not need to be removed for testing. Bacteria can kill cells and alter the chemical response, leading

to inaccurate data. Utilizing the system features and designing the correct protocol will help maintain a sterile environment.

This bioreactor is capable of creating higher loads and greater displacements than previous systems used for compressing explants[1, 3, 4, 10]. The Biopress system (Flexcell International, Hillsborough, NC) is not capable of pressures higher than 0.1 MPa since the pressure is applied by air into a flexible bottom. Since our system applies load using a linear actuator, loads up to 2225 N can be added. In Frank, et. al., 2000, a biaxial tissue-loading device can load 12 explants in shear and compression [10]. An advantage our system has is that it can create displacements over 10 mm with a resolution of 0.4 μm. The Frank, et. al., 2000 creates displacements up to 100μm. Our actuator also has a bi-directional repeatability of ±7.62μm compared to the ±25μm used in Sah, et al., 2003. In addition, the present system is capable of 1 Hz cyclic compression in a sinusoidal type wave using displacement or load control. The flexibility of the Smartmotor Interface will allow various alterations of test programs. Frequency, amplitude, and number of cycles can be easily changed. The bioreactor can be used to compress any tissue that fit under an 8mm compression rod and in a 10 mm deep well. All surfaces are machined to a smooth, frictionless finish, to ensure the sample is exposed to pure unconfined compression.

A verification test has been performed to prove that the system remains accurate in the incubator environment. A 2 hour, 1 Hz displacement controlled test was run with the incubator at 37˚C. The displacement accuracy did not change at any point during the testing in the incubator. Additional tests were performed to prove that the plunger, dish, and cap assembly could maintain a sterile environment from the culture hood to the

incubator and back. A practice run of the test protocol using only culture medium showed no sign of bacteria after four days of culture. This is evidence that the system can remain sterile through the testing procedure of explants.

The bioreactor has some limitations that need to be compensated for. This system can only perform unconfined compression. As the sample is compressed, the top and bottom surfaces of the sample can expand. To keep explants from slipping to one side of the compression rods, the top and bottom surface of the explant needs to be trimmed to be parallel. The design is ideal for an explant that is approximately 6 mm in diameter. This is because the compression rod is 8 mm in diameter so the smaller explant will stay under the compression rod as long as it is centered. The placement of each sample in the well has to be exact to ensure the sample stays under the compression rod. Once the cap is put on and the test starts running, the samples cannot be viewed to determine if they are being compressed correctly. The only indication of this is the orientation of the explants when the test is completed and when they are removed.

Another limitation is the machining of each component within the system. The most accurate machining procedures used can create a part within 0.0254mm. This is accurate enough for most applications but requires extra compensation for the bioreactor. Since the displacements in this system are so small, the machine error has to be measured and accounted for. The gap measurement using the body filler provides a method for compensation. The results show that well 5 has the smallest gap and should therefore produce different results than the other wells.

Despite, the limitation described above the explant compression system has features that are advantageous to tissue compression experimentation. The system

maintains a sterile environment throughout the assembly and testing procedures. The components in direct contact with the tissue sample are made of material that can be autoclaved or rinsed with alcohol. Six tissue explants are exposed to uniaxial unconfined compression simultaneously. The system can compress these samples using load or displacement control settings. Waveforms can be manually programmed into the linear actuator using the interface software to customize each test. During the test, displacement and load are recorded at 2 Hz. (min. and max. of each cycle), with a resolution of 0.4μm and 1.30 N respectively. This system can be utilized to produce useful test data about tissue response to physiological loading.

ACKNOWLEDGMENT

The authors are grateful to the Whitaker Foundation for their financial support.

Table 2.1 Precision data of ultra low pressure film.

Pressure Film Repeatablity Test (.477 MPa Applied Pressure)

	Test 1	Test 2	Test 3	Test 4	Test 5	Test 6	Test 7	Average	Std. Dev.
Press.	0.4776	0.4769	0.4776	0.4770	0.4775	0.4771	0.4776	0.4773	0.0003

Table 2.2 Results of pressure film verification at two different loads.

.477MPa	**Pressure (MPa)**								
Test #	Rod 1	Rod 2	Rod 3	Rod 4	Rod 5	Rod 6	Average	Std. Dev.	% Error
1	0.4773	0.4768	0.4771	0.4771	0.4768	0.4768	0.4770	0.0002	0.0912
2	0.4768	0.4769	0.4768	0.4768	0.4769	0.4772	0.4769	0.0001	0.0788
3	0.4773	0.4768	0.4769	0.4770	0.4769	0.4771	0.4770	0.0002	0.1108
4	0.4773	0.4768	0.4769	0.4768	0.4769	0.4768	0.4769	0.0002	0.1056
5	0.4778	0.4771	0.4769	0.4771	0.4771	0.4768	0.4771	0.0003	0.1986
.564MPa									
1	0.5732	0.5783	0.5715	0.5715	0.5425	0.5758	0.5688	0.0132	6.6006
2	0.5541	0.5447	0.5194	0.5816	0.5047	0.5508	0.5426	0.0272	15.2409
3	0.5591	0.5857	0.5870	0.5718	0.5715	0.5441	0.5698	0.0163	7.8899
4	0.5756	0.5841	0.5818	0.5626	0.5571	0.5730	0.5724	0.0106	4.8354
5	0.5785	0.5548	0.5803	0.5762	0.5702	0.5457	0.5676	0.0142	6.3441

Table 2.3 Displacement accuracy using gap measurement.

Gap Measurement (mm)

	Well 1	Well 2	Well 3	Well 4	Well 5	Well 6	Max. Diff.	Avg.	Std. Dev.
Test 1	3.0556	3.1013	3.1090	3.1166	3.0353	3.0582	0.0813	3.0793	0.0338
Test 2	3.0353	3.0785	3.0861	3.0734	3.0048	3.0353	0.0813	3.0522	0.0320
Test 3	3.3934	3.4519	3.4468	3.4417	3.3655	3.3858	0.0864	3.4142	0.0370
Test 4	3.4036	3.4493	3.4671	3.4315	3.3782	3.4036	0.0889	3.4222	0.0331
Test 5	3.3985	3.4493	3.4544	3.4519	3.3731	3.4036	0.0813	3.4218	0.0345

Avg. Diff. 0.0838

Table 2.4: Data showing how far each well was from the average for each test. The average variation from average for each well is displayed in the last row. Negative number show the well had a smaller gap than the average for each test, positive values are gaps that are greater than the average.

Gap Variation

	Well 1	Well 2	Well 3	Well 4	Well 5	Well 6
Test 1	-0.0237	0.0220	0.0296	0.0373	-0.0440	-0.0212
Test 2	-0.0169	0.0262	0.0339	0.0212	-0.0474	-0.0169
Test 3	-0.0207	0.0377	0.0326	0.0275	-0.0487	-0.0284
Test 4	-0.0186	0.0271	0.0449	0.0093	-0.0440	-0.0186
Test 5	-0.0233	0.0275	0.0326	0.0301	-0.0487	-0.0182
Avg.	-0.0207	0.0281	0.0347	0.0251	-0.0466	-0.0207

List of Figures

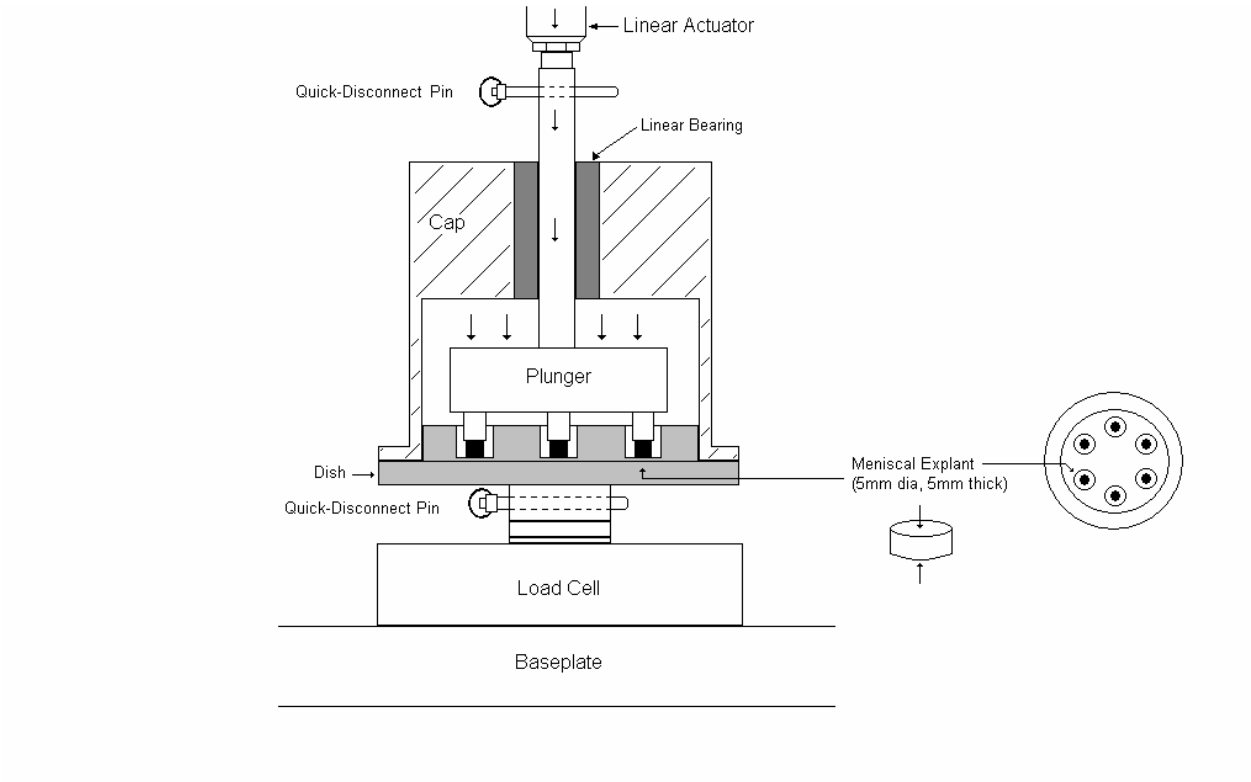

Figure 2.1: Plunger/Dish/Cap assembly: The linear actuator is attached to the plunger using a quick-disconnect pin. The dish is attached to the load cell in the same manner. The cap improves alignment of the plunger by utilizing a linear bearing.

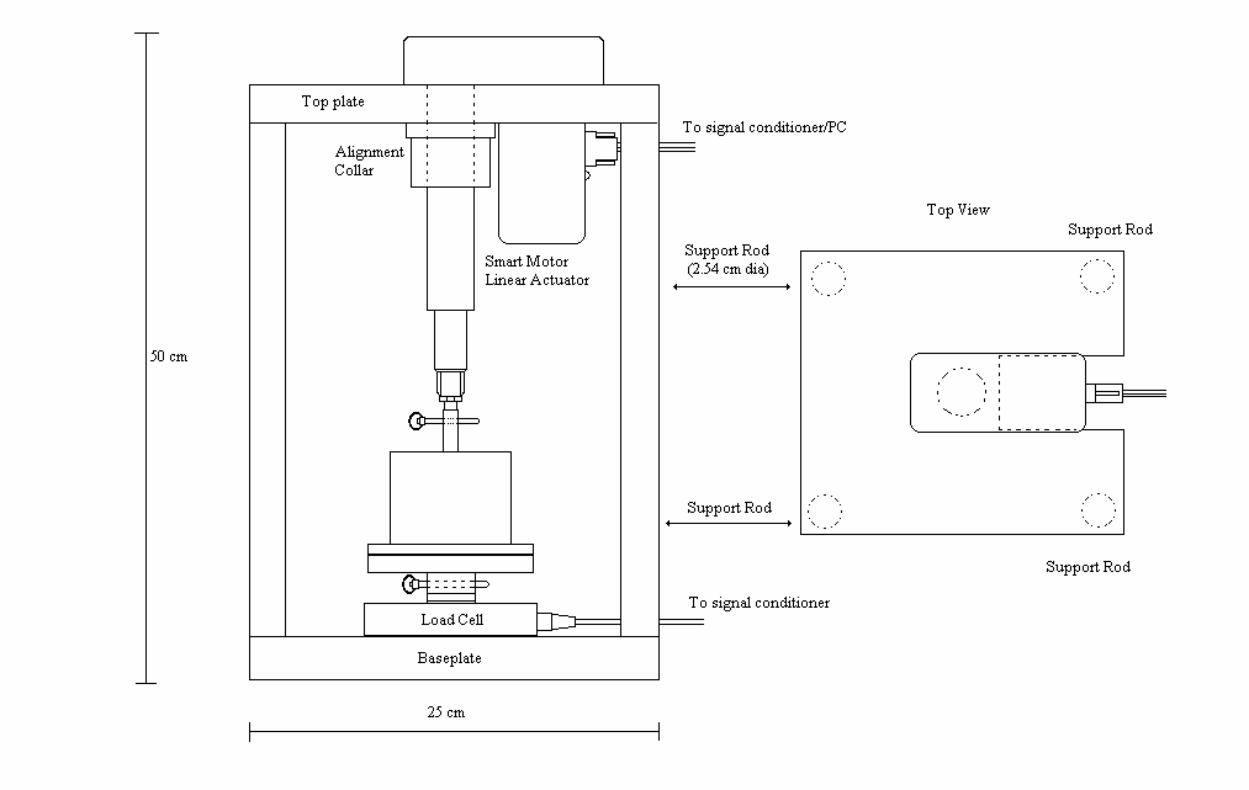

Figure 2.2: Test Frame: The test frame is composed of two aluminum plates supported by aluminum rods. The actuator is positioned in a centered hole in the top plate and tighten into alignment with an adjustable collar.

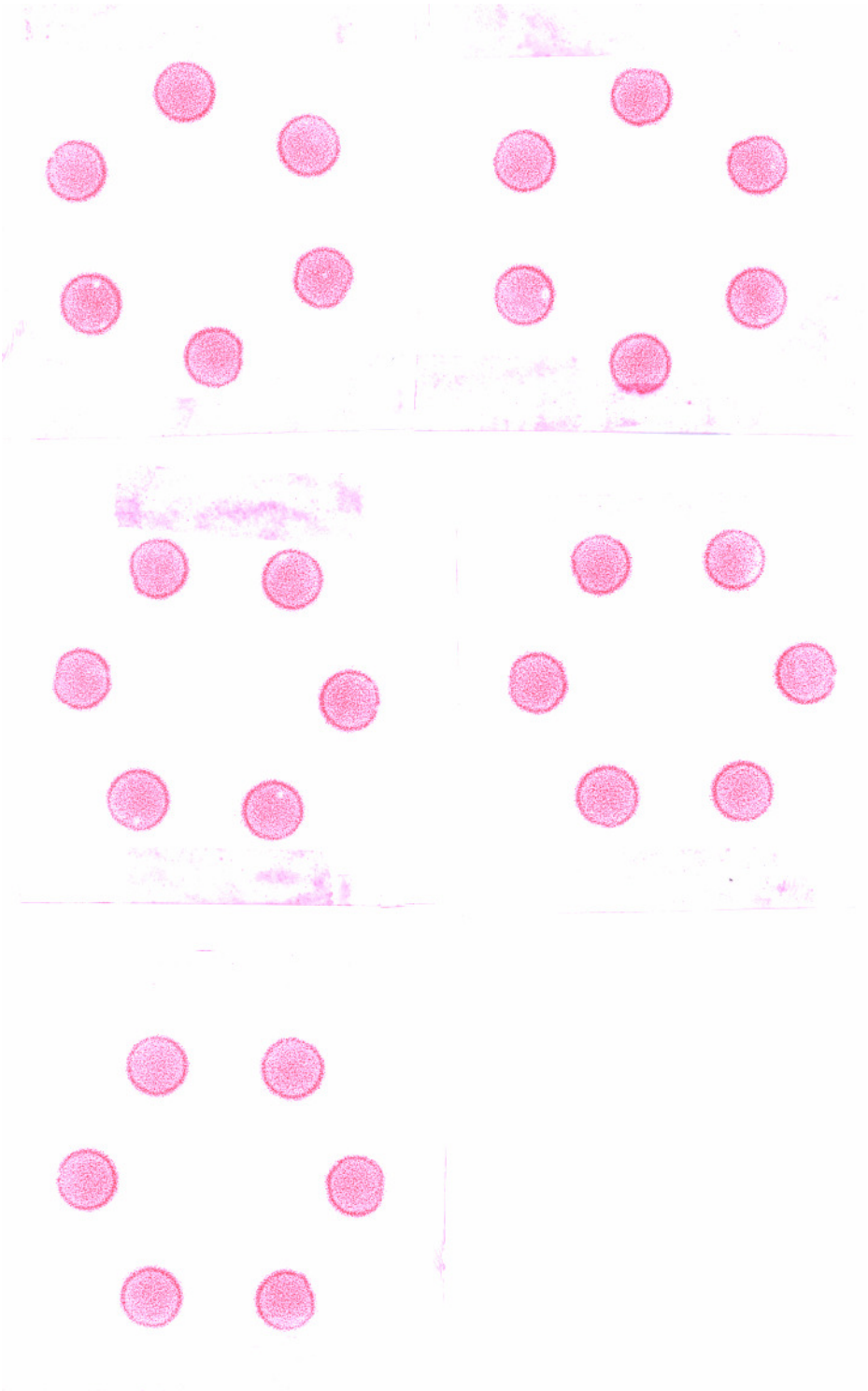

Figure 2.3: Pressure film impressions at 0.477 MPa pressure

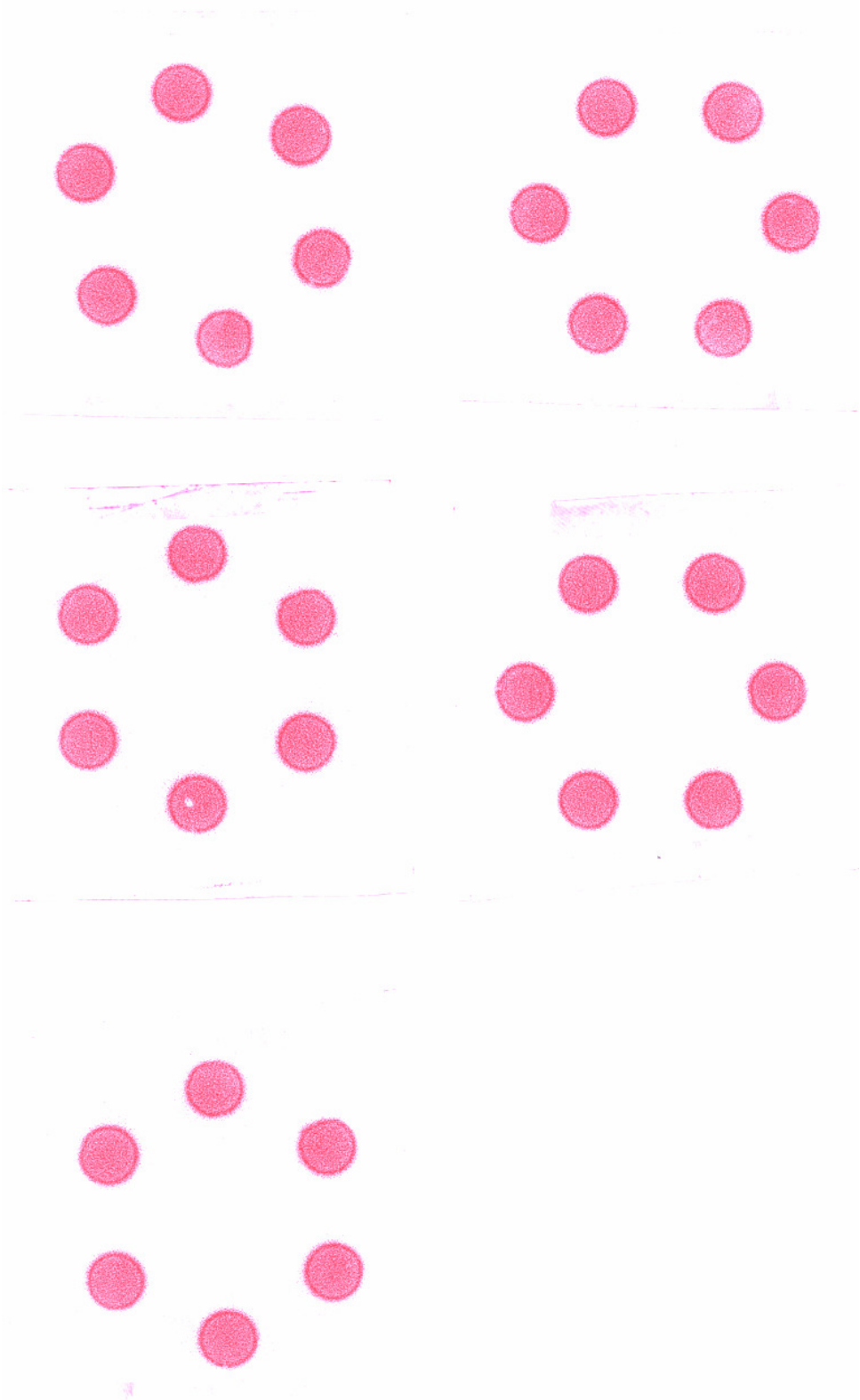

Figure 2.4: Pressure film impressions at 0.564 MPa pressure.

Figure 2.5: Calibration curve for pressure film correlating density of film to applied pressure.

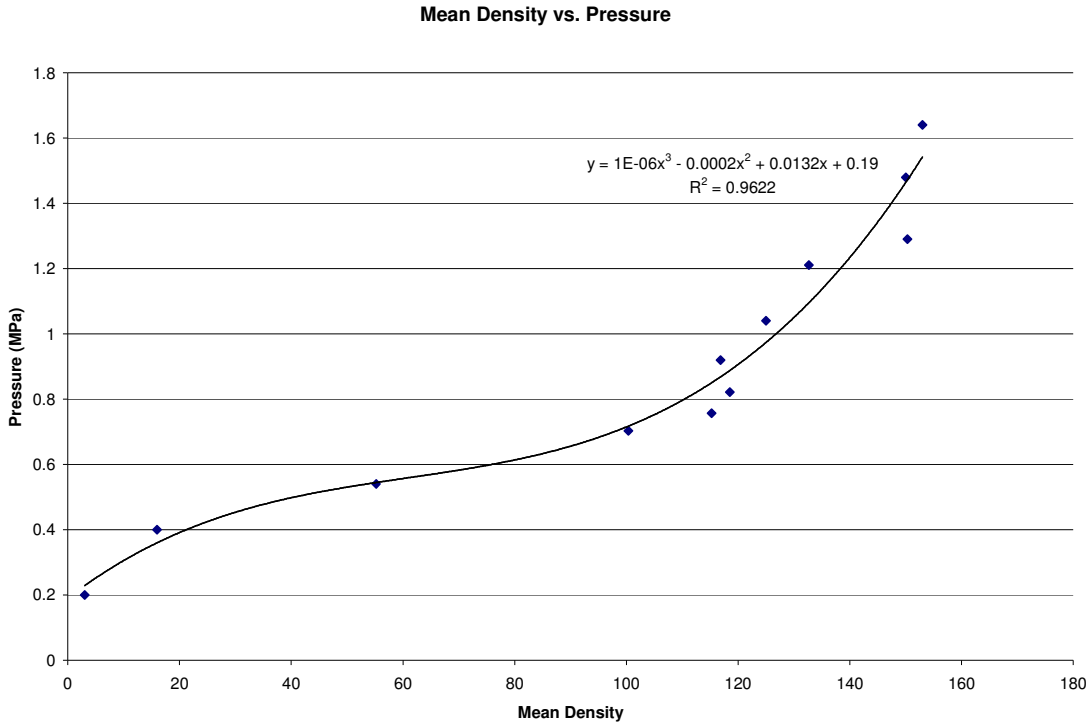

REFERENCES

1. Fink, C., et al., *The effect of dynamic mechanical compression on nitric oxide production in the meniscus.* Osteoarthritis and Cartilage, 2001: p. 1-8.
2. Sah, R.L., et al., *Biosynthetic response of cartilage explants to dynamic compression.* Journal of Orthopaedic Research, 1989. **7**: p. 619-636.
3. Shin, S.J., et al., *Regulation of matrix turnover in meniscal explants: role of mechanical stress, interleukin-1, and nitric oxide.* J Appl Physiol, 2003. **95**(1): p. 308-13.
4. Upton, M.L., et al., *Differential effects of static and dynamic compression on meniscal cell gene expression.* J Orthop Res, 2003. **21**(6): p. 963-9.
5. van Griensven, M., et al., *Cyclic mechanical strain induces NO production in human patellar tendon fibroblasts--a possible role for remodelling and pathological transformation.* Exp Toxicol Pathol, 2003. **54**(4): p. 335-8.
6. Grodzinsky, A.J., et al., *Cartilage tissue remodeling in response to mechanical forces.* Annu Rev Biomed Eng, 2000. **2**: p. 691-713.
7. Spilker, R.L., Donzelli, P.S., *A biphasic finite element model of the meniscus for stress-strain analysis*, in *Knee Meniscus;Basic and Clinical Foundations*, V.C. Mow, Arnoczky, S.P., Jackson, D.W., Editor. 1992, Raven Press: New York.
8. Spilker, R.L., P.S. Donzelli, and V.C. Mow, *A transversely isotropic biphasic finite element model of the meniscus.* Journal of Biomechanics, 1992. **25**(9): p. 1027-45.
9. Zielinska, *3D Finite Element Model of Medial Meniscus Meniscectomy; Changes in Contact Behavior.* Journal of Biomechanical Engineering, 2005.
10. Frank, E.H., et al., *A versatile shear and compression apparatus for mechanical stimulation of tissue culture explants.* J Biomech, 2000. **33**(11): p. 1523-7.

CHAPTER THREE

NITRIC OXIDE PRODUCTION

Nitric Oxide Production by Menical Explants Following Dynamic Compression

Jeffrey A. McHenry and Tammy L. Haut Donahue

3.1 Abstract

This paper describes the dynamic compression of porcine meniscal explants using a custom-built tissue compression bioreactor capable of various displacement and load control testing. The goal was to better understand the relationship of mechanical stress to nitric oxide production in the meniscus during physiological conditions and determine the identity of nitric oxide producing cells. Cyclic compression testing was conducted on 6mm diameter explants, 5mm in height, at a frequency of 1 Hz. for two hours. Compression magnitudes included 5%, 10%, 15%, 20% strain as well as 0.05 MPa and 0.1 MPa tests compared to a 0%strain/0MPa control representing an unloaded state. These magnitudes were chosen to cover the range of stress and strain experienced in the normal meniscus and to investigate how unloading and overload affects nitric oxide production. Result from testing showed 5% and 10% strain produced less nitric oxide than control samples in both the surface and deep zones of the explants. The 15 % strain testing showed comparable results to control while the 20% strain testing produced the greatest amount of nitric oxide in both zones. Statistical analysis showed a significant

quadratic relationship (p=0.000) for both zones and no significant difference between means of surface and deep. Results from load control provided inconclusive data. These findings suggest a complicated relationship between mechanical stress and nitric oxide production. Physiological strain levels and durations may reduce nitric oxide produced by meniscal fibrochondocytes.

3.2 Introduction

The menisci are specialized structures that are vital to normal function of the knee. In addition to distributing load from the femoral condyles to the tibial plateau, the meniscal attachments aid in maintaining knee joint stability and congruency. Meniscal tissue is approximately 75% water. Fibrochondocytes maintain an extra-cellular matrix containing proteoglycans and Type I collagen [1-11]. Mechanical stimuli are believed to contribute to maintaining meniscal matrix metabolism, however it is yet unclear how these signals are propagated [3, 10, 12-17, 19, 21, 22]. A better understanding of the relationship between mechanical loading and biochemical response could aid in understanding the poor healing characteristics of the meniscus and it role in the onset of osteoarthritis (OA).

The meniscus has been shown to be a mechanically sensitive tissue with specific loading conditions resulting in various biosynthetic responses. Unloading the meniscus has been shown to result in a decrease in production of matrix molecules such as aggrecan and collagen [12, 13]. Conversly, extended periods of dynamic compressive stress (0.1 MPa, 0.5 Hz., 24hr) increase gene expression of cyclooxygenase (COX-2), and

inducible nitric oxide synthase (iNOS), causing an increase in mediators prostaglandin E_2 (PGE_2) and nitric oxide (NO), respectively[14-19].

NO is a gaseous free radical that acts as a messenger and is believed to regulate matrix metabolism by inducing the release of proteoglycans from the matrix, decreasing collagen production by fibrochondrocytes, and possibly causing cell apoptosis [16, 18, 20-22]. Since meniscal tissue produces NO spontaneously, baseline levels may be responsible for balancing the remodeling process of fibrochondrocytes.

Previous studies employing 24 hours of cyclic compression at a load resulting in 10% strain have shown that increasing compressive strain in the meniscus leads to an up-regulation of NO [14, 19]. *In vivo*, partial mensicectomy results in elevated strain levels in the meniscus [23, 24], and has been shown to lead to osteoarthritis (OA). Portions of the inner two thirds of the tissue is often removed, leaving the remaining tissue to carry increased load. Strain increases from approximately 10% for an intact meniscus to up to 30% strain for a partial meniscectomy where 60% of the inside tissue is removed. This increased strain may be partially responsible for the high level of NO found in the osteoarthritic knee. Indeed, *in vivo* experimental osteoarthritis models, including partial meniscectomy and ACL transection have been shown to result in increased NO liberation in the meniscus [25, 21]. In addition, Kobayashi et al., 2001, showed that following a partial medial meniscectomy in rabbits, there was a spatial variation in NO production with the tissue adjacent to the location of the meniscectomy producing significantly more NO than the peripheral meniscal tissue [25]. Similar spatial trends were seen with iNOS expression [25].

The source of NO in the meniscus is fibrochondrocytes. However, these cells are represented by two distinct populations separated by layer. The superficial layer is composed of cells that appear and behave more like fibroblasts while the deep zones are composed of cells that are more like chondrocytes. Fink, et al., 2001 showed that following mechanical stimulation, the surface zone of the meniscus produced higher levels of NO when compared to the deep zone. Recently, these same research group added IL-1, a proinflammatory cytokine secreted by cells, to the media during compression and found a synergistic increase in NO compared to compression alone [19]. However, in each of these studies, only one level of pressure was investigated. Interestingly, in contrast to mechanical stimulation data, direct stimulation with a chemical signal (IL-1), in the absence of mechanical loading, demonstrated increase NO production in deep zone cells, compared to little or no production from the surface zone [16].

Currently there is a lack of data relating short periods of physiological strain that may result from walking or exercise to NO production. It is our goal to determine how NO production changes through a range of compressive strain that covers physiological levels seen in the intact meniscus and following meniscectomy for periods of normal activity. Comparing these results to results with 0% strain will determine how activity compares to inactivity in terms of NO production and therefore meniscal health. Another goal is to show how strain relates to load during unconfined compression of meniscal explants. Investigating meniscal compression using load and displacement control will accomplish these goals as well as demonstrate the creep properties of meniscal explants.

These goals will be evaluated for the superior and deep zones to determine how each unique population of fibrochodrocyte responds to compression.

3.3 Methods and Materials

Meniscus Samples

Meniscal samples were obtained from porcine knees typically harvested from 4-month-old female pigs within 24 hours of death. Left and right knees from 12 animals were dissected aseptically to retrieve the medial and lateral menisci. Six explants were removed from each meniscus using a 6 mm diameter biopsy punch (FRAY Products Corp, Buffalo, NY). Samples were cut parallel to the superior surface to maximize the amount of superior tissue saved. The explants were then transferred to a microtome and trimmed to achieve parallel top and bottom surfaces at a height of 5mm. To allow for full recovery of the tissue, samples were then incubated for 48 hours in culture medium (44.5% Dulbecco's modified Eagle's medium, 44.5% Ham's F-12, 10% Fetal Bovine Serium, and 1% penicillin/streptomycin) at 37°C with 5% CO_2 and 95% air. The media was changed after the first 24 hours of this 48-hour incubation.

Meniscal Compression

Explants were compressed for 2 hrs at 1 Hz to simulate physiological conditions equivalent to two hours of walking. Tests were performed in a custom designed bioreactor previously described [27]. Briefly, the system is capable of both load and displacement control and utilizes a linear actuator (Ultramotion, Mattituck, NY) to compress 6 explants simultaneously in unconfined compression. The system is contained within a CO_2 incubator at 37°C. Explants were centered in each well and covered with

400 µl of test medium (48.5% Dulbecco's modified Eagle's medium, 48.5% Ham's F-12, 2% Fetal Bovine Serum, 1 % penicillin/streptomycin). The explants were transferred to the bioreactor and preloaded using the weight (132.05 grams) of the plunger containing the compression rod.

Displacement tests were run at 0% (n=8), 5% (n=6), 10% (n=6), 15% (n=6), and 20% (n=4) strain calculated from the original height of the meniscal explants. These explants were taken from both the anterior portion of the medial and lateral menisci of both the left and right knees. The range of strains was chosen to encompass strains above and below physiological conditions experienced by an intact menicus. The tests ran at 1 Hz in a sinusoidal fashion, with time, position, and load recorded throughout the test using system software (SmartMotor Interface).

Load control tests were run in a similar way, to 0.00 MPa (n=8), 0.05 MPa (n=3), and 0.1 MPa (n=4) load levels. Higher loads levels were investigated on two sets of samples (0.5 and 1.0 MPa), however tissue integrity was compromised at the end of the two hour loading regime. Again, the weight of the plunger (132.05 grams) was used as the preload and starting position. Samples were loaded at 1 Hz for two hours while time, load, and position were recorded.

Upon completion, samples were removed from the dish and cut into superior and deep zones. The wet weight of each half of the explant was determined prior to incubation for 24 hrs in test media (48.5% Dulbecco's modified Eagles medium, 48.5% Ham's F-12, 2% Fetal Bovine Serum, 1% penicillin/streptomycin). A preliminary study that tested NO production following 15% strain with post incubation times of 24, 48, and

72 hours showed maximal expression at 24 hours. Following post-incubation the media was immediately stored at -80°C until NO quantification.

NO Quantification

Nitric oxide was measured from each explant by using a total NO assay as detailed by the manufacturer (Cayman Chemical, Ann Arbor, MI). The assay measured the stable form of NO, nitrite and nitrate, by converting all nitrate to nitrite using the Greiss reaction. The reaction produces a colored azo dye that absorbs light at 540 nm, which can be read in a microplate reader. The resulting absorptivity was converted to concentration using a standard curve created from known concentrations of nitrite. The resulting concentrations were then normalized by the weight (grams) of each tissue sample.

Statistical Analysis

Regression analysis was used to determine the relationship between strain level and nitric oxide production. Data points with quadratic regression lines and 95% confidence intervals were plotted. R-squared and P-values were used to determine the fit of the regression. $P<0.05$ was considered significant. NO production from the superficial and deep zones was compared, for a given load or strain level, using paired t-tests.

3.4 Results

Meniscal Compression

Data collected from each test confirmed the bioreactor reached target compressive displacement (± 0.001 mm) or load (± 0.01 MPa) during each cycle. Displacement controlled tests showed a rapid drop in load within the first 1000 cycles with little change

following 4000 cycles (Figure 1). For displacement tests below 15 % strain, load settled at or below 0.05 MPa while the 20% strain test remained above 0.1 MPa throughout the duration of the test. The difference of load measured from start to finish can be seen in Table 1A. Load controlled tests (Figure 2) showed a rapid increase in compressive displacement within the first 1000 cycles. The 0.05 MPa load level reached maximum displacement near 3000 cycles and remained at that level to the end of the tests. The 0.1 MPa tests reached 18% strain near 3000 cycles but steadily increased to 20.7% strain by the final cycle. These differences in strain from start to finish of these tests can be seen in Table 1B.

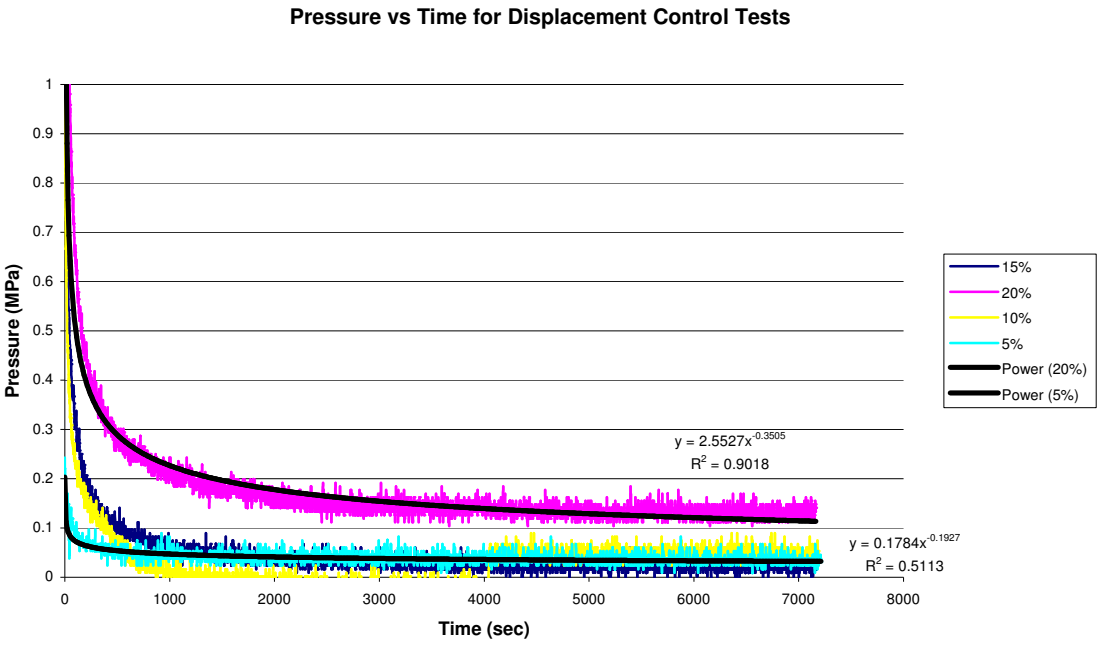

Figure 3.1: Representative data of Pressure vs. Time displays the stress relaxation characteristics of meniscal explants. Regression equations with R^2 values are displayed for the 5% and 20% strain test. The data shows significant relaxation within the first 1000 cycles of the 7200 cycle test. The test frequency was 1 Hz. for a duration of 2 hrs.

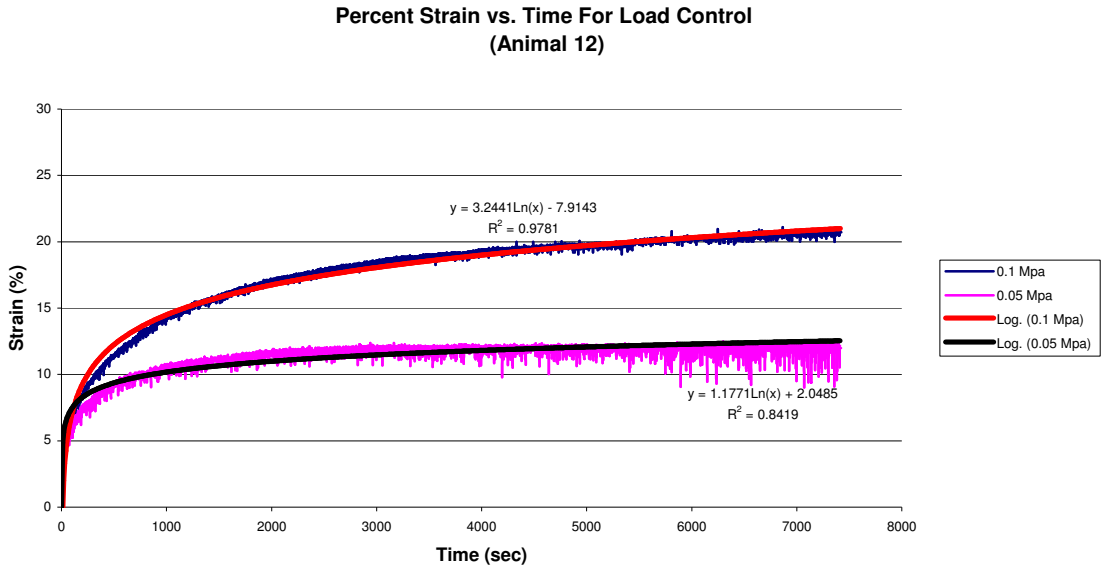

Figure 3.2: Representative plot of load control tests displayed creep characteristics with the plot of compressive Strain vs. Time. Regression equations and R^2 values are displayed next to each data set. These results show large increases in compressive displacement within the first 1000 cycles. At the end of the test, the 0.1 MPa test required 0.4 mm more compression than the 0.05 MPa test.

	Pressure (MPa)	
Strain	Start	End
5%	0.166 ± 0.108	0.038 ± 0.010
10%	1.141 ± 0.103	0.046 ± 0.010
15%	2.185 ± 0.827	0.035 ± 0.026
20%	3.548 ± 0.429	0.128 ± 0.020

A

	Strain (%)	
Press. (MPa)	Start	End
0.05	2.6 ± 0.53	11.6 ± 1.36
0.10	3.0 ± 0.12	20.1 ± 1.45

B

Table 3.1: A: Average and standard deviation pressure at start and end of displacement control test at all tested strain levels. **B:** Average of displacements at the start and end of load control test for both tested load levels.

Nitric Oxide Production

Nitric oxide (NO) production was not significantly influenced by location within the explant. There was no significant difference between NO production of the superficial and deep zones of the explants (0% p = 0.898, 5% p = 0.443, 10% p = 0.176, 15% p= 0.978, 20 % p = 0.351) using a paired t-test. However, a distinct trend did appear with both displacement and load controlled tests. For displacement control, the 20% strain level produced the greatest amount of NO with 15% being lower and comparable to the 0% strain (control) samples. The 5% strain produced the next lowest amount of NO while the 10% strain level produced the least amount of NO out of all strain levels. The relationship of NO production to strain level fits the quadratic model $NO\ Production=225.5 -30.66*Strain\ Level +1.972*Strain\ Level^2$ for the superficial zone with R^2=0.435(Figure 3). The quadratic term was significant (p = 0.000) as well as the constant (p = 0.001), while the linear term was not found to be significant (p = 0.100). The deep zone showed a similar trend with 10% strain producing the least NO. The quadratic $NO=234.6 -19.4*Strain\ Level+1.158*Strain\ Level^2$ fit the data with R^2=.213 (Figure 4). The quadratic term was statistically significant (p = 0.016) as well as the constant (p = 0.000), while the linear term was not significant (p = 0.459).

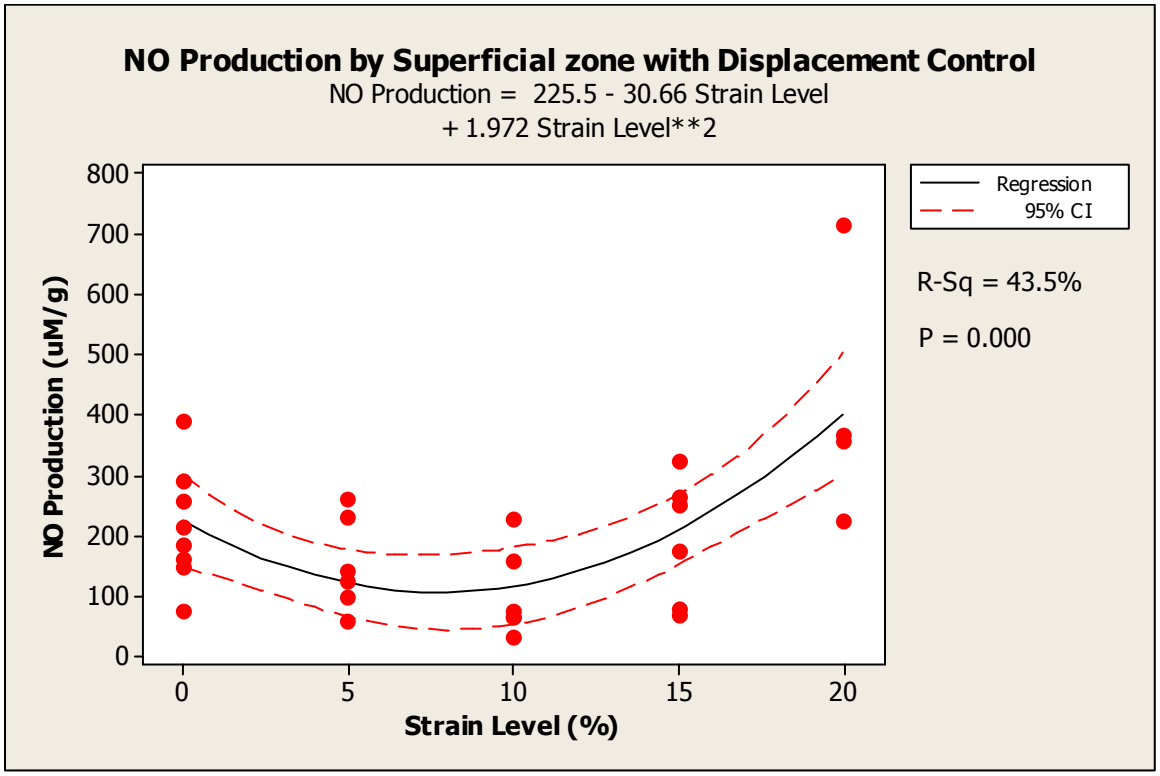

Figure 3.3: Displacement control graph showing quadratic fit to NO produced by superficial zone of explants with 95% confidence interval displayed. R^2=0.435. For 0%: n=8; 5%: n=6; 10%: n=6; 15%: n=6; 20%: n=4.

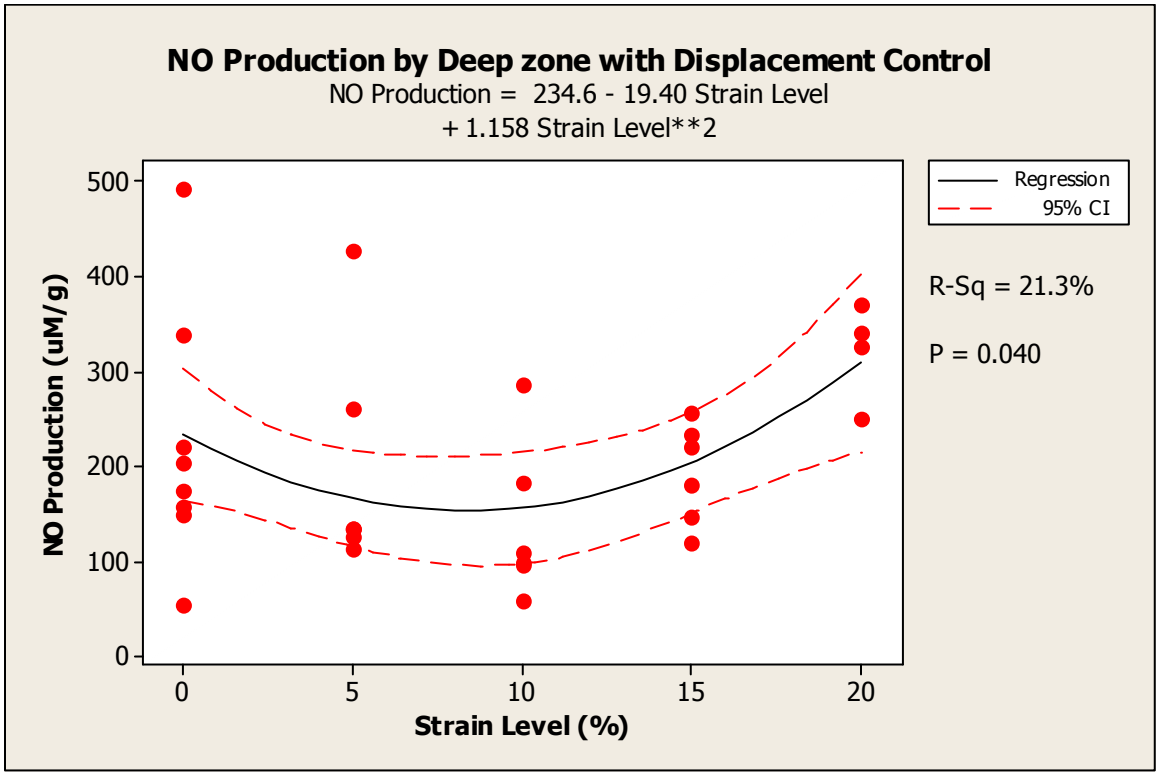

Fiqure 3.4: Displacement control graph showing NO production of deep zone of explants compared to a quadratic fit with 95% confidence interval. R^2=0.213. 0%: n=8; 5%: n=6; 10%: n=6; 15%: n=6; 20%: n=4.

Results from the 0.05 MPa and 0.1 MPa load controlled tests were not statistically significant (0 MPa p = 0.898, 0.05 MPa p = 0.361, 0.01 MPa p = 0.252) for comparison of superficial to deep zones using paired t-test. There were also no significant terms in the regression equations for the data other than the constants. The trends show higher NO production than the 15% strain control test and less then the 20% strain. The superficial zone showed a quadratic increase from zero load condition (Figure 5), while the NO production for the deep zone increased for 0.05 MPa and decreased again for 0.1 MPa (Figure 6).

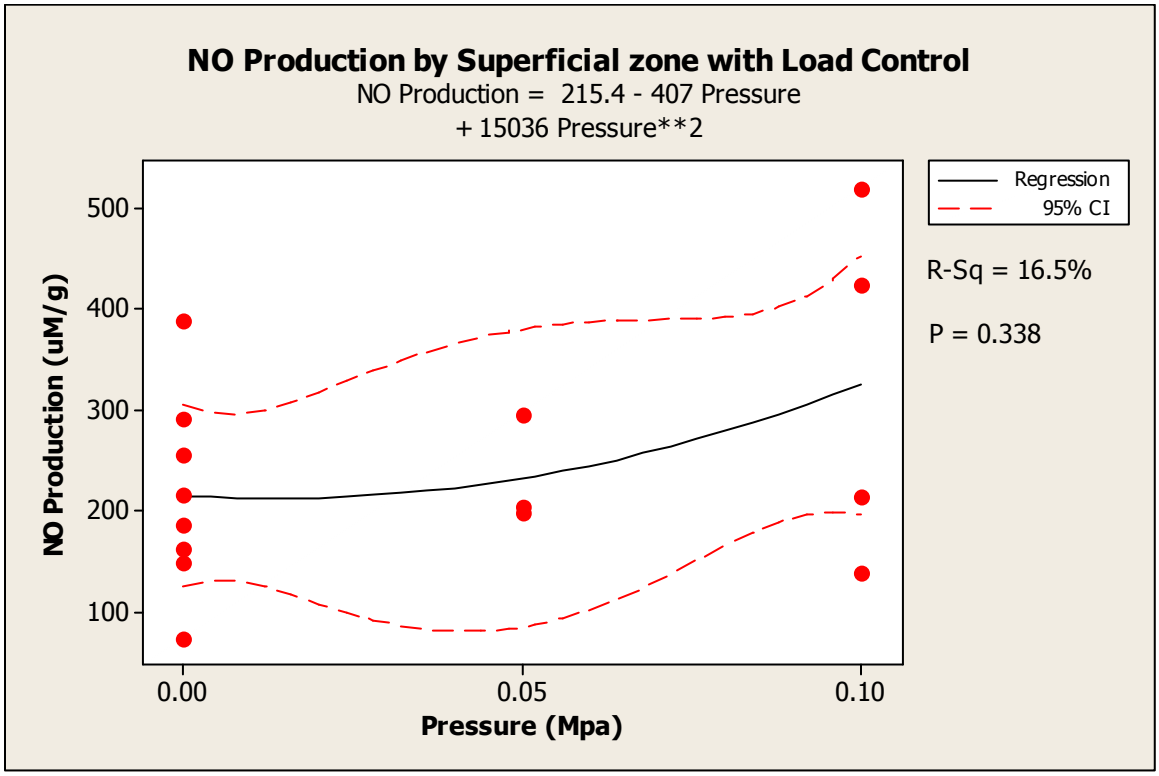

Figure 3.5: Load control graph showing quadratic regression with 95% confidence interval for superficial zone of explants. R^2=0.165. 0 MPa: n=8; 0.05 MPa: n=3; 0.1 MPa: n=4.

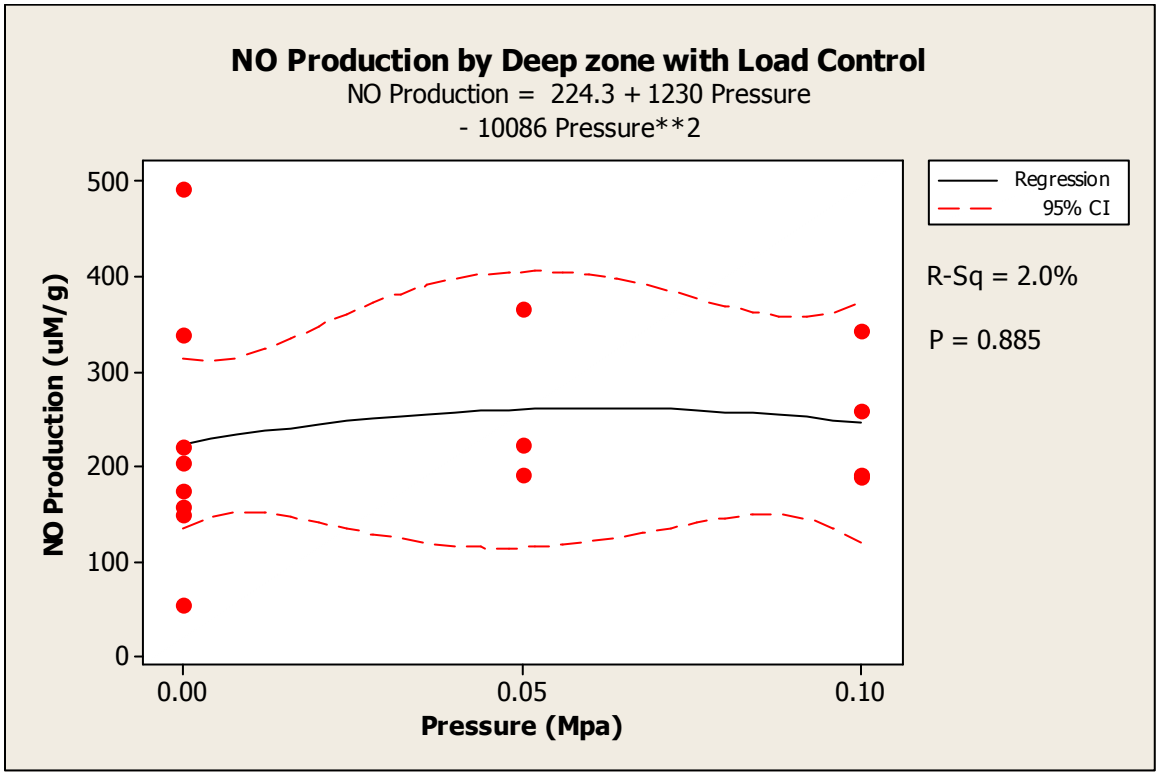

Figure 3.6: Load Control graph showing quadratic regression with 95% confidence interval for deep zone of explants . R^2=0.02. 0 MPa: N=8; 0.05 MPa: N=3; 0.1 MPa: N=4.

3.5 Discussion

The findings of this research suggest a relationship between mechanical compression and nitric oxide production by meniscus. The experimental setup (1 Hz; 2 hrs) simulates a short period of activity for comparison to inactivity in an attempt to determine how this affects NO production and ultimately meniscal health. The data suggests that inactivity (0 pressure/strain) as well as overstrain produces high amount of NO in comparison to physiological strain levels. The results of this study also show that physiological pressures (~1 MPa) applied to meniscal explants in unconfined compression do not produce equivalent physiological strains. Load controlled tests targeting 1 MPa produced approximately 30% strain and 0.1 MPa tests produced

approximately 20 % strain. It requires much lower pressure (<0.05 MPa) to achieve physiological strain (5-10%) during unconfined compression. The data also suggests that NO production is not dependent on location within each explant. Nitric oxide is linked to inflammation and tissue degradation in articular cartilage and meniscus and is believed to be a direct result of compression [14, 19]. Previous studies have reported that dynamic compression of meniscal explants results in an up-regulation of NO [14, 19]. However, these experiments were performed for an extended period of time and at only one strain level, which would not be considered normal activity. Some studies have also reported that meniscal explants produce NO spontaneously without compression [14, 16, 19, 21, 25, 26]. The results from our study also show that NO is produced spontaneously but do not support the simple relationship that compression up-regulates NO production in the meniscus. Our data suggest that physiological strain levels for short periods of time that could be considered normal activity actually decreases NO production in the meniscus. The data also shows that overstrain, as experienced by meniscectomized tissue, up-regulates NO above both the zero load/strain condition and physiological levels of strain.

These findings challenge the conclusion of others that dynamic compression increases NO production [14, 19]. The 5% and 10% strain levels are physiological and appear to reduce NO production by meniscal explants compared to 0% strain. If this is in fact the case for the meniscus, moderate levels of NO may be required for maintenance of normal, healthy tissue. NO is typically linked to tissue degradation, but its role in matrix metabolism is not completely understood. It is possible that NO modulates matrix resorbtion to allow for the addition of newly remodeled matrix constituents by

fibrochondrocytes. If this were the case, excessive NO production would lead to an unbalance of matrix metabolism in favor of resorbtion and result in tissue degradation.

Differences in response of superficial and deep zone to compression were not demonstrated in this study. Previous studies showed that fibroblastic cells produced higher NO levels than the deep chondrocytic cells [14, 19]. In this study, the trends produced by both regions were similar. Further investigation is required to reconcile differences between this investigation and previous.

There were several limitations to this study that prevent further defining the relationship between compression and NO production. These tests were performed using unconfined compression, which may not be physiological. The results show that physiological strain produces sub-physiological stresses experienced in the meniscus throughout the test. This may be caused by excessive fluid flow out of the explant due to its unconfined treatment. To date, only 6 animals have been used for each level of strain (n=8 for control, 0% and n=4 for 20%) and only 3 animals for load levels.

Recommedations

Meniscal location (lateral or medial) and explant location from anterior to posterior are other factors that may respond differently to compression. Other compressions studies using confined compression would be beneficial in determining how compression affects NO production. However, to completely understand the mechanism of NO production and its role in matrix metabolism, chemical factors must be investigated along with mechanical factors. One chemical factor of particular interest is interleukin-1 (IL-1) for its apparent link to NO. IL-1 is a proinflammatory cytokine that is believed to induce NO production. Blocking this cytokine during compression may

reduce NO production during physiological strain for normal activity periods. Such a result could change treatment of meniscal lesions and improve tissue healing. In order to create the best healing response by the meniscus, chemical as well as mechanical treatment may be required. Understanding this mechanism is crucial to improving medical treatment to common meniscal injury.

Acknowledgement

The authors are grateful to the Whitaker foundation for their financial support.

REFERENCES

1. Aagaard, H. and R. Verdonk, *Function of the normal meniscus and consequences of meniscal resection.* Scand J Med Sci Sports, 1999. **9**(3): p. 134-40.
2. Ahluwalia, S., et al., *Distribution of smooth muscle actin-containing cells in the human meniscus.* J Orthop Res, 2001. **19**(4): p. 659-64.
3. Collier, S. and P. Ghosh, *Effects of transforming growth factor beta on proteoglycan synthesis by cell and explant cultures derived from the knee joint meniscus.* Osteoarthritis Cartilage, 1995. **3**(2): p. 127-38.
4. Gershuni, D.H., A.R. Hargens, and L.A. Danzig, *Regional nutrition and cellularity of the meniscus. Implications for tear and repair.* Sports Med, 1988. **5**(5): p. 322-7.
5. Ghadially, F.N., J.M. Lalonde, and J.H. Wedge, *Ultrastructure of normal and torn menisci of the human knee joint.* J Anat, 1983. **136 (Pt 4)**: p. 773-91.
6. Peters, T.J. and I.S. Smillie, *Studies on the chemical composition of the menisci of the knee joint with special reference to the horizontal cleavage lesion.* Clin Orthop, 1972. **86**: p. 245-52.
7. Roughley, P.J., et al., *The presence of a cartilage-like proteoglycan in the adult human meniscus.* Biochem J, 1981. **197**(1): p. 77-83.
8. Roughley, P.J. and R.J. White, *The dermatan sulfate proteoglycans of the adult human meniscus.* J Orthop Res, 1992. **10**(5): p. 631-7.
9. Tanaka, T., K. Fujii, and Y. Kumagae, *Comparison of biochemical characteristics of cultured fibrochondrocytes isolated from the inner and outer regions of human meniscus.* Knee Surg Sports Traumatol Arthrosc, 1999. **7**(2): p. 75-80.
10. Leslie, B.W., et al., *Anisotropic response of the human knee joint meniscus to unconfined compression.* Proc Inst Mech Eng [H], 2000. **214**(6): p. 631-5.
11. Proctor, C.S., Schmidt, M.B., Whipple, R.R., Kelly, M.A., Mow, V.C., *Material Properties of the normal medial bovine meniscus.* Journal of Orthopaedic Research, 1989. **7**(6): p. 771-782.
12. Djurasovic, M., et al., *Knee joint immobilization decreases aggrecan gene expression in the meniscus.* Am J Sports Med, 1998. **26**(3): p. 460-6.
13. Dowdy, P.A., et al., *The effect of cast immobilization on meniscal healing. An experimental study in the dog.* Am J Sports Med, 1995. **23**(6): p. 721-8.
14. Fink, C., et al., *The effect of dynamic mechanical compression on nitric oxide production in the meniscus.* Osteoarthritis and Cartilage, 2001: p. 1-8.
15. LeGrand, A., et al., *Interleukin-1, tumor necrosis factor alpha, and interleukin-17 synergistically up-regulate nitric oxide and prostaglandin E2 production in explants of human osteoarthritic knee menisci.* Arthritis Rheum, 2001. **44**(9): p. 2078-83.
16. Cao, M., et al., *Generation of nitric oxide by lapine meniscal cells and its effect on matrix metabolism: stimulation of collagen production by arginine.* J Orthop Res, 1998. **16**(1): p. 104-11.
17. Maneiro, E., et al., *Aceclofenac increases the synthesis of interleukin 1 receptor antagonist and decreases the production of nitric oxide in human articular chondrocytes.* J Rheumatol, 2001. **28**(12): p. 2692-9.

18. Murrell, G.A., et al., *Nitric oxide: an important articular free radical.* J Bone Joint Surg Am, 1996. **78**(2): p. 265-74.
19. Shin, S.J., et al., *Regulation of matrix turnover in meniscal explants: role of mechanical stress, interleukin-1, and nitric oxide.* J Appl Physiol, 2003. **95**(1): p. 308-13.
20. Taskiran, D., et al., *Nitric oxide mediates suppression of cartilage proteoglycan synthesis by interleukin-1.* Biochem Biophys Res Commun, 1994. **200**(1): p. 142-8.
21. Hashimoto, S., et al., *Nitric oxide production and apoptosis in cells of the meniscus during experimental osteoarthritis.* Arthritis Rheum, 1999. **42**(10): p. 2123-31.
22. Upton, M.L., et al., *Differential effects of static and dynamic compression on meniscal cell gene expression.* J Orthop Res, 2003. **21**(6): p. 963-9.
23. Zielinska, *3D Finite Element Model of Medial Meniscus Meniscectomy; Changes in Contact Behavior.* Journal of Biomechanical Engineering, 2005.
24. Spilker, R.L., Donzelli, P.S., *A biphasic finite element model of the meniscus for stress-strain analysis*, in *Knee Meniscus;Basic and Clinical Foundations*, V.C. Mow, Arnoczky, S.P., Jackson, D.W., Editor. 1992, Raven Press: New York.
25. Kobayashi, K., et al., *Chondrocyte apoptosis and regional differential expression of nitric oxide in the medial meniscus following partial meniscectomy.* Journal of Orthopaedic Research, 2001. **19**: p. 802-808.
26. Kobayashi, K., et al., *The suppressive effect of hyaluronan on nitric oxide production and cell apoptosis in the central region of meniscus following partial meniscectomy.* Iowa Orthop J, 2002. **22**: p. 39-41.
27. McHenry, J., et al., *Nitric Oxide Production of Meniscal Explants Following Dynamic Compression.* Thesis 2005: Ch. 2, p. 25-45.

APPENDIX A

SUPPLEMENTARY INFORMATION ON CHAPTER 2
(VALIDATION OF BIOREACTOR)

A.1 Description of Bioreactor Components and Features

The bioreactor used in these experiments is a specially design unit with a unique combination of components. The system is set in a dimensionally critical frame that able to fit in an incubator. The device utilizes a Smartmotor 1720. This is a belt driven linear actuator made by Ultramotion. It is capable of thrusting to 500 lbs with bidirectional repeatability of 0.0003 in and a unidirectional repeatability of 0.0001 in. at a maximum speed of 20 in/sec. Attached to the actuator are the compression surfaces contained by an aluminum cap with a linear bearing. The plunger is attached to the actuator while an aluminum dish is attached to a load cell from interface (Figure A.1). The load cell used was a 300 lb capacity load cell to increase accuracy and resolution above a previously used 2000lb capacity load cell with similar dimensions. The signal from the force transducer connects directly to a 2100 series signal condition and amplifier (Vishay). This unit allow for easy adjustment of signal balancing and amplification. That conditioned signal connects directly to the actuator to provide a continuous load reading (Figure A.2). The connection supplies a voltage to the input pins, which is read through the Smartmotor as an analog signal that is converted to an encoder count. The actuator is then connected to the PC which uses an Animatics control system and Smartmotor (SMI) interface.

Figure A.1: The dish and load cell assembly of the bioreactor.

Figure A.2: The amplified load cell signal connection to the SmartMotor actuator (white cable) to input pins.

The system stands 50 cm tall and 25 cm in length and width allowing it to be contained in an incubator (Figure A.3). The 1-inch thick aluminum plates (Al 6061) at the top and bottom of the bioreactor are supported by 1-inch aluminum rods. The plunger is also made of aluminum and has six Teflon-filled Delrin compression rods 8mm in diameter. The dish is also machined out of aluminum allowing the compression surface assembly (plunger and dish) to be sterilized by alcohol or autoclave.

Figure A.3: The bioreactor frame allows the system to fit in an incubator and contains many components that can be sterilized.

A.2 Validation of Even Well Pressure

Validation of the bioreactor required collecting evidence that the system compressed all six explants to the same pressures and strains. The first method involved placing pressure film between the surfaces used for compression. To do this, the pressure film was calibrated in the Instron materials testing machine to pressures from below to above the pressure range of the film (Figure A.4, Table A.1). Also several samples were loaded to the same pressure to determine the repeatability of the film (Figure A.5, Table A.2). Next, the dish was measured using micrometers to make sure the top surface, the bottom of the well, and the compression rod surfaces were all parallel. A 3/8 in thick uniform machined circular piece of steel was added onto the top of the dish. At this point a uniform piece of rubber was placed on top of that followed by the pressure film. The plunger was then pressed into the pressure film to a specific displacement. That was repeated five times at two different displacements. These were then compared to the calibration done on the Instron using Scion image to determine the pressure differences between wells.

A second technique was used to collect a physical measurement of the gap between the bottom of each compression rod and the bottom of each well. To do this, each well was filled with auto body filler and the plunger was quickly lowered into the aluminum dish until body filler surrounded each compression rod. The actuator remained at this position until the body filler hardened to a rigid body. The assembly was removed, at which point the body filler was measured using a micrometer; this was repeated five times. It was also necessary to verify the load program was reading accurately the load it was recording on the computer. This was done first by calibration of the load cell by

incrementally adding known weight while recording voltage read by the oscilloscope and the encoder counts read through the SMI software. Calibration curves were made to ensure linear relationships (Figure A.4 and A.5). A sample load program was then run and monitored on the oscilloscope to determine if the peak voltage matched encoder counts and the target load.

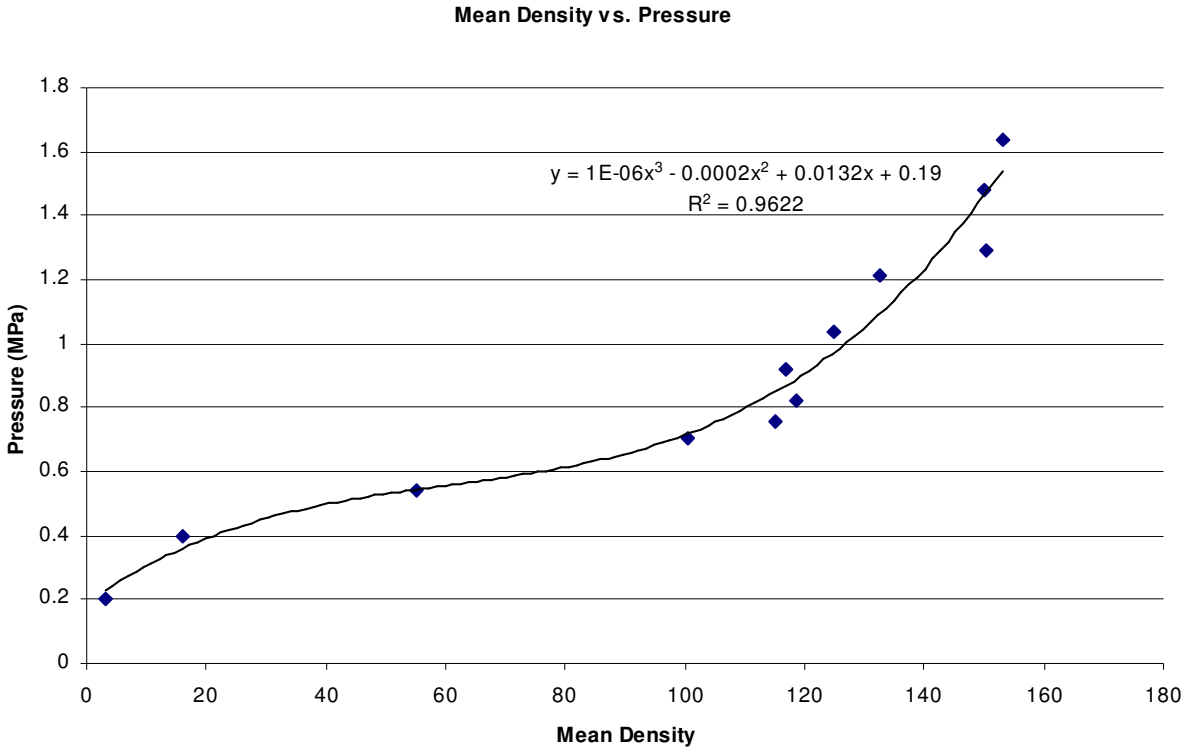

Figure A.4: The calibration of the pressure film showing the relationship of mean density measured with Scion Image and pressure in MPa. The regression equation is also displayed.

Pressure (MPa)	Density
0.2	3.03
0.4	15.95
0.54	55.18
0.703	100.39
0.757	115.23
0.822	118.52
0.92	116.87
1.04	124.97
1.211	132.69
1.29	150.31
1.48	150.06
1.64	153

Table A.1: Data collected from calibration of the pressure film used to create the calibration curve.

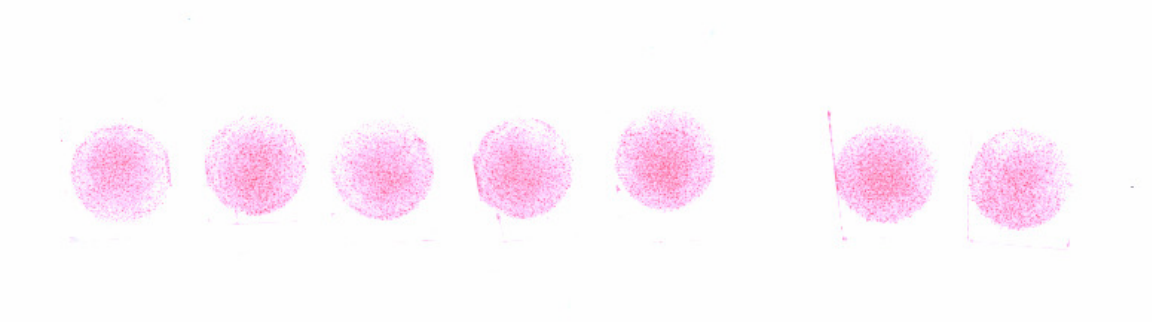

Figure A.5: Pressure film impressions made during a repeatability test on the Instron material testing machine at a target pressure of 0.477 MPa (70 psi.).

Pressure Film Repeatability Test (.477 MPa)

	Test 1	Test 2	Test 3	Test 4	Test 5	Test 6	Test 7	Max. Diff.	% Error
Density	64.92	70.78	65.04	70.41	78.53	76.87	65.00	13.61	20.96

A

Pressure Film Repeatability Test (.477 MPa Applied Pressure)

	Test 1	Test 2	Test 3	Test 4	Test 5	Test 6	Test 7	Average	Std. Dev.
Press.	0.4776	0.4769	0.4776	0.4770	0.4775	0.4771	0.4776	0.4773	0.0003

B

Table A.2: A: Data collected from the repeatability test in term of density measure using Scion Image. **B:** Result of the repeatability test using the calibration curve found in A.4.

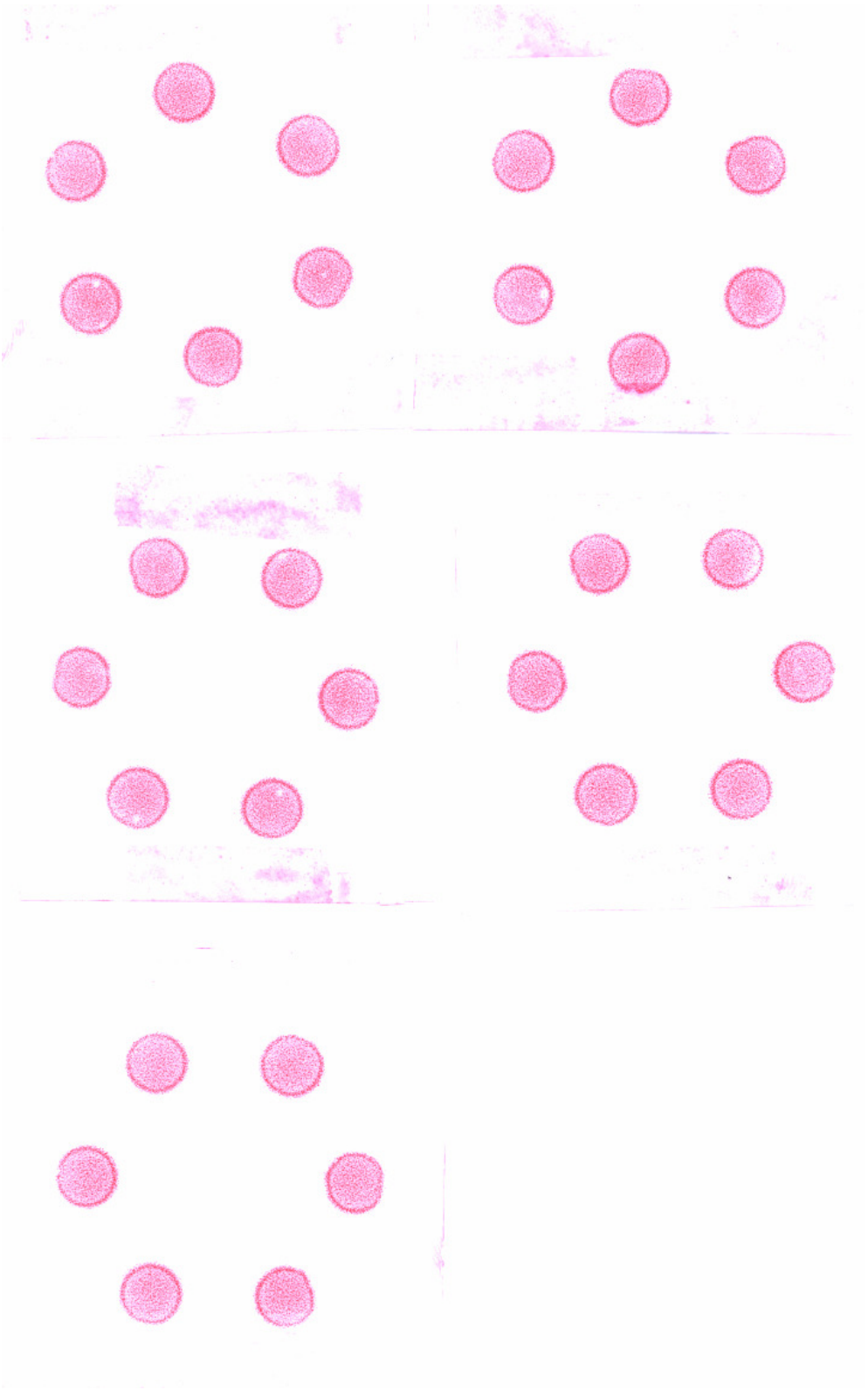

Figure A.6: Impressions made at a load level resulting in 0.477 MPa (70 psi.)

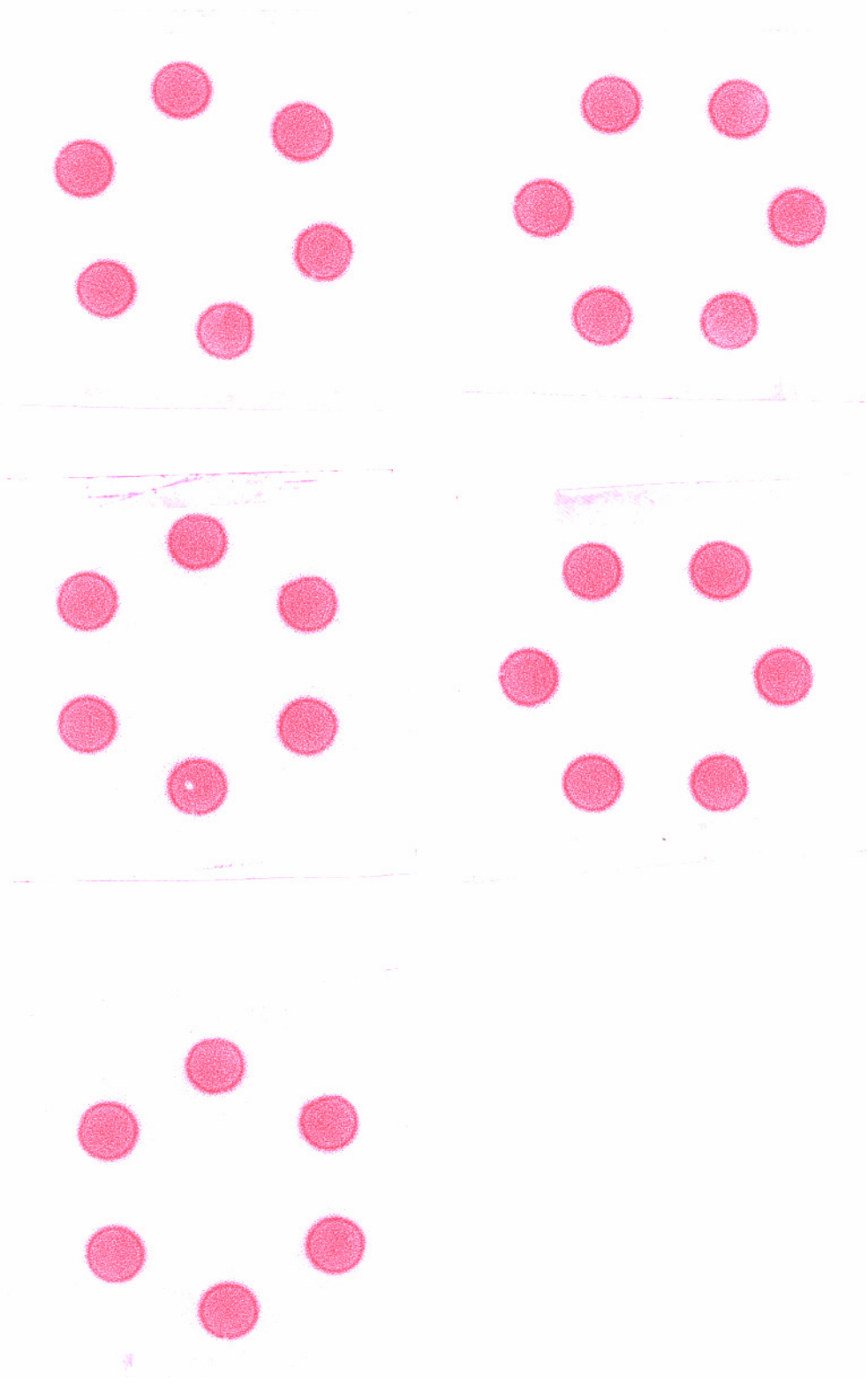

Figure A.7: Impressions made at a load level resulting in 0.564 MPa (82 psi.)

.477Mpa Denstiy (0-255)

Test #	Rod 1	Rod 2	Rod 3	Rod 4	Rod 5	Rod 6	Average	Max. Diff.	% Error
1	67.78	74.05	69.24	68.79	73.98	72.37	71.04	6.27	9.25
2	72.01	75.51	72.11	74.36	74.96	68.07	72.84	7.44	10.93
3	67.14	73.10	71.74	70.38	71.35	68.72	70.41	5.96	8.88
4	67.33	73.13	71.22	73.25	75.78	73.33	72.34	8.45	12.55
5	63.55	69.32	71.56	76.93	68.83	72.05	70.37	13.38	21.05
.564Mpa									
1	113.40	114.17	113.13	113.13	107.99	113.79	112.60	6.18	5.72
2	110.20	108.44	102.70	114.67	98.25	109.59	107.31	16.42	16.71
3	111.08	115.26	115.45	113.17	113.12	108.31	112.73	7.14	6.59
4	113.76	115.03	114.70	111.67	110.74	113.37	113.21	4.29	3.87
5	114.21	110.32	114.47	113.86	112.92	108.62	112.40	5.85	5.39

A

.477MPa Pressure (MPa)

Test #	Rod 1	Rod 2	Rod 3	Rod 4	Rod 5	Rod 6	Average	Std. Dev.	% Error
1	0.4773	0.4768	0.4771	0.4771	0.4768	0.4768	0.4770	0.0002	0.0912
2	0.4768	0.4769	0.4768	0.4768	0.4769	0.4772	0.4769	0.0001	0.0788
3	0.4773	0.4768	0.4769	0.4770	0.4769	0.4771	0.4770	0.0002	0.1108
4	0.4773	0.4768	0.4769	0.4768	0.4769	0.4768	0.4769	0.0002	0.1056
5	0.4778	0.4771	0.4769	0.4771	0.4771	0.4768	0.4771	0.0003	0.1986
.564 MPa									
1	0.5732	0.5783	0.5715	0.5715	0.5425	0.5758	0.5688	0.0132	6.6006
2	0.5541	0.5447	0.5194	0.5816	0.5047	0.5508	0.5426	0.0272	15.2409
3	0.5591	0.5857	0.5870	0.5718	0.5715	0.5441	0.5698	0.0163	7.8899
4	0.5756	0.5841	0.5818	0.5626	0.5571	0.5730	0.5724	0.0106	4.8354
5	0.5785	0.5548	0.5803	0.5762	0.5702	0.5457	0.5676	0.0142	6.3441

B

Table A.3: A: Density measurements using Scion Image for all the impressions made on ultra low pressure film with 255 representing a saturated sample. The average density, standard deviation, and percent error for each test are calculated. **B:** The data from table A is converted to pressure using calibration results from figure A.4.

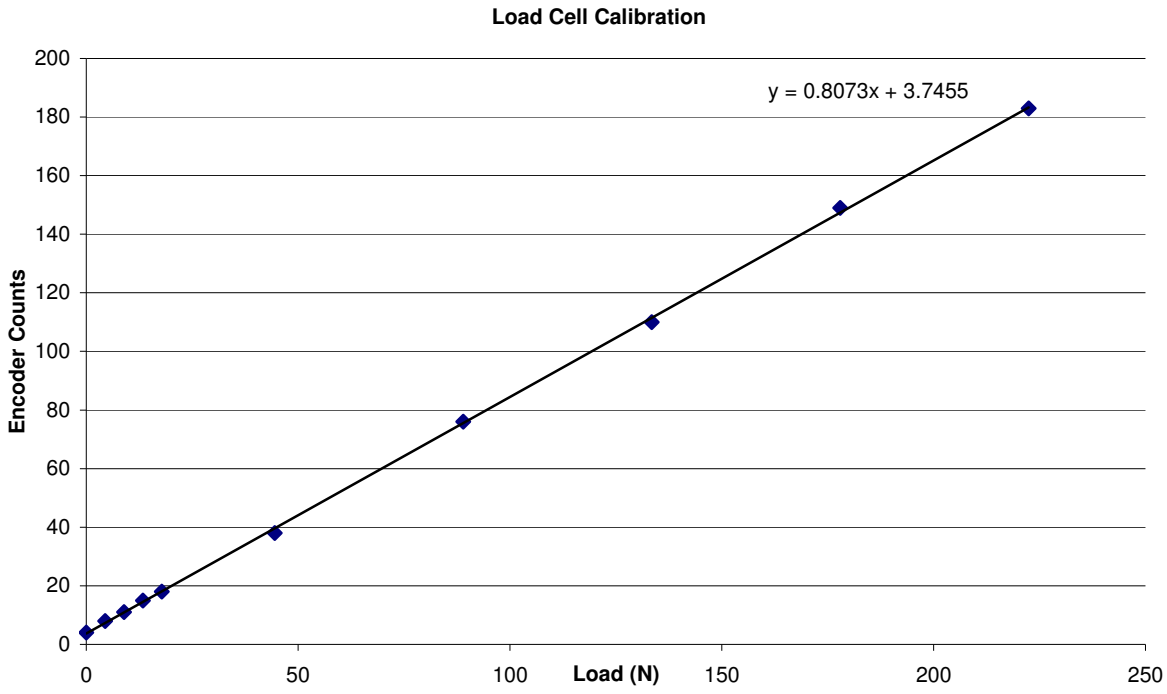

Figure A.8: Calibration of load cell relating encoder counts to known loads applied.

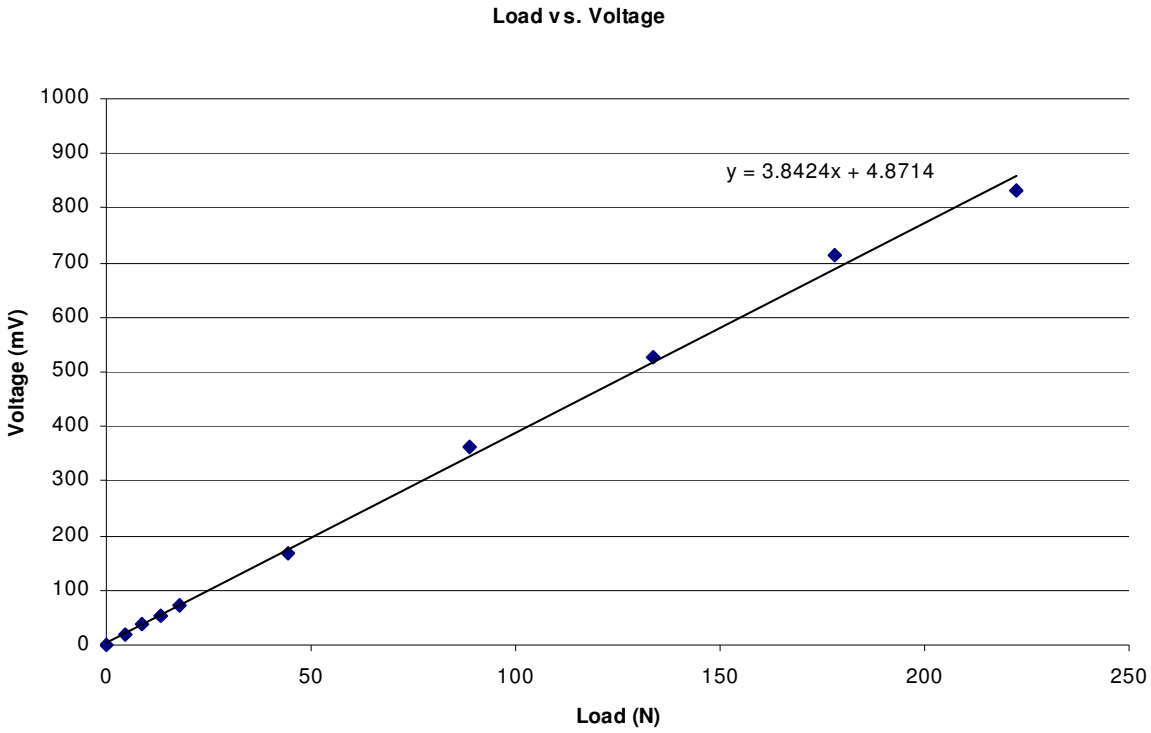

Figure A.9: Calibration of the load cell relating known loads applied to voltage measured on the oscilloscope.

Load (lbs)	Load (N)	Counts	voltage (mV)
0	0	4	0
1	4.4482	8	20.3
2	8.8964	11	37.5
3	13.3446	15	54.7
4	17.7928	18	71.9
10	44.482	38	167
20	88.964	76	363
30	133.446	110	525
40	177.928	149	713
50	222.41	183	831

Table A.4: Table showing data used to create calibration of load cell in A.5 and A.6.

A.3 Validation Protocols

LOAD CELL REPLACEMENT AND CALIBRATION PROTOCOL

Equipment List:

1. Weights
2. 3/16” Alan wrench
3. Adjustable wrench
4. Oscilloscope

Load Cell Replacement:

1. Unscrew lower attachment post from load cell.
2. Remove all alan bolts with 3/16” alan wrench.
3. Disconnect load cell cable.
4. Replace load cell with dimensionally similar load cell.
5. Orient load cell to align wires and tighten down alan bolts evenly.
6. Tightly screw in the lower attachment post.
7. Assemble dish, plunger, and cap and secure on lower attachment pin with quick disconnect pin.
8. Turn on the power module to the motor and open the SmartMotor Interface in the marrow folder.
9. Manually lower the actuator into the top of the plunger.
   * Code example:
   ```
   MP
   A=1000
   V=100000
   D=-60000
   G
   ```
   * For distance (D) 2500 = 1mm; Down is neg.
10. Loosen nut on actuator and turn end piece until holes line up. Slide second quick disconnect pin into plunger/actuator.
11. Retighten actuator nut.
12. Attach load cell cable.

Load Cell Calibration:

1. Turn on 2100 system (switch in lower right hand corner).
2. Power up motor and SMI as previously described
3. Go to *File-Open* and open the file *checkload.sms* in the C: Program Files/ Program Editor folder and click open.
4. Make sure the cursor is in the program window and click T on the tool bar to transmit the program.
   * The actuator may need to be raised to provide room to add weights.
5. Attach the aluminum dish to the lower attachment post for a weight platform.
6. On channel 2 of the 2100 system, turn the balance dial until both lights are extinguished.

7. Click R on the tool bar and note the encoder counts in the command window. One number should show up after the RUN command. This value is the initial offset of the load reading.
8. Attach an oscilloscope to the output of the 2100 system.
9. Hit the *Cursors* button and use the dial to the left of it to align the Y1 cursor at the starting point of the load signal. The RUN/STOP button should be green and the signal should be rolling across the screen. If not hit the MAIN/DELAYED button and select ROLL. Also hit the ACQUIRE button and select AVERAGING.
10. Add a weight on top of the aluminum dish.
11. Click R on the tool bar and note the resulting encoder counts.
12. On the oscilloscope hit the CURSORS button and select the Y2 cursor and move it to the new location of the signal using the dial to the left or the CURSORS button.
13. Note the ΔY value.
14. Repeat steps 10-13 for several different weight increments.
15. To increase or decrease amplification turn the GAIN dial directly below the BALANCE dial until the desired amplification is reached.
    * The voltage output of the 2100 system should exceed 5V since the SmartMotor and only read a maximum of 5V.
16. For larger changes in amplification, turn the multiplier switch next to the GAIN to 2x, 20x, or 200x amplification.
17. Plot results of load vs. counts and load vs. voltage to determine linearity. Use a linear regression trend line to determine relationship between load and encoder counts.
    - For 300 lb load cell: GAIN should be at 200x with the dial set at 1.35.
        - 3.84 mV = 1 Newton; 0.8073 counts = 1 Newton.

    - For 2000 lb load cell: Calibrate to 500 lb:
        - 2.25 mV = 1 Newton: 0.46 counts = 1 Newton

VALIDATION PROTOCOL FOR EVEN WELL PRESSURE

Objective:

To determine the greatest difference in pressure between all six well of the bioreactor. This will be done using Ultra Low pressure film, which will be placed between each compression rod and each sample to be compressed. The film will be analyzed using Scion Image to check the density. The density values will be related to pressure using calibration and the results will determine the accuracy of even well pressure.

Pressure Film Calibration

- Using a punch, cut six identical cylindrical pieces of sample material (rubber) of constant thickness. Measure dimensions of samples.
- Cut matching samples of Pressurex Ultra Low pressure film (28 psi – 85 psi).
- Place the sample material on the lower platen of the Instron 8872 tensile testing hydraulic press and place the pressure film on top of the sample. The dull sides of each layer of film have to be in contact.
- Change the display of the Instron to read load measured in Newtons. Using the fine adjustment, manually lower the upper platen and compress to a known load within the pressure range of the pressure film. Immediately unload.
- Remove and discard translucent sheet of pressure film
- Perform 12 compressions using different loads each time. Load at increments of 5 psi, going from 30 to 85 psi.
- Using Scion Image, measure the mean density of each pressure film compression. Use the results to create a calibration curve of density vs. pressure.

Testing Well Pressure

- Place sample material (rubber) in the bottom of each well. Make sure each rubber sample is sitting flat in the bottom of each well with some clearance around the edges. Place pressure film on top of each sample.
- Assemble the well plate, plunger, and lid, and connect to load cell and actuator. The load cell is connected first, and then the actuator is lowered to meet the connection with the plunger. Pick a target load within the range of the pressure film to compress the samples.
- To move the actuator, refer to the commands in chapter's 2 &3 of the SmartMotor user's manual.
- Double Click the Marrow folder on the desktop and open Smartmotor Interface shortcut.
- Open the file titled target load.sms.
- Change the voltage value for load to the desire amount. To change pressure to voltage, determine the number of Newton's on each sample, multiply by 6 (number of wells), and then multiply by .46. This value goes into the "f = " for the user input for force.
- Click the T (transmit) button.
- When the program is finished transmitting, click R (run) to start the program.
- When the program is finished, raise the actuator back up and take out the dish and film cutouts.
- Perform a total of 15 tests at three different loads.
- Scan results and measure density of each well for each test.
- Using calibration results, find pressure by using density for each sample and each test.
- Calculate differences in pressure between each well and determine percent error.

Compare target pressure with pressure found from film, and using load from load cell.

A.4 Validation Programs

The following are programs written in SmartMotor programming language, which were used in various ways during validation of the bioreactor.

```
'Check current load reading'

RUN?
UAI
b=UAA
Rb
END
```

checkload.sms: This program is a simple code used to check the current load measured by the load cell.

```
'Check load after one compressive displacement'

RUN?
O=0
MP
A=1000
V=100000
D=-500   'Change value to increase or decrease compressive displacement'
G
TWAIT
UBI
b=UBA
Rb
P=0
G
TWAIT
END
```

findload.sms: This program is used to check the load after a set displacement before returning to the starting location. This program was used during validation due to the high repeatability of the displacement of the actuator. I was also used when determining the resistance of samples to different displacements.

```
'Moves actuator until desire load is reached, then returns'

RUN?

O=0             'resets the preload position to the zero position


A=1000
V=100000

j=1             'user input for cycles

i=0

WHILE i<j               'start of load cycling
        i=i+1
        C7
f=198           'user input for force
        q=-5            'position increment value
        UAI
        b=UAA

                WHILE b<=f              'run until voltage reaches user input for force

                        UAI
                        b=UAA
                        D=q             'position increment
                        G
                        TWAIT


                LOOP                    'once loop is ended, the load will have been found
        TWAIT
        UAI
        b=UAA
        Rb                      'reports voltage where the max load occured (user input for load)
LOOP

        P=0                     'moves actuator back to position where preload occured (unloads sample)
        G




END
```

target load.sms: This program is used to compress as sample to a desired load and then return to the starting location. This program was used during validation to apply repeated load to multiple pressure film samples.

APPENDIX B

SUPPLEMENTARY INFORMATION ON CHAPTER 3
(NITRIC OXIDE PRODUCTION)

B.1 Compression Programming

Load and displacement control programs were written in SmartMotor programming language. The displacement programs compresses to a target displacement and then returns to the starting location. The velocity and acceleration are adjusted to achieve 1 Hz motion. At the peak and valley of each cycle, the SmartMotor Interface (SMI) software on the PC records load, position, and time. This repeats for a desired number of cycles at which point the actuator returns to the starting position. Load control works by displacing a distance determine by the size of the error signal of the difference from the current load to the target load. The larger this error signal is, the greater the displacement. Following each movement, the program checks the load signal and moves again, a smaller distance for a smaller error signal. This loop continues until the target load is reached and then returns to the starting location of the test. This program also records the load, position, and time at the peak and valley of each cycle. An example of these programs can be seen below.

```
'10% Strain'

RUN?        'Run followed by ? enables program not to run when the motor is first powered up

UBI         'opens the A/D port containing the load cell signal

v=UBA           'this will be the voltage in counts from the load cell

C9
s=0         'user input for the preload

ss=-25      'position increment value for finding the preload

MP          'specifies position control
A=100
V=1000000

TWAIT           'waits until actuator is done moving to continue running the program
A=10000
V=1000000


'At this point the preload has been found

WAIT=8000       'wait 2 seconds
O=0             'sets the zero position to the position where the preload exists
CLK=0           'resets the clock
RP
UAI
b=UAA
Rb              'reports the position at start of test, should always be 0
RCLK            'reports the clock, should always be 0
GOTO1               'this tells the program to go to label C1


    'POSITION CONTORL IN THE NEXT PORTION OF CODE
C1
C8
x=7200      'user input for number of cycles

a=0
WHILE a<x
    a=a+1
    A=775       'this is the needed acceleration to achieve 1Hz loading

C7
V=44000
P=-1250     'VARIABLE SPEED DEPENDING ON USER DISPLACEMENT
    'USER INPUT POSITION

u=P         'sets u equal to the user position input
G
TWAIT
```

```
RP              'reports position at the displaced value
UAI
b=UAA
Rb
RCLK            'reports clock at displaced value
D=-u            'moves the opposite distance of what the user inputed for displacement
G
TWAIT                   'waits til actuator reaches the preload position
RP              'reports position at the preload position
UAI
b=UAA
Rb
RCLK            'reports clock at the preload position
LOOP            'end of position cycle

END
```

```
'0.1 MPa Load Control'

RUN?


UAI                 'opens the A/D convert port containing the load cell signal
b=UAA               'this will be the voltage in counts from the load cell
C9
s=2                 'user input for the preload
ss=-25          'position increment value
uu=25
MP                  'specifies position control

A=1000
V=1000000


        'WHILE b!=s
        '           UAI             'run until voltage reaches user input for preload
        '           b=UAA
        '       IF b>s
        '           D=uu            'position increment
        '       ELSEIF b<s
        '           D=ss
        '       ELSE b=s
        '           D=0
        '       ENDIF
        '           G
        '           TWAIT

        'LOOP

WAIT=8000   'waits at the preload position for 2 seconds
O=0         'resets the preload position to the zero position
CLK=0       'resets the clock
RP          'reports position at start
UAI         'sets A pin to input
b=UAA           'set variable b to analog of pin A
Rb          'reports voltage from pin A
RCLK        'reports clock

A=10000
V=1000000

GOTO1               'tells program to go to the label C1

C1


                        'END OF PRELOAD
                        'BEGINING OF LOAD CONTROL

C8
```

```
j=7200                  'user input for cycles

i=0

WHILE i<j               'start of load cycling
        i=i+1
        C7
f=18            'user input for force


        q=-10  'position increment value
        r=-100
        y=-200

        UAI
        b=UAA

A=10000
V=1000000

ll=f/3
mm=f/2
ee=CLK
                WHILE b<=f              'run until voltage reaches user input for force
                        UAI
                        b=UAA
                    IF b<ll
                        D=y
                    ELSEIF b<mm
                        D=r
                    ELSE
                        D=q
                    ENDIF
                        G
                    TWAIT


                LOOP                    'once loop is ended, the load will have been found

        TWAIT
        nn=CLK
        RP                      'reports position at max load
        UAI
        b=UAA
        Rb                      'reports voltage where the max load occured (user input for load)
        RCLK                    'reports clock where max load occured
        dd=nn-ee
        WAIT=2000-dd

        A=10000
        V=500000
        P=0                     'moves actuator back to position where preload occured (unloads sample)
        G
        aa=CLK
```

```
        cc=aa-ee
        WAIT=4000-cc                'waits 0.5 seconds before loading. may need to be changed if 1Hz is
critical
        RP
        UAI
        b=UAA
        Rb                  'reports voltage at preload
        RCLK                'reports clock at preload position
        LOOP

END
```

B.2 Design Drawings

Experiments performed in this research required some additional fixture and equipment to be made to increase accuracy and improve setup procedures. The fixtures made include a microtome for trimming explants and a fixture for loading and unloading explants. The first design for trimming the explants was not made. These drawings can be seen from pages 83-89. The simple form of the microtome used just a rectangular aluminum post with a cylinder cut to hold the explant while razors were used to trim both sides. These drawing can be seen in pages 90 and 91.

The fixture for loading and unloading the explants was a frame that set in the culture hood. The components were made of aluminum and feature a centering hole for the aluminum dish, and a rod used to suspend the plunger and cap above the dish during loading, preloading, and addition of media. The drawing of this fixture can be seen in pages 92-95.

Figure B.1: A picture of the setup frame assembled with the dish, plunger, and cap showing arrangement of fixture during sample loading and unloading.

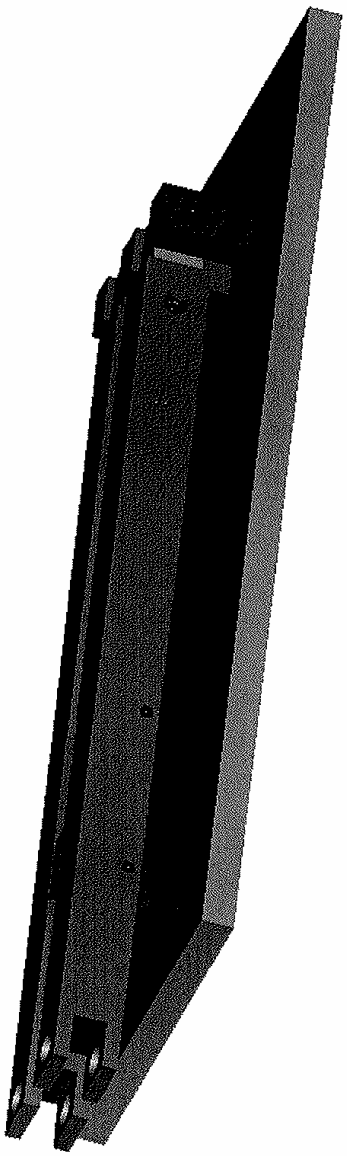

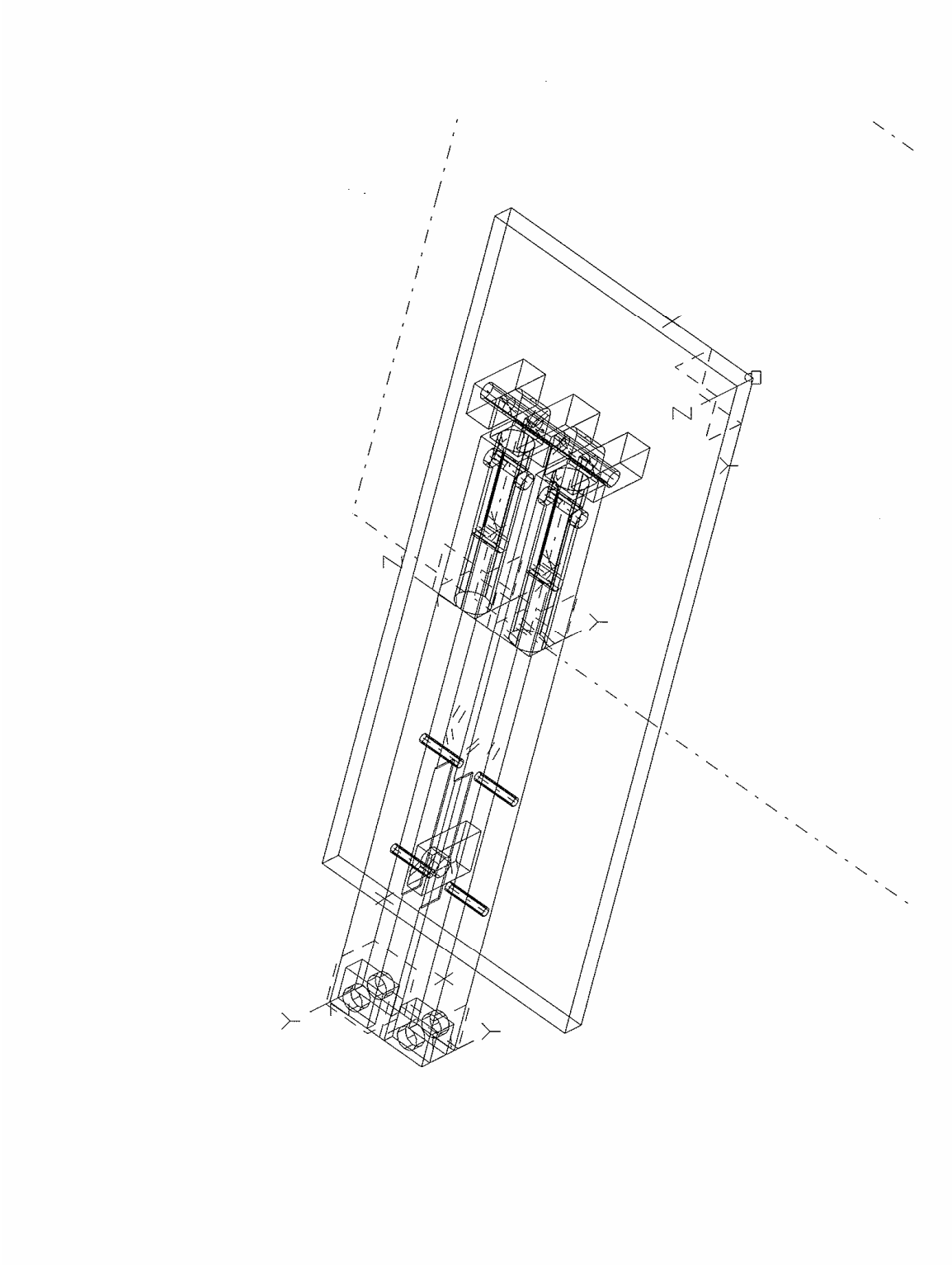

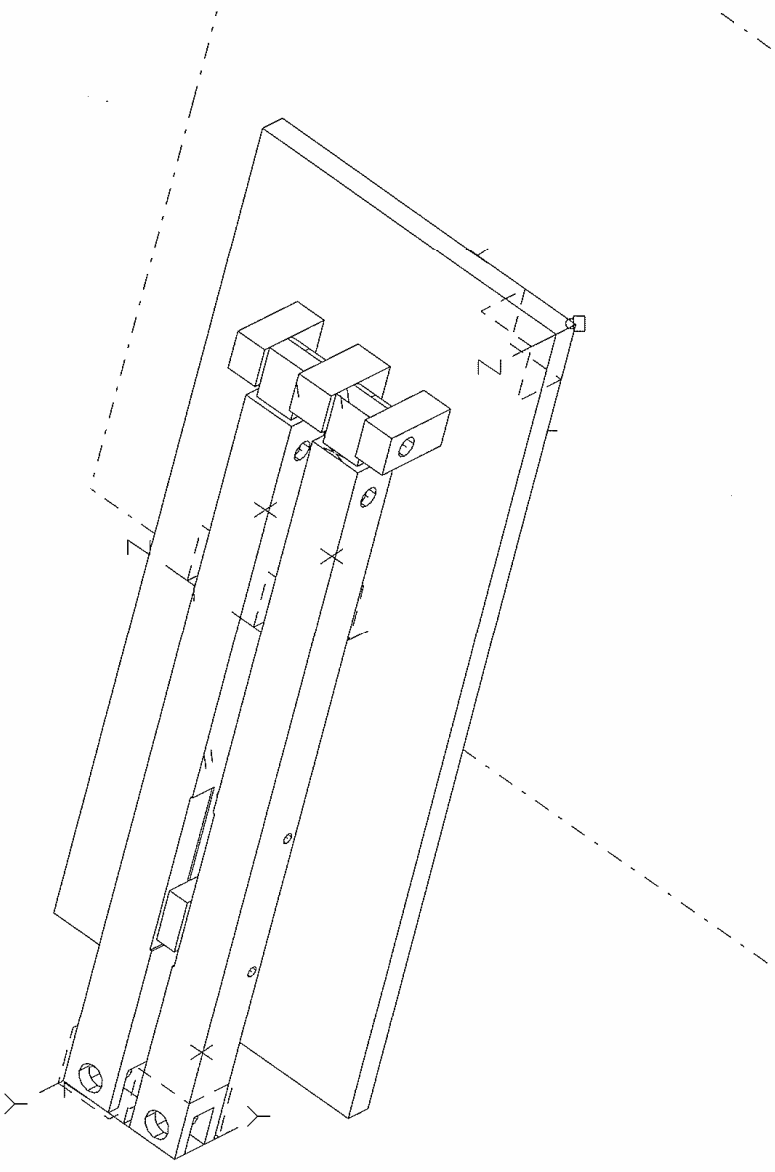
Z
Z
Y
Y

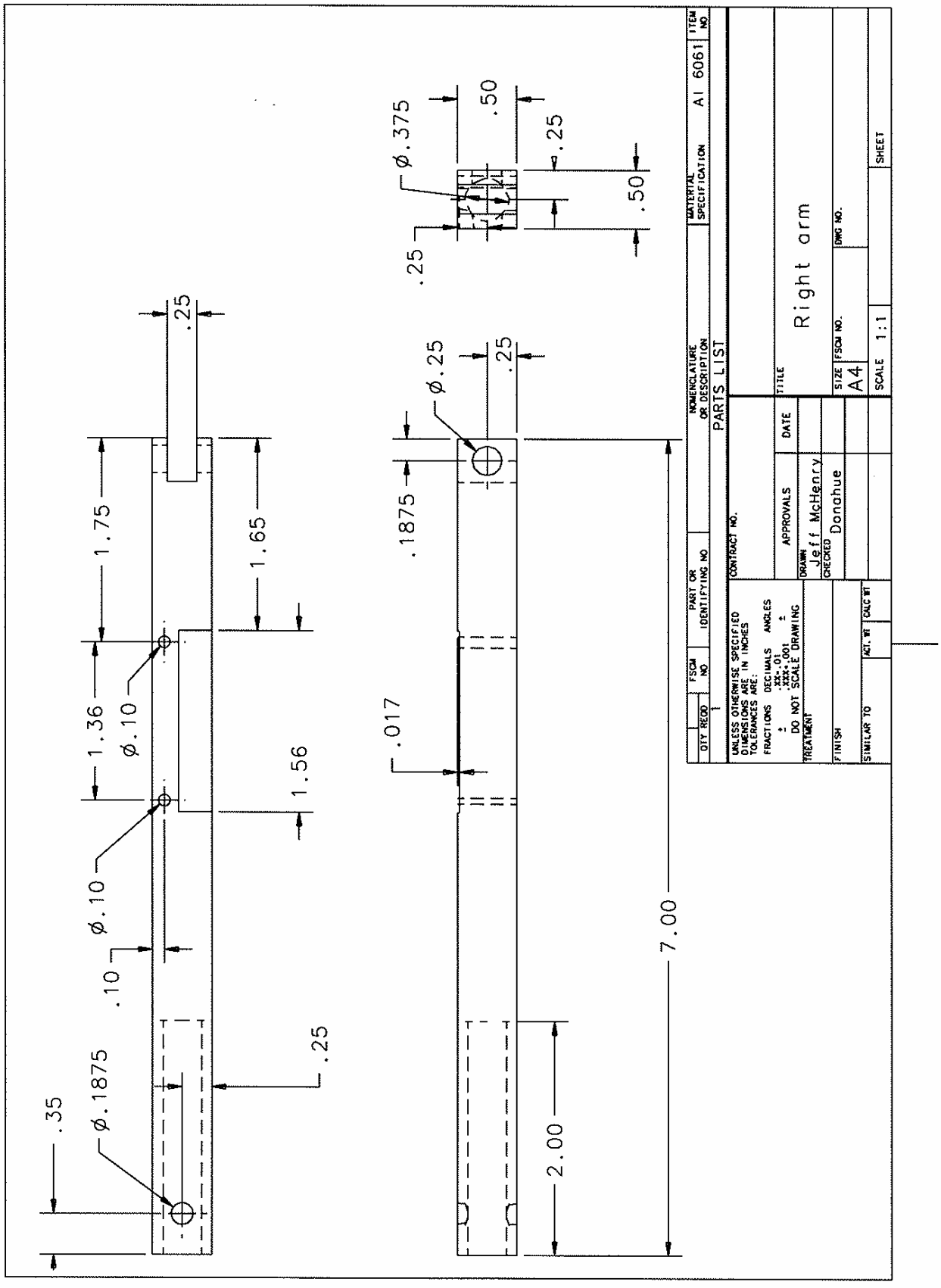
.35
Ø.1875
.10
Ø.10
Ø.10
1.36
1.75
1.56
1.65
.25
.25
2.00
.017
.1875
Ø.25
.25
7.00
Ø.375
.25
.50
.25
.50
ITEM NO.
1
QTY REQD
FSCM NO
PART OR IDENTIFYING NO
NOMENCLATURE OR DESCRIPTION
PARTS LIST
MATERIAL SPECIFICATION
Al 6061
CONTRACT NO.
UNLESS OTHERWISE SPECIFIED DIMENSIONS ARE IN INCHES TOLERANCES ARE:
FRACTIONS DECIMALS ANGLES
.XX ±.01
.XXX ±.001
DO NOT SCALE DRAWING
TREATMENT
FINISH
SIMILAR TO
MAT. WT
CALC WT
APPROVALS
DATE
DRAWN
Jeff McHenry
CHECKED
Donahue
TITLE
Right arm
SIZE
A4
FSCM NO.
DWG NO.
SCALE 1:1
SHEET

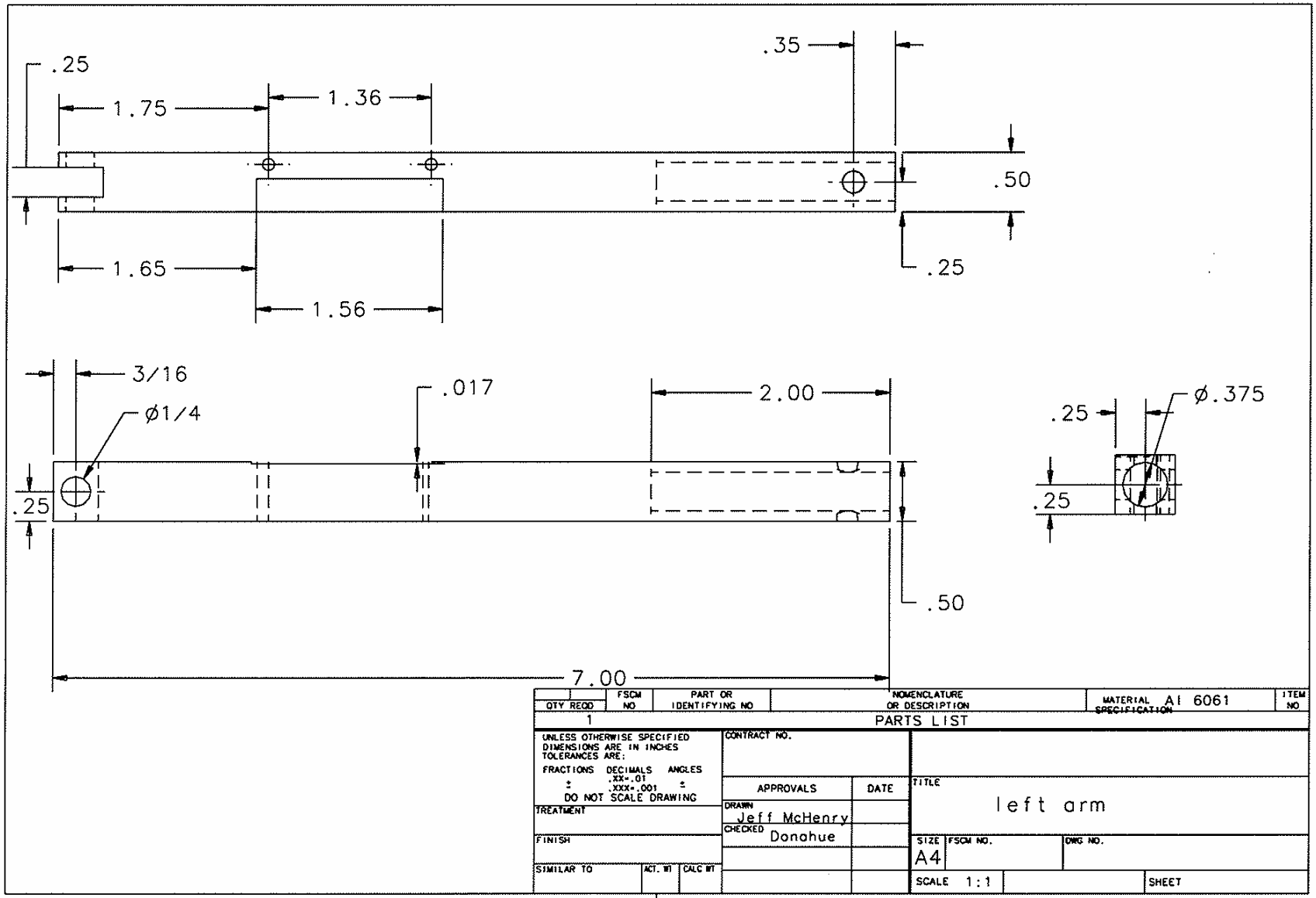
.25
1.75
1.36
.35
.50
1.65
1.56
.25
3/16
Ø1/4
.017
2.00
.25
.25
Ø.375
.50
7.00
QTY REQD
FSCM NO
PART OR IDENTIFYING NO
NOMENCLATURE OR DESCRIPTION
MATERIAL Al 6061
ITEM NO
1
PARTS LIST
UNLESS OTHERWISE SPECIFIED DIMENSIONS ARE IN INCHES TOLERANCES ARE:
FRACTIONS DECIMALS ANGLES
± .XX=.01 ±
.XXX=.001
DO NOT SCALE DRAWING
CONTRACT NO.
APPROVALS
DATE
DRAWN
Jeff McHenry
CHECKED
Donahue
TREATMENT
FINISH
SIMILAR TO
ACT. WT
CALC WT
TITLE
left arm
SIZE
A4
FSCM NO.
DWG NO.
SCALE 1:1
SHEET

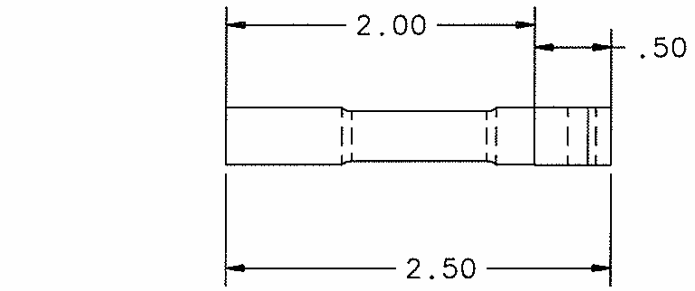

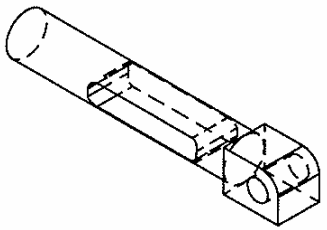

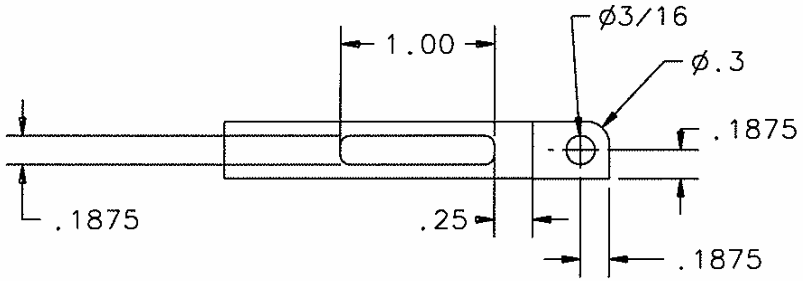

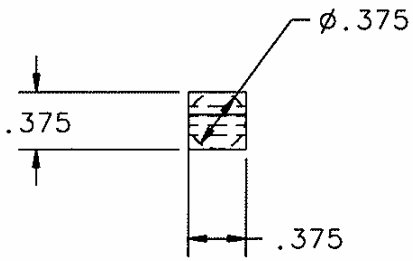

QTY REQD	FSCM NO	PART OR IDENTIFYING NO.	NOMENCLATURE OR DESCRIPTION	MATERIAL SPECIFICATION	ITEM NO
2			PARTS LIST	Al 6061	

UNLESS OTHERWISE SPECIFIED DIMENSIONS ARE IN INCHES
TOLERANCES ARE:
FRACTIONS DECIMALS ANGLES
± .XX=.01 ±
.XXX=.001
DO NOT SCALE DRAWING

TREATMENT

FINISH

SIMILAR TO | ACT. WT | CALC WT

CONTRACT NO.

APPROVALS	DATE
DRAWN Jeff McHenry	
CHECKED Donahue	

TITLE: lower arm

SIZE A4 | FSCM NO. | DWG NO.

SCALE 1:1 | SHEET

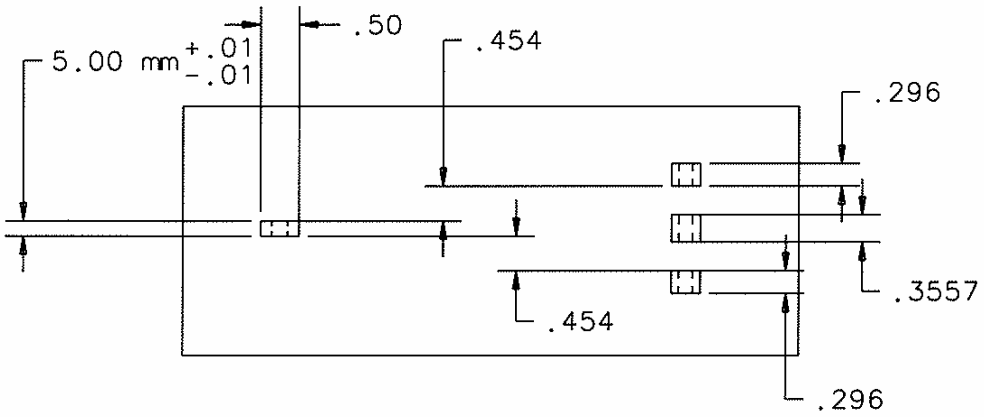

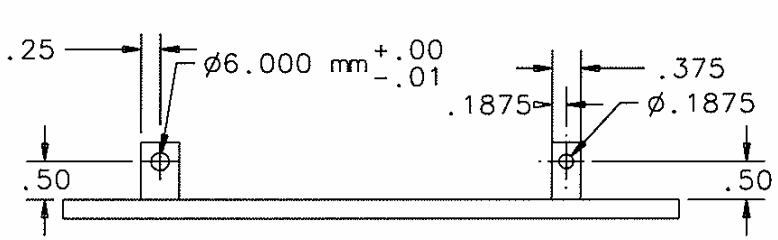

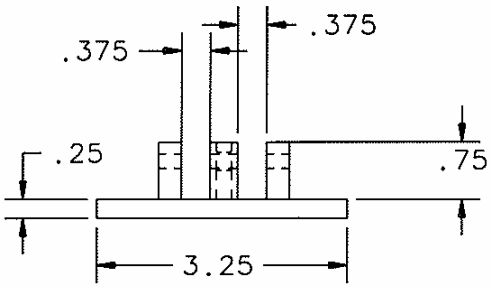

QTY REQD	FSCM NO	PART OR IDENTIFYING NO	NOMENCLATURE OR DESCRIPTION	MATERIAL SPECIFICATION	ITEM NO
1			PARTS LIST	Al 6061	

UNLESS OTHERWISE SPECIFIED DIMENSIONS ARE IN INCHES
TOLERANCES ARE:
FRACTIONS DECIMALS ANGLES
± .XX-.01 ±
.XXX-.001
DO NOT SCALE DRAWING

TREATMENT

FINISH

SIMILAR TO | ACT. WT | CALC WT

CONTRACT NO.

APPROVALS	DATE
DRAWN Jeff McHenry	
CHECKED Donahue	

TITLE: Base

SIZE A4 | FSCM NO. | DWG NO.

SCALE 1:1 | SHEET

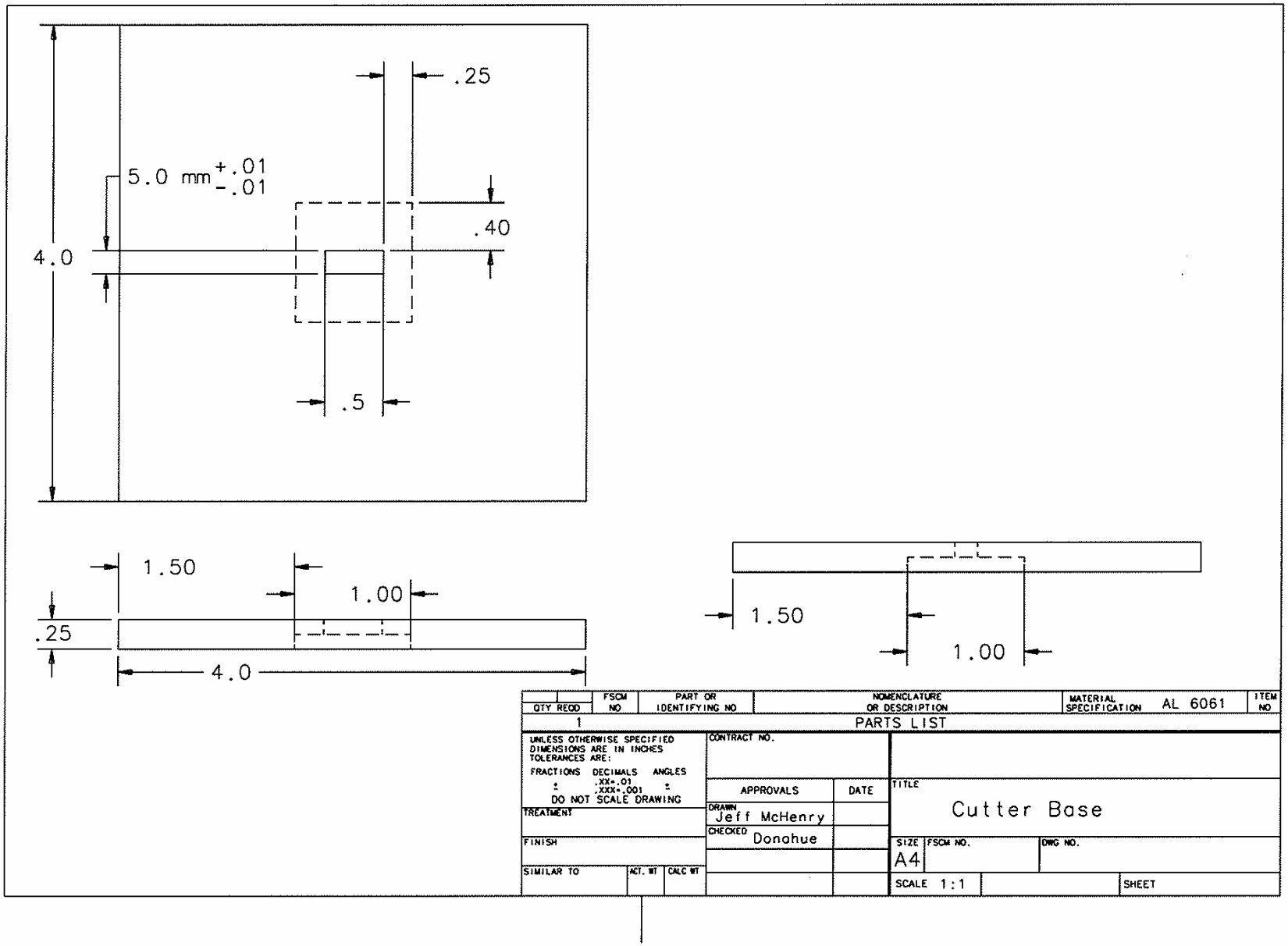
.25
5.0 mm +.01 -.01
.40
4.0
.5
1.50
1.00
.25
4.0
1.50
1.00
QTY REQD
FSCM NO
PART OR IDENTIFYING NO
NOMENCLATURE OR DESCRIPTION
MATERIAL SPECIFICATION
AL 6061
ITEM NO
1
PARTS LIST
UNLESS OTHERWISE SPECIFIED DIMENSIONS ARE IN INCHES TOLERANCES ARE:
FRACTIONS DECIMALS ANGLES
± .XX=.01 ±
.XXX=.001
DO NOT SCALE DRAWING
CONTRACT NO.
APPROVALS
DATE
DRAWN Jeff McHenry
CHECKED Donahue
TREATMENT
FINISH
SIMILAR TO
ACT. WT
CALC WT
TITLE
Cutter Base
SIZE A4
FSCM NO.
DWG NO.
SCALE 1:1
SHEET

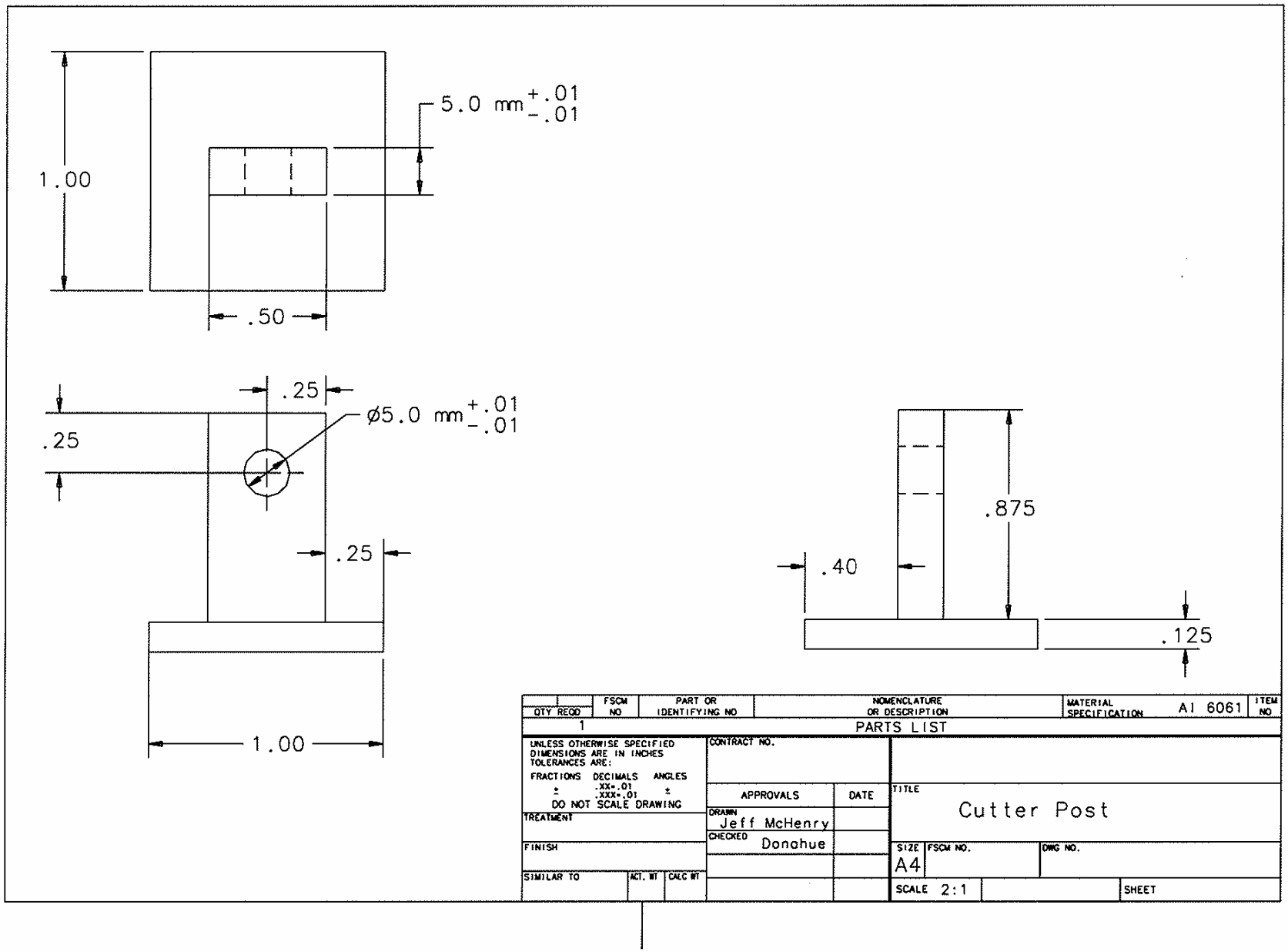
5.0 mm +.01 -.01
1.00
.50
.25
.25
Ø5.0 mm +.01 -.01
.25
1.00
.875
.40
.125
QTY REQD
FSCM NO
PART OR IDENTIFYING NO
NOMENCLATURE OR DESCRIPTION
MATERIAL SPECIFICATION
Al 6061
ITEM NO
1
PARTS LIST
UNLESS OTHERWISE SPECIFIED DIMENSIONS ARE IN INCHES TOLERANCES ARE:
FRACTIONS DECIMALS ANGLES
± .XX=.01 ±
.XXX=.01
DO NOT SCALE DRAWING
CONTRACT NO.
APPROVALS
DATE
DRAWN
Jeff McHenry
CHECKED
Donohue
TREATMENT
FINISH
SIMILAR TO
MAT. WT
CALC WT
TITLE
Cutter Post
SIZE
A4
FSCM NO.
DWG NO.
SCALE 2:1
SHEET

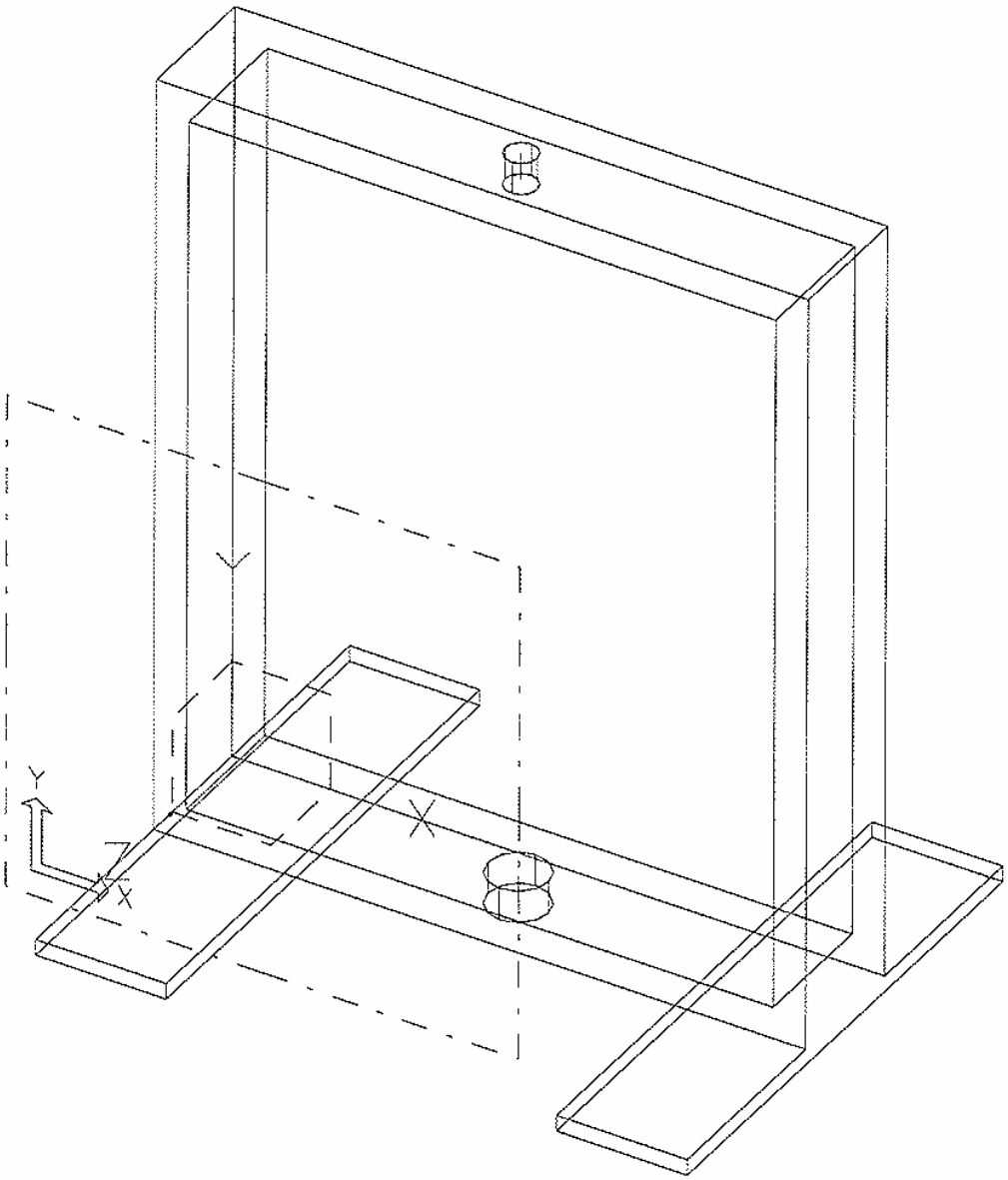
Y
Z
X
Y
X

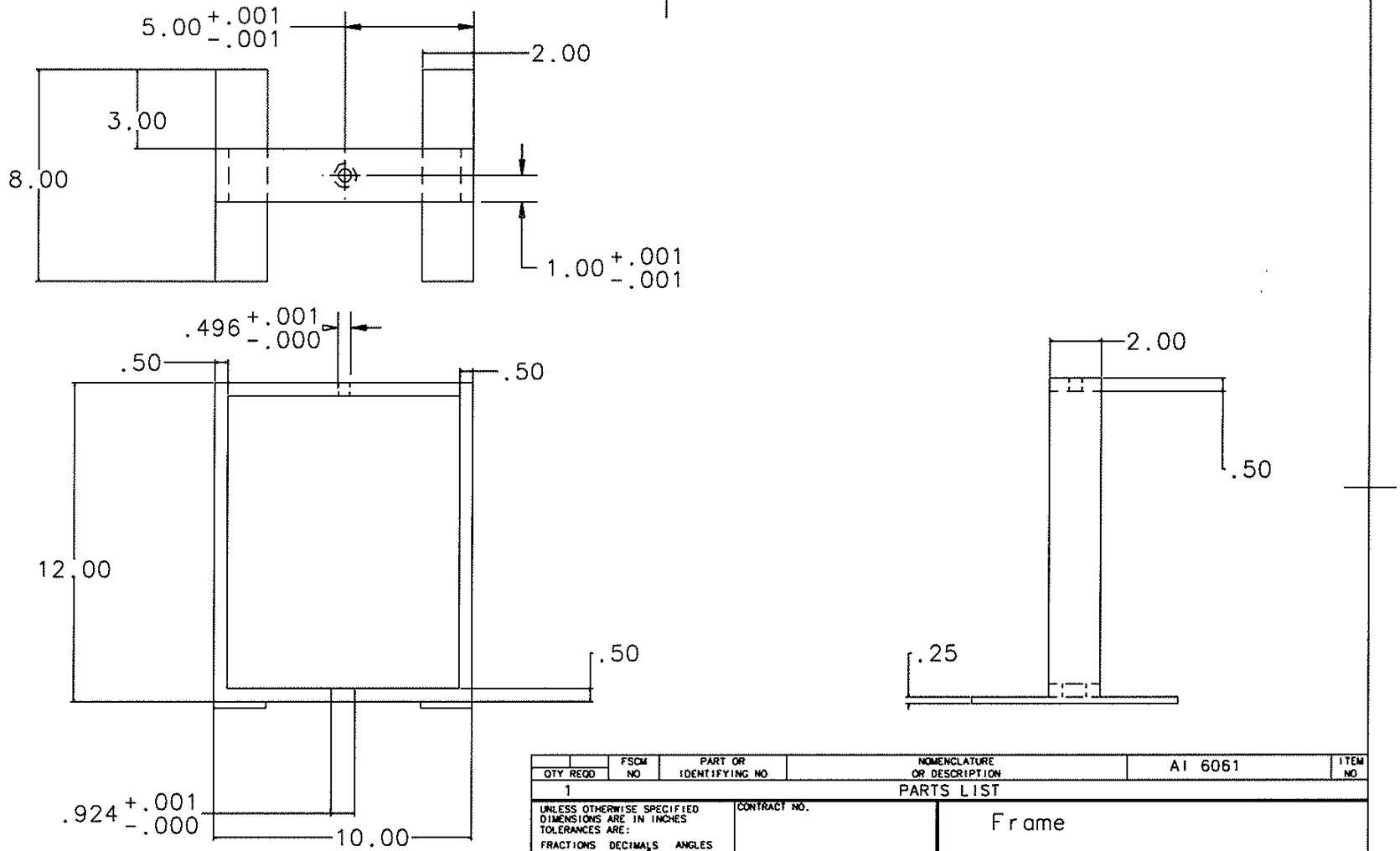

QTY REQD	FSCM NO	PART OR IDENTIFYING NO.	NOMENCLATURE OR DESCRIPTION	Al 6061	ITEM NO
1			PARTS LIST		

UNLESS OTHERWISE SPECIFIED DIMENSIONS ARE IN INCHES TOLERANCES ARE: FRACTIONS ± DECIMALS .XX-.5 .XXX- ANGLES ± DO NOT SCALE DRAWING	CONTRACT NO.	Frame
TREATMENT	APPROVALS / DRAWN	DATE / TITLE
FINISH	CHECKED	SIZE A4 / FSCM NO. / DWG NO.
SIMILAR TO / ACT. WT / CALC WT		SCALE / SHEET

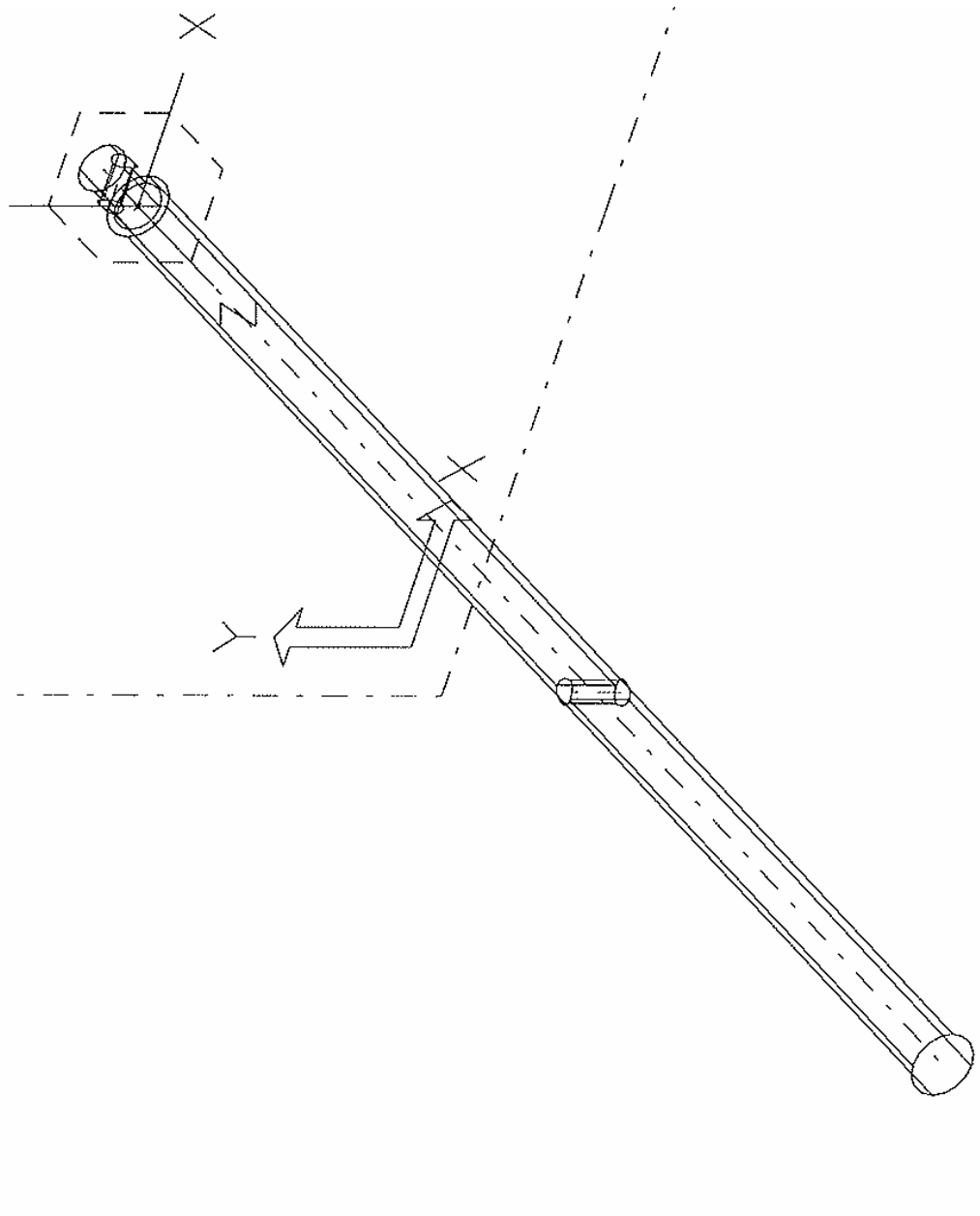

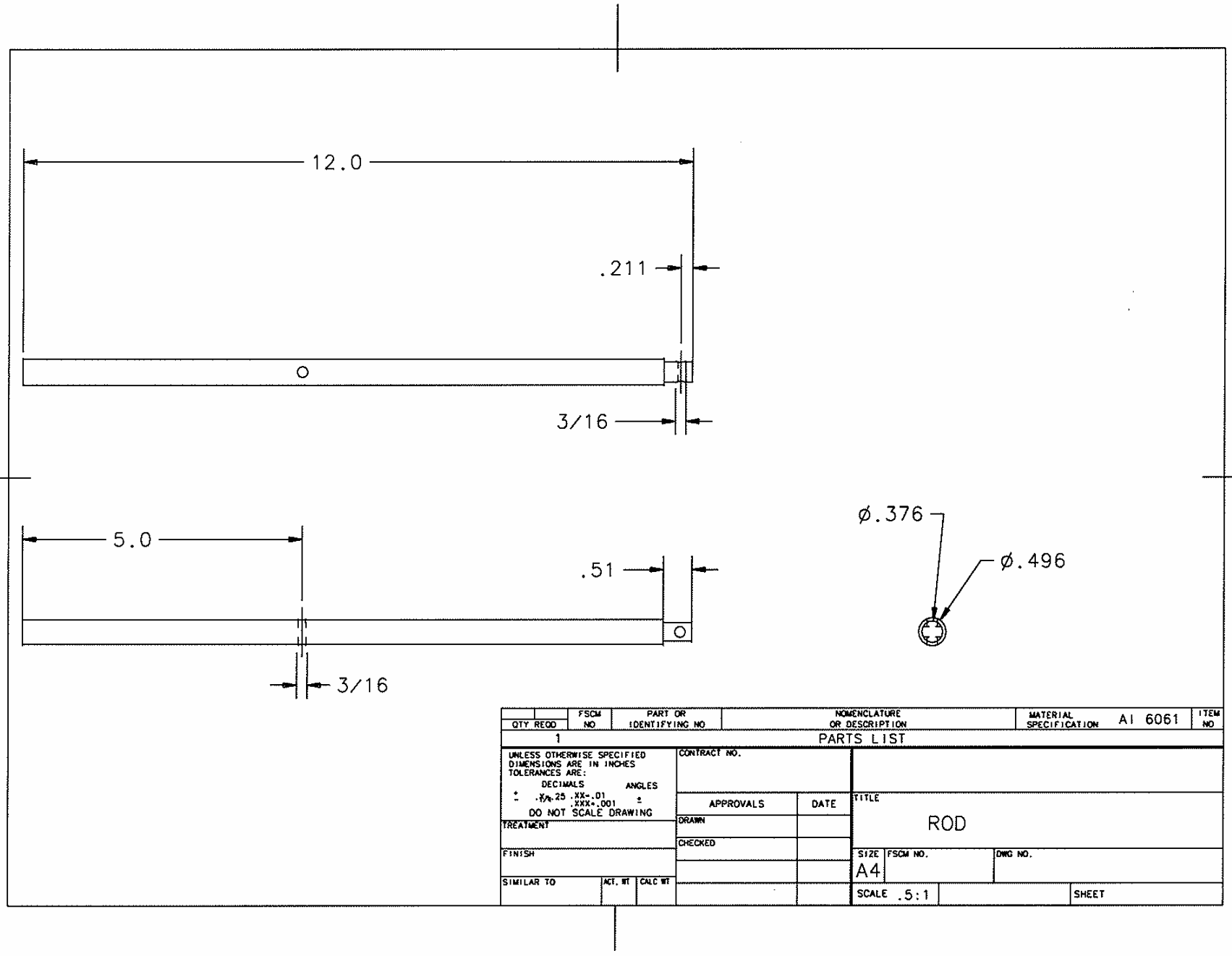
12.0
.211
3/16
5.0
.51
3/16
ø.376
ø.496
QTY REQD
FSCM NO
PART OR IDENTIFYING NO
NOMENCLATURE OR DESCRIPTION
MATERIAL SPECIFICATION
Al 6061
ITEM NO
1
PARTS LIST
UNLESS OTHERWISE SPECIFIED DIMENSIONS ARE IN INCHES TOLERANCES ARE:
DECIMALS
ANGLES
± .X/8 .25 .XX±.01 .XXX±.001 ±
DO NOT SCALE DRAWING
CONTRACT NO.
APPROVALS
DATE
DRAWN
CHECKED
TREATMENT
FINISH
SIMILAR TO
ACT. WT
CALC WT
TITLE
ROD
SIZE
A4
FSCM NO.
DWG NO.
SCALE .5:1
SHEET

B.3 Experiment Protocols

EXPLANT COMPRESSION EXPERIMENT

Time Period-	Setup (Day 1)	3 hrs
	Run Time (Day 2)	2.5 hrs/test (4 tests)
	Clean Up	0.5hrs
	Total	13.5 hrs

Equipment List:

Day 1:

1. Media: 2 80ml bottles, DMEM, Ham's F-12, FBS, Penn/Strep, 100-1000 µl pipette and tips,
2. Dissection Tools(sterile): Scalpel w/ 2 extra blades, tweezers, hemostat, drop cloth, PBS, culture dish
3. Explant tools: Dermal punches (3), Plexiglas plate, Alan wrench, microtome, razor, tweezers, microplate, media, pipette/tips, scalpel w/ blade, 96-well plate

Day 2:

4. Compression Setup: Frame w/ rod, 2 Alan wrenches, 6-well dish, plunger, cap, 100-1000 µL pipette and tips, media, tweezers, paper clip, culture dish, scale

Day 3:

5. Post compression: 24-well microplate, tweezers scalpel, frame, post-compression media, 100-1000 µl pipette and tips

A. Autoclave/Sterilize

1. Autoclave as much of the equipment as possible following the autoclave protocol.
2. Sterilize inside of culture hood using spray bottle of 75% isopropanol and wipe down.
3. Sterilize the remaining equipment by spraying with alcohol and placing in the culture hood.

B. Make Growth and Flow Media

Growth Media: 44.5% DMEM/F-12, 10% FBS, 1% Penn/Strep
Post Comp. Media: 48.5 % DMEM/F-12, 2% FBS, 1% Penn/Strep

1. Place all ingredients into 37˚C water bath for ~15 min.
2. Mix media in culture hood:
    - 20 ml growth media per animal
    - 40 ml post comp. media per animal
3. Make sure media is 37˚C before use with any tissue.

C. Dissection and Explant Removal

1. Dissect fresh porcine knee in culture hood using sterilized tools only.
2. Using cleans scalpel and tweezers remove medial and lateral meniscus and place in dish containing sterile Phosphate Buffered Saline 1X (PBS)
3. For explant removal place meniscus on clean surface (Plexiglas)
4. Remove 6 outer and 6 inner explants from each meniscus:
    - Place sharp dermal punch flat against top surface of meniscus and cut using turning motion.
    - Push tissue from punch into microtome using Alan wrench.
    - Using razor and sawing motion, trim explants removing as little top surface as possible.
    - Remove from microtome using tweezers.
5. Place in 96-well microplate keeping top surface up.
6. Fill wells with ~300 µl of growth media.
7. Label plates and place in incubator for 48 hours
8. After 24 hrs. remove old media with pipette and refill with fresh growth media.

D. Compression Testing

Compression Program:

1. On PC, open marrow folder on desktop and double click on SmartMotor Interface Icon.
2. Go to *File→Open* and select compression program out of C: Program File/ Program Editor
3. The following displacement control files are available for use: 5% disp.sms ; 10% disp.sms ; 15% disp. Sms ; 20 % disp.sms
4. The load control programs are: .1 Mpa.sms ; .5 Mpa.sms; 1 Mpa.sms
5. Make sure j equals the number of cycles desired and u equals the displacement desired.
    - 2500 counts = 1mm; (-) is the downward direction.
    - For load (300 lb load cell): f is the load variable and 0.8073 counts = 1 Newton
6. Turn the motor on (the switch on the power unit on top of the PC) and transmit the program by clicking the T button on the tool bar.
7. Turn on the 2100 System power by the switch on the lower right (below the channel dial):
    - Gain should be set to 200x with the dial at 1.35
    - Channel selector should be on channel 2.
    - Excit switch on channel 2 should be on.
    - Bridge volts on meter should read 10 volts.
    - For help use 2100 system manual.
8. The test is now ready to run after samples are loaded.

Loading Samples:

9. Make sure post comp. media is at 37°C

10. Place frame, dish, plunger, cap, and tools in the culture hood and sterilize.
11. Assemble the components into the frame (as shown in Figure 1) and place the explant in the center of each well top side up.
12. Maintain order of explants in each well. Well 1 is the well with alignment holes on each side.
13. Lower the plunger into contact with the explants keeping the cap suspended above with Alan wrench.
14. Fill each well with 400 µl of flow media using pipette.
15. Lower cap, remove from frame, and bring to bioreactor keeping it level and steady to prevent spilling from wells.
16. Attach the bottom pin first and then manually lower the actuator to match the top hole and attach top pin.
17. Turn the balance knob on channel 2 of the 2100 system until both light (at the top of channel 2) are extinguished.
18. Click the R button on the tool bar to run the test.
19. When test is complete, remove top pin, raise actuator (D=70000), and remove lower pin before bringing back to the culture hood.
20. Remove samples and media as desired and place in 24-well plates with post comp. media (2% FBS).
    - Explants need to be cut into superficial and deep zones using tweezers and scalpel.
    - Weight each explant half (with scale placed in incubator) and put in separate wells in 24 well plate.
    - Add 1 ml of flow media into each well.
    - Place into incubator with CO_2 supply.
21. Incubate 24 hours.
22. After incubation time, immediately separate media and tissue samples into clean, labeled 1.5 ml centrifuge tubes and immediately put on ice.
    - Use parafilm on centrifuge tubes containing media samples.
23. Immediately bring samples to -80˚C freezer. Place media sample directly into freezer. Tissue sample must be frozen in liquid Nitrogen tank for 24 hrs prior to being placed into freezer.

Testing Data:

24. Place the cursor at the bottom of the data sting in the smart motor command window. Highlight the data by moving to the top of the data string and pressing SHIFT + Left Mouse Button.
25. Go to *Edit-Copy* and then paste in Excel spreadsheet.
26. Go to *File-Open* go to local C, open *Excel Macro* folder and open *Macrotest* to open the Excel spreadsheet that contains the macro to separate the data into columns. Minimize that window.
27. Highlight the first cell of the data string.
28. Go to *Tools-Macro-Macros…,* highlight *dispwload* and click *Run*. This will separate the data into time, load, and displacement columns.
29. Divide the time column by 4000 (=A1/4000) to get time in seconds; Divide the displacement by 2500 to convert to millimeters.

* The time column is the column with the greatest values; The displacement column contain negative numbers representing compression.

30. For load: subtract the initial load reading from all of the value to start at zero load. Then divide the data by 0.8073 to get load in Newtons.

Nitric Oxide assay:

1. Follow the protocol given in the Nitric Oxide assay kit instructions.
2. Turn the microplate reader on: Switch on back right.
3. Log into the computer and open the SOFTmax PRO software on the desktop.
4. On the top tool bar that says (READ), click on the thermometer icon and set the temperature to 37°C.
   * Wait until the read out on the upper left reaches 37°C before performing the test.
5. On the top menu, click on *Assays*, then click on *Set Folder*, *Select Directory* will pop up, double click on SOFTmax PRO 4.0 and in that folder open *Basic Protocols.*
6. Again on the top menu, click on *Assays*, and open up *Basic Endpoint Protocols*.
7. In the *Plate #1* section click on setup and open setup menu.
8. Turn the wavelength to 540 nm.
9. Turn *automix* on at the default 5 sec. before first read.
10. Click OK in the lower right and close the setup menu.
11. Click on *Template* and open the menu.
12. Click and drag the sections of Standards, Controls, Unknowns, and Blanks to each section of wells by the using the pull down menu in the upper left.
13. Set the Standards and Unknowns in *Series* to help with data graphs.
14. Close template.
15. ***Click READ and run the experiment.***

LOAD PROGRAM ADJUSTMENT

1. Determine the total Newton force that will be applied by the SmartMotor (Newtons per explant multiplied by 6)
2. Multiply the total Newton force by 0.8073 and then add 3. This puts the force in counts for the SmartMotor to read. The addition of three accounts for the intial reading when both lights are extinguished on the 2100 system.
3. Change the f =… value in the load program code to the value found in step 2 (Highlighted below).

```
.
.

C8
j=7200          'user input for cycles

i=0

WHILE i<j               'start of load cycling
        i=i+1
        C7
f=27            'user input for force


        q=-10   'position increment value
        r=-100
        y=-200

        UAI
        b=UAA

A=10000
V=1000000

ll=f/3
mm=f/2
ee=CLK
                WHILE b<=f              'run until voltage reaches user input for force
                                UAI
                                b=UAA
                        IF b<ll
                                D=y
                        ELSEIF b<mm
                                D=r
                        ELSE
                                D=q
                        ENDIF
```

Save program with pressure as file name, transmit (T), and run (R) the program.

LIVE/DEAD ASSAY PROTOCOL

Sample Prep.	10 min
Incubation	30 min
Fluor. Detect	30 min
Clean up	10 min
Total	80 min

Equipment List:

1. Live/Dead assay kit w/ fluorescent dye (L3224, Molecular Probes)
2. Fluorescent microscope
3. Microscope slides
4. Tweezers
5. Scalpel
6. 96-well plate
7. Phosphate Saline Buffer (PBS)
8. 100-1000 µl pipette w/ tips
9. Aluminum foil
10. 10 ml centrifuge tubes
11. Insulated container

Stain Solutions:

1. Allow staining chemicals to warm to room temperature before use.
2. Stain is photosensitive, keep staining chemicals and mixtures out of direct light. (Turn off light in culture hood.)
3. In two 10 ml centrifuge tubes mix chemicals with sterile PBS to the following concentrations:
   ~1 µM calcein AM; 8 µM ethidium homodimer-1
   - 4 ml vol: 16 µl eth. H-1 + 4 ml PBS
   - 4 ml vol: 1 µl cal. AM + 4 ml PBS
4. Wrap tube is aluminum foil to keep out light.

Sample Preparation:

1. Using pipette, fill 1 column of 96-well plate with PBS (~300 µl per well)
2. Using scalpel and tweezers, cut a thin (< 1mm) slice of meniscal tissue keeping track top and bottom of tissue.
3. Cut tissue into top and bottom halves and place/wash in wells filled with PBS.
4. Transfer tissue into blank wells.
5. Cover each piece of tissue with stain (~100 µl of each stain)
   * May require more stain depending on sample size.
6. Wrap plate in aluminum foil and incubate at 37°C for 30-60 min.

Fluorescent Detection:

1. Following incubation place plate in insulated container along with tweezers and microscope slide.
2. Wash/ place the tissue sample is clean PBS.
3. Turn on fluorescent lamp, computer, and monitor.
   * Fluorescent lamp must remain on a minimum of 30 min.
4. Open the desktop icons *DP Controller* and *DP Manager.*
5. Place tissue on slide and align in microscope using either the 10x or 20x lens.
6. Turn shutter switch on and view under red (dead) and green (live) fluorescence (~500 nm for red: setting 4; ~600 nm for green: setting 3)
   * Focus using red fluorescence first due to image clearity.
7. Make sure slide bar on top right of microscope is halfway out allowing eyepiece and camera viewing.
8. On *DP controller*, under Capture tab (far left), click on the play button (far left) just next to the capture button (camera icon).
9. Decrease the pixel size to 1360x1024 in the drop down box next to the capture button.
10. Lower the intensity under the Intensity tab by moving the arrow to the right on graph (far left) until the image is clear.
11. Under capture tab click on the capture button (picture of a camera) to record the picture on the screen.
12. The image appears on the DP manager for saving to different directories.

Image Merging:

1. Go to *Start* and open *My Computer*.
2. Open *Local C* and click on the *SPOTC*am folder.
3. Double Click on the *SPOT32* icon.
4. Go to *File-Open Image File* and open the first image you want to merge.
5. Go to *Edit-Merge Images*
6. Check the red and green channels.

Whatever color the initial image is, select *CurrentlyOpen* on that channel. For the other channel select *Image File* and click the (…) button. Select the file and Click OK to merge the two files.

B.4 Nitric Oxide Production Raw Data

Nitric oxide produced by the meniscal explants was measured using a total nitric oxide assay by Cayman Chemical (Ann Arbor, MI). The media samples were filtered and loaded into 96 well plates according to the protocol supplied by the assay kit. Wells were organized and recorded using abbreviations for animal, location, and layer tested. For example A6LL2T represents **A**nimal **6**, **L**eft knee, **L**ateral, **2**nd explant from anterior, **T**op of explant; A12RM3B represents **A**nimal **12**, **R**ight knee, **M**edial, **3**rd explant from anterior, **B**ottom of explant. The data collected required converting the microplate to nitrite concentration using the standard curve produced in the assay. The data was then normalized by wet weight of the tissue samples and divided into categories of strain/load level for data analysis. The following tables show the explants tested, the strain/load levels, the raw data, and the conversion to normalized and arranged data.

	1	2	3	4	5	6	7	8	9	10	11	12
A	0	A1LM2T	A3RL2T	A1LL2T	A4LL2T	A2RL1T	A4LM2T	A4RM2T	A2LM2T	A9LL1T	A9RL3T	
B	5	A1LM2B	A3RL2B	A1LL2B	A4LL2B	A2RL1B	A4LM2B	A4RM2B	A2LM2B	A9LL1B	A9RL3B	
C	10	A1LM3T	A3RL3T	A1LL3T	A4LL3T	A2RL2T	A4LM3T	A4RM3T	A2LM3T	A9LL3T	A9RL4T	
D	15	A1LM3B	A3RL3B	A1LL3B	A4LL3B	A2RL2B	A4LM3B	A4RM3B	A2LM3B	A9LL3B	A9RL4B	
E	20	A2LM4T	A3LL2T	A2LL2T	A3RM3T	A1RL3T	A3LL4T	A3LM2T	A1RL2T	A9LM2T	A9LL2T	
F	25	A2LM4B	A3LL2B	A2LL2B	A3RM3B	A1RL3B	A3LL4B	A3LM2B	A1RL2B	A9LM2B	A9LL2B	
G	30	A2LM5T	A2RM3T	A2LL3T	A3RM2T	A1RL4T	A3LM4T	A3LL3T	A1RL3T	A9LM3B	A9LM6T	
H	35	A2LM5B	A2RM3B	A2LL3B	A3RM2B	A1RL4B	A3LM4B	A3LL3B	A1RL3B	A9LM3T	A9LM6B	

	1	2	3	4	5	6	7	8	9	10	11	12
A	Std.	c	c	10%	10%	15%	15%	5%	5%	20	0.1	
B	Std.	c	c	10%	10%	15%	15%	5%	5%	20	0.1	
C	Std.	c	c	10%	10%	15%	15%	5%	5%	20	0.1	
D	Std.	c	c	10%	10%	15%	15%	5%	5%	20	0.1	
E	Std.	c	c	10%	10%	5%	15%	5%	5%	0.05	c	
F	Std.	c	c	10%	10%	5%	15%	5%	5%	0.05	c	
G	Std.	c	c	10%	10%	15%	15%	5%	5%	0.05	c	
H	Std.	c	c	10%	10%	15%	15%	5%	5%	0.05	c	

Table B.1: This table shows the arrangement of the first 96-well microplate that was set up for the total NO assay kit. The top section shows the samples used and the bottom shows what strain/load level was represented by each sample.

READINGS	1	2	3	4	5	6	7	8	9	10	11	12
A	0.003	0.039	0.064	0.025	0.03	0.03	0.039	0.039	0.031	0.097	0.072	-0.0005
B	0.143	0.046	0.063	0.031	0.051	0.062	0.045	0.046	0.039	0.086	0.059	-0.003
C	0.301	0.09	0.064	0.027	0.039	0.039	0.05	0.046	0.042	0.072	0.057	-0.004
D	0.452	0.022	0.062	0.035	0.046	0.029	0.043	0.117	0.039	0.081	0.051	-0.006
E	0.576	0.045	0.117	0.039	0.061	0.027	0.097	0.056	0.05	0.07	0.061	-0.006
F	0.733	0.063	0.075	0.048	0.079	0.055	0.083	0.132	0.056	0.111	0.108	0.035
G	0.815	0.034	0.034	0.027	0.063	0.032	0.066	0.065	0.055	0.069	0.068	-0.004
H	0.96	0.04	0.026	0.034	0.059	0.047	0.058	0.053	0.043	0.078	0.086	-0.007

5.684982	13.01099	1.582418	3.047619	3.047619	5.684982	5.684982	3.340659	22.68132	15.35531
7.736264	12.71795	3.340659	9.201465	12.42491	7.443223	7.736264	5.684982	19.45788	11.54579
20.63004	13.01099	2.168498	5.684982	5.684982	8.908425	7.736264	6.564103	15.35531	10.95971
0.703297	12.42491	4.512821	7.736264	2.754579	6.857143	28.54212	5.684982	17.99267	9.201465
7.443223	28.54212	5.684982	12.13187	2.168498	22.68132	10.66667	8.908425	14.76923	12.13187
12.71795	16.23443	8.322344	17.40659	10.37363	18.57875	32.93773	10.66667	26.78388	25.90476
4.21978	4.21978	2.168498	12.71795	3.6337	13.59707	13.30403	10.37363	14.47619	14.18315
5.978022	1.875458	4.21978	11.54579	8.029304	11.25275	9.787546	6.857143	17.11355	19.45788

Weight(g)										
0.0689	0.0875	0.0562	0.0707	0.049	0.0553	0.0693	0.0658	0.0496	0.0605
0.077	0.044	0.0677	0.084	0.062	0.0473	0.0671	0.0602	0.0524	0.0552
0.0297	0.0742	0.06	0.0655	0.0717	0.0553	0.0612	0.0585	0.0595	0.0621
0.0931	0.032	0.0645	0.07	0.0711	0.0441	0.0711	0.071	0.0634	0.0525
0.0765	0.0618	0.0583	0.0829	0.0606	0.0464	0.0881	0.0523	0.0759	0.0455
0.0574	0.0424	0.063	0.0471	0.0752	0.0516	0.0726	0.0734	0.0516	0.0378
0.0828	0.0825	0.0631	0.0745	0.0655	0.071	0.0915	0.0606	0.0678	0.0862
0.0626	0.0774	0.0628	0.0563	0.0391	0.0515	0.0557	0.0752	0.0432	0.0639

µM/g										
82.51062	148.697	28.1569	43.10635	62.19631	102.8026	82.03437	50.7699	457.2847	253.8068
100.471	289.0443	49.34504	109.5413	200.4017	157.362	115.2945	94.43491	371.3335	209.1628
694.614	175.3503	36.14164	86.79361	79.28845	161.0927	126.4095	112.2069	258.0725	176.4848
7.554207	388.2784	69.96621	110.5181	38.74232	155.4908	401.4364	80.07016	283.7961	175.266
97.29704	461.8467	97.51255	146.3434	35.7838	488.8215	121.0745	170.3332	194.588	266.6345
221.5671	382.8876	132.1007	369.5667	137.9472	360.0534	453.6877	145.3224	519.0675	685.3112
50.96353	51.14885	34.36606	170.7107	55.47633	191.508	145.3992	171.182	213.5131	164.5377
95.49556	24.23072	67.19395	205.0762	205.353	218.4999	175.719	91.18541	396.1471	304.5051

Table B.2: The top section show the reading produced by the microplate reader. The next portion is the concentration as determined by the standard curve produce by column 1. The next section shows the weight (g) of each sample for normalization and final concentration in µM/g.

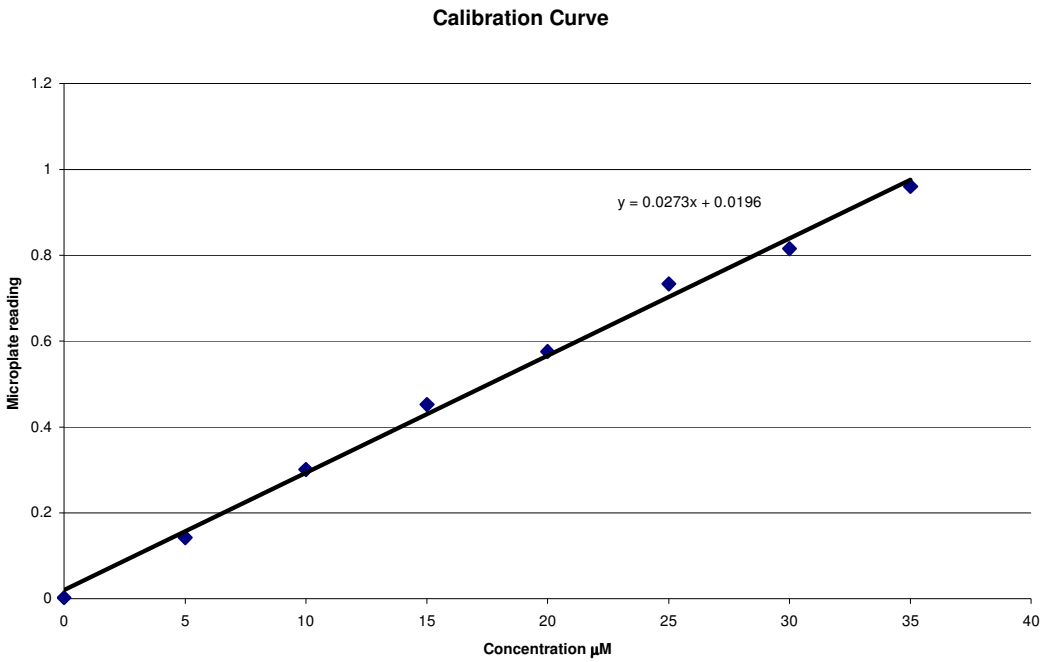

Figure B.2: The calibration curve used for the first NO assay to convert microplate reading to concentration of nitrite.

	1	2	3	4	5	6	7	8	9	10	11	12
A	0 A8LL1T	A7LL1T	A5LL1T	A6RL1T	A7RM1T	A9RM3T	A11RL1T	A11LL3T	A12RL1T	A12LM2T		
B	5 A8LL1B	A7LL1B	A5LL1B	A6RL1B	A7RM1B	A9RM3B	A11RL1B	A11LL3B	A12RL1B	A12LM2B		
C	10 A8LL2T	A7LL2T	A5LL2T	A6RM2T	A7RM2T	A9RM4T	A11RL2T	A11LL5T	A12RL2T	A12LM3T		
D	15 A8LL2B	A7LL2B	A5LL2B	A6RM2B	A7RM2B	A9RM4B	A11RL2B	A11LL5B	A12RL2B	A12LM3B		
E	20 A8LM1T	A7LM1T	A6LL3T	A6LM3T	A7RL1T	A11LL1T	A11RM1T	A12LL1T	A12RM1T			
F	25 A8LM1B	A7LM1B	A6LL3B	A6LM3B	A7RL1B	A11LL1B	A11RM1B	A12LL1B	A12RM1B			
G	30 A8LM2T	A7LM2T	A6LL4T	A6LM4T	A7RL2T	A11LL2T	A11RM2T	A12LL2T	A12RM4T			
H	35 A8LM2B	A7LM2B	A6LL4B	A6LM4B	A7RL2B	A11LL2B	A11RM2B	A12LL2B	A12RM4B			

20%	5	15	15	LPS	C	.05	C	.05	C
20%	5	15	15	LPS	C	.05	C	.05	C
20%	5	15	15	LPS	C	.05	C	.05	C
20%	5	15	15	LPS	C	.05	C	.05	C
.1	10	5	10	15	20	.1	20	.1	
.1	10	5	10	15	20	.1	20	.1	
.1	10	5	10	15	20	.1	20	.1	
.1	10	5	10	15	20	.1	20	.1	

Table B.3: This table shows the arrangement on the microplate and strain/load levels of the samples used for the second total NO assay.

weight (g)		0.0408	0.0528	0.0551	0.0883	0.0607	0.0638	0.0632	0.0704	0.059	0.0631
		0.0869	0.061	0.0753	0.0565	0.0907	0.058	0.0717	0.0534	0.073	0.0657
		0.047	0.0803	0.0713	0.0664	0.0682	0.0555	0.08	0.0872	0.0754	0.0652
		0.0671	0.0557	0.06	0.0683	0.071	0.0535	0.051	0.0475	0.0546	0.0516
		0.0532	0.0514	0.0607	0.0722	0.0489	0.074	0.0653	0.0661	0.057	
		0.073	0.0707	0.0723	0.0686	0.0671	0.048	0.0724	0.0605	0.0504	
		0.0586	0.0537	0.0503	0.0703	0.0489	0.0621	0.0729	0.068	0.0592	
		0.0671	0.0657	0.0847	0.072	0.0622	0.049	0.0675	0.058	0.0591	
conc.(uM)	standards					microplate reading					
0	0.007	0.232	0.1	0.118	0.16	0.147	0.055	0.11	0.095	0.098	0.124
5	0.158	0.174	0.074	0.109	0.09	0.142	0.077	0.094	0.073	0.112	0.062
10	0.3	0.139	0.136	0.095	0.111	0.137	0.069	0.074	0.094	0.073	0.113
15	0.437	0.169	0.089	0.089	0.067	0.15	0.059	0.066	0.078	0.076	0.061
20	0.58	0.154	0.031	0.099	0.131	0.038	0.183	0.068	0.112	0.173	
25	0.727	0.178	0.065	0.127	0.096	0.071	0.12	0.109	0.122	0.113	
30	0.822	0.201	0.039	0.081	0.079	0.032	0.127	0.066	0.082	0.131	
35	1.022	0.122	0.037	0.075	0.075	0.024	0.092	0.068	0.069	0.068	

calc conc.(uM)									
38.84752	15.44326	18.63475	26.08156	23.7766	7.464539	17.21631	14.55674	15.08865	19.69858
28.56383	10.83333	17.03901	13.67021	22.89007	11.36525	14.37943	10.65603	17.57092	8.705674
22.35816	21.82624	14.55674	17.39362	22.00355	9.946809	10.83333	14.37943	10.65603	17.74823
27.6773	13.49291	13.49291	9.592199	24.30851	8.173759	9.414894	11.54255	11.18794	8.528369
25.01773	3.20922	15.26596	20.93972	4.450355	30.15957	9.769504	17.57092	28.38652	
29.27305	9.237589	20.2305	14.73404	10.30142	18.98936	17.03901	19.34397	17.74823	
33.35106	4.62766	12.07447	11.71986	3.386525	20.2305	9.414894	12.25177	20.93972	
19.34397	4.27305	11.01064	11.01064	1.968085	14.02482	9.769504	9.946809	9.769504	

Conc. (uM/g)									
952.145	292.486	338.1988	295.3744	391.7067	116.999	272.41	206.7718	255.7399	312.1804
328.6977	177.5956	226.2816	241.9507	252.3712	195.9526	200.55	199.5511	240.6976	132.5064
475.7054	271.8087	204.1618	261.9521	322.6326	179.2218	135.4167	164.9018	141.3266	272.2121
412.4785	242.2425	224.8818	140.4421	342.3734	152.7805	184.6058	243.0011	204.9074	165.2785
470.2581	62.43618	251.4985	290.0238	91.0093	407.5618	149.6095	265.8233	498.0092	
401.0007	130.659	279.8132	214.782	153.5234	395.6117	235.3454	319.7351	352.1474	
569.1308	86.17616	240.0491	166.7121	69.25409	325.7729	129.1481	180.1731	353.7114	
288.2857	65.03881	129.9957	152.9255	31.64124	286.2209	144.7334	171.4967	165.3046	

Table B.4: This table shows the weight of the explants in the top section, then the microplate reading, the calculated concentration using the calibration, and last the concentration normalized by weight of the tissue. This data corresponds to the data in Table B.3.

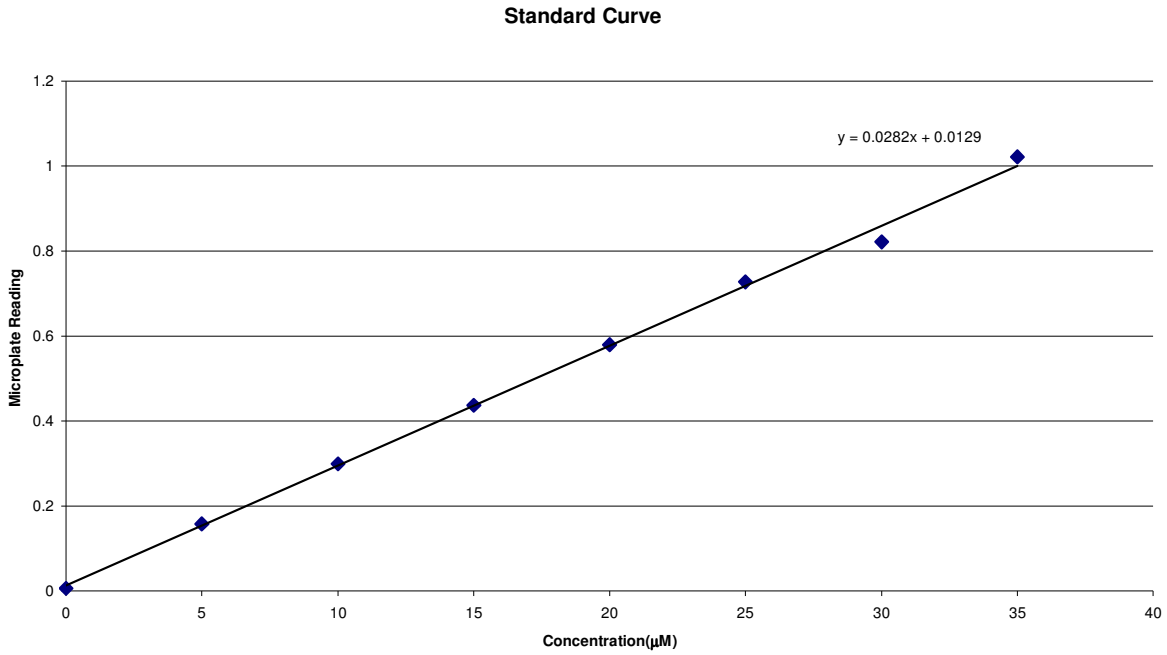

Figure B.3: This is the standard curve created for the second nitric oxide assay. This was used to convert the microplate readings to concentration in μM.

	Averages (μM/g)									
	Control		5%		10%		15%		20%	
	T	B	T	B	T	B	T	B	T	B
	388.5623	54.01258	58.90908	126.6209	32.14927	59.65563	70.74238	119.572	357.6786	327.5648
	74.13028	158.5313	123.742	427.562	65.9393	99.64733	79.13945	181.3575	713.9252	370.5881
	162.0236	338.6613	98.08456	135.0769	64.94998	110.0297	324.9571	257.7721	222.9982	249.9541
	256.4978	203.5591	141.27	112.6963	158.5271	287.3214	264.8534	222.3908	366.6674	340.9163
	215.5861	494.9081	231.834	134.3905	74.30617	97.84888	249.7681	233.4162		
	292.1962	148.8925	261.6536	261.0279	228.3679	183.8537	176.4807	146.9828		
	185.8368	221.2761								
	148.1104	174.3665								
AVG	215.3679	224.276	152.5822	199.5624	104.04	139.7261	194.3235	193.5819	415.3173	322.2558
STD DEV.	96.93882	135.3564	78.5898	124.124	74.10579	82.92744	103.8958	53.54527	209.6365	51.44558

A

	Averages(μM/g)			
	.05 Mpa		.1 Mpa	
	Top	Bottom	Top	Bottom
	198.5333	222.8025	519.6944	344.6432
	203.9133	192.5779	425.8603	258.726
	295.3675	366.2903	139.3788	190.0394
			215.1458	192.2144
AVG	232.6047	260.5569	325.0198	246.4057
STD DEV	54.42073	92.80652	177.5781	72.8383

B

Table B.5: A. This is the table for the strain data with the repeat for each meniscal location averaged together. The data was used to create the regressions used in Chapter 2. **B.** The is the table for the load data with the repeat for each location averaged to give the data used in Chapter 2. The control samples used for comparison are in B.5A. which incorporated control sample take from animals used in both strain and load controlled tests.